# PHOTODETACHMENT OF GAS-PHASE HALOGEN MOLECULAR ANIONS AND THE ENOLATE ANION OF ACETOPHENONE

by

Ronald O. Daubach

A DISSERTATION PRESENTED TO THE GRADUATE COUNCIL
OF THE UNIVERSITY OF FLORIDA IN
PARTIAL FULFILLMENT OF THE REQUIREMENTS
FOR THE DEGREE OF DOCTOR OF PHILOSOPHY

1983

Copyright 1983

by
Ronald O. Daubach

# ACKNOWLEDGEMENTS

The author thanks Dr. John R. Eyler for his instruction, assistance, and direction in this research effort. In addition, the patience and concern of Dr. Eyler in all stages of this research and manuscript preparation are gratefully acknowledged.

The stimulation provided by fellow graduate students was valuable. Particular thanks are extended to Dr. L. Morgenthaler, R. J. Doyle,and D. A. Atherton. The design of the microcomputer interface was initially generated by Dr. Ed Voigtman without whose assistance no subsequent progress would have been possible.

The construction of the apparatus used in this work involved the efforts of many. The professional workmanship of Mr. Art Grant, Mr. Ed Whitehead, Mr. Rudy Strohschein, Mr. James Chamblee,and Mr. Robert Dugan is thankfully commended.

The author thanks Ms. Constance Miller for the patient and careful preparation of this dissertation.

The impetus to accomplish when the desire lagged was provided by the love, concern,and devotion of Joni Meno Daubach which is deeply appreciated.

Funding for this research has been provided by the Division of Sponsored Research and the Department of Chemistry.

## TABLE OF CONTENTS

Page

ACKNOWLEDGEMENTS . . . . . . . . . . . . . . . . . . . . . . . . . . iii

LIST OF TABLES . . . . . . . . . . . . . . . . . . . . . . . . . . vi

LIST OF FIGURES . . . . . . . . . . . . . . . . . . . . . . . . . . vii

ABSTRACT . . . . . . . . . . . . . . . . . . . . . . . . . . . . ix

CHAPTER I INTRODUCTION . . . . . . . . . . . . . . . . . . 1

- Historical and Scientific Interest in Negative Ions . . . . . . . . . . . . . . . 1
- Electron Affinity . . . . . . . . . . . . . . . 3
- Experimental Techniques . . . . . . . . . . . . 5
- Theoretical Techniques . . . . . . . . . . . . 6
- Outline of Dissertation . . . . . . . . . . . . 9

CHAPTER II THEORY OF ION CYCLOTRON RESONANCE . . . . . . . 10

- Ion Motion in Static Fields . . . . . . . . . . 10
- Ion Motion in an RF Electric Field . . . . . . . 19
- Ion Detection . . . . . . . . . . . . . . . . . 25

CHAPTER III EXPERIMENTAL APPARATUS . . . . . . . . . . . . . 31

- Trapping Cell . . . . . . . . . . . . . . . . . 31
- Vacuum Apparatus . . . . . . . . . . . . . . . . 34
- Optical Apparatus . . . . . . . . . . . . . . . 39
- Pulsed Electronics . . . . . . . . . . . . . . . 46
- Microcomputer . . . . . . . . . . . . . . . . . 52
  - Microcomputer and Modifications . . . . . . 53
  - Microcomputer Interface Hardware . . . . . . 55
  - Microcomputer Software . . . . . . . . . . . 58
  - Run Time Operation . . . . . . . . . . . . . 59
- Derivation of the Expression for the Photodetachment Cross-Section . . . . . . . . . . 75

CHAPTER IV EXPERIMENTAL RESULTS AND DISCUSSION OF THE HALOGEN ANION STUDIES . . . . . . . . . . . 80

- Chlorine Molecular Anion-Formation of $Cl_2^-$ . . . 80
- Photodetachment of $Cl_2^-$ . . . . . . . . . . . . 95

Page

Analysis of $Cl_2^-$ Results. . . . . . . . . . . . . 104
Computation of Franck-Condon Factors . . . . . . . 106
Bromine Molecular Anion-Formation of $Br_2^-$ . . . . 120
Photodetachment of $Br_2^-$ . . . . . . . . . . . . . 123
Analysis of $Br_2^-$ Results. . . . . . . . . . . . . 123
Bromine Monochloride Molecular Anion . . . . . . 131
Analysis of $BrCl^-$ Results. . . . . . . . . . . . 131

CHAPTER IV PHOTODETACHMENT STUDY OF THE ENOLATE ANION OF ACETOPHENONE. . . . . . . . . . . . . . . . . 135

Formation of the Enolate Anion . . . . . . . . . . 135
Analysis of the Acetophenone Enolate Anion Results. . . . . . . . . . . . . . . . . . . . 142

CHAPTER V SUMMARY. . . . . . . . . . . . . . . . . . . . 150

APPENDIX I ON-BOARD MICROCOMPUTER HARDWARE MODIFICATION . . 152

APPENDIX II MICROCOMPUTER CONTROL REGISTERS. . . . . . . . . 153

APPENDIX III MICROCOMPUTER PROGRAMS . . . . . . . . . . . . . 155

APPENDIX IV SAMPLE PREPARATION . . . . . . . . . . . . . . . . 181

APPENDIX V NUMERICAL VALUES OF THE RKR POTENTIALS AND THE FRANCK-CONDON OVERLAP PROGRAM OUTPUT . . . . 183

REFERENCES . . . . . . . . . . . . . . . . . . . . . . 205

BIOGRAPHICAL SKETCH . . . . . . . . . . . . . . . . . . . . . . . 212

# LIST OF TABLES

Table Page

1 Laser Dyes and Observed Lasing Wavelength Regions. . 41

2 Grating Characteristics as a Function of Wavelength for a 1200 line/mm Grating in Autocollimation . . . . . . . . . . . . . . . . . . 45

3 Factors in the Relative Errors in the Cross-Section for a Range of $\Delta$ Values and f Equal to 1.0 and 0.75. 78

4 Variation of ICR Operating Parameters During Studies to Maximize Formation of the Nitrite Ion from Nitromethane . . . . . . . . . . . . . . . . . . . 82

5 Empirical Electron Affinities for $NO_2$ in eV. . . . . 92

6 Spectroscopic Constants Used in the Determination of the Rydberg-Klein-Rees Potential Curve for $Cl_2$. . 113

7 Spectroscopic Constants Used in the Determination of the Rydberg-Klein-Rees Potential Curve for $Cl_2^-$ . 114

8 Correlation of the Observed Peaks ($\lambda$, $T_{exp}$) in the $Cl_2^-$ Photodetachment Spectrum with Calculated Transitions Energies ($T_{calc}$) and Franck-Condon Factors. . . . . . . . . . . . . . . 117

9 Adiabatic Electron Affinity Values for Chlorine Determined from the Assignment of the Photodetachment Spectrum Structure. . . . . . . . . . . 121

10 Comparison of Literature Values for the Electron Affinity of Chlorine . . . . . . . . . . . . . . . 122

11 Experimental Wavelengths ($\lambda$) and Term Values ($T_{exp}$) and First Differences ($\Delta^1$) for the Observed Photoreduction of Bromine Molecular Negative Ions. . 129

12 Rate Coefficients for the Reaction of $Cl_2^-$ with $Br_2$. . . . . . . . . . . . . . . . . . . . . . . . 134

13 Values for Instrumental Parameters Pertinent to Acetophenone Anion Production and $OH^-$ and $F^-$ Precursor Anions . . . . . . . . . . . . . . . . 141

# LIST OF FIGURES

Figure | | Page
---|---|---
1 | Trochoidal Trajectory of a Charged Particle in Uniform and Static Crossed Electric and Magnetic Fields. . . . . . . . . . . . . . . . . . . | 13
2 | Trapped Ion Cyclotron Resonance Cell Schematic . . . | 16
3 | Time-Dependent Radii for Non-Resonant Particles. . . | 24
4 | GLC Circuit Emulation of ICR Detection . . . . . . . | 28
5 | Trapped Ion Cyclotron Resonance Cell . . . . . . . . | 33
6 | Schematic Diagram of the Digital Pulse Electronics . | 36
7 | Vacuum System Schematic. . . . . . . . . . . . . . . | 38
8 | Dye Laser Apparatus and Orientation. . . . . . . . . | 43
9 | A Typical Pulsed ICR Experiment Pulse Sequence . . . | 48
10 | Operator/Microcomputer Interaction Flowchart . . . . | 61
11 | Main Program Branch Flowchart. . . . . . . . . . . . | 63
12 | Baseline MO Data Flowchart . . . . . . . . . . . . . | 65
13 | Resonant Baseline Data Flowchart . . . . . . . . . . | 67
14 | Laser Status Flowchart . . . . . . . . . . . . . . . | 69
15 | Microcomputer RAM Memory Map . . . . . . . . . . . . | 71
16 | Negative Ion Mass Spectrum of Nitromethane . . . . . | 84
17 | Negative Ion Mass Spectrum for a Chlorine/ Nitromethane Mixture . . . . . . . . . . . . . . . . | 87
18 | Time-Dependent Mass Spectra of the Major Peaks of a Chlorine/Nitromethane Mixture . . . . . . . . . | 89

Figure Page

19 Photodetachment of $Cl_2^-$. . . . . . . . . . . . . . . . . 97

20 Photoproduction of $Cl^-$. . . . . . . . . . . . . . . . . 100

21 $Cl_2^-$ Photodetachment Cross-Section as a Function of Wavelength. . . . . . . . . . . . . . . . . . . . 103

22 Rydberg-Klein-Rees Potential Energy Curves for $Cl_2$ and $Cl_2^-$ . . . . . . . . . . . . . . . . . . . . 112

23 The Negative Ion Mass Spectrum of a Mixture of Chlorine/Bromine and Nitromethane. . . . . . . . . . 125

24 Photodetachment Spectrum of $Br_2^-$ . . . . . . . . . . 127

25 Negative Ion Mass Spectrum with $BrCl^-$. . . . . . . . 133

26 Acetophenone Signal Intensity. . . . . . . . . . . . 138

27 Photoreduction of the Enolate Anion. . . . . . . . . 140

28 Photodetachment of Acetophenone as a Function of Wavelength at 150 ms Delay . . . . . . . . . . . . . 144

29 Photodetachment of Acetophenone as a Function of Wavelength at 200 ms Delay . . . . . . . . . . . . . 146

30 Photodetachment of Acetophenone as a Function of Wavelength at 250 ms Delay . . . . . . . . . . . . . 148

Abstract of Dissertation Presented to the Graduate Council of
the University of Florida in Partial Fulfillment of the
Requirements for the Degree of Doctor of Philosophy

# PHOTODETACHMENT OF GAS-PHASE HALOGEN MOLECULAR ANIONS AND THE ENOLATE ANION OF ACETOPHENONE

By

Ronald O. Daubach

December 1983

Chairman: Dr. John R. Eyler
Major Department: Chemistry

The photodetachment of electrons from negative halogen molecular ions has been investigated. An ion cyclotron resonance mass spectrometer was employed for the generation, containment and detection of the ions. Photoprocesses were induced by means of an integrated, tunable dye laser system.

Structure was observed in the photodetachment spectra of chlorine and bromine molecular anions. This structure was correlated to vibronic fine structure of the photodetachment transition. An adiabatic electron affinity value for chlorine of $2.36\,^{+0.27}_{-0.32}$ eV was obtained. The absence of structure in the bromine photodetachment cross-section attributable to the anion precluded estimation of the electron affinity of bromine. The interhalogen molecular anion of bromine monochloride was generated but was of low signal intensity. The photodetachment spectrum of the enolate anion of acetophenone exhibited behavior which supported previous explanations of the source of the structure in the cross-section near threshold.

# CHAPTER I
# INTRODUCTION

## Historical and Scientific Interest in Negative Ions

The study of negative ions in the gas phase has elicited increasing interest since Wildt ascertained the importance of $H^-$ to the explanation of the anomalous infrared opacity of the solar spectrum (1). This insight was founded upon the investigation of the "affinity continuum" associated with the radiative attachment of an electron to an atom by Gerlach and Gromann (2). Wildt further proposed that the radiative behavior of diatomic negative ions of neutral diatomics of established astrophysical importance such as $H_2$, $C_2$, $O_2$, NH, OH,and CH might be of significance in stellar radiation spectral analysis. Subsequent study of negative ions for astrophysical applications has been largely concerned with defining the wavelength dependence of the interaction of light with the selected ions (3). Following the recognition of the import of negative ions in stellar plasmas, an awareness of negative ions evolved in atmospheric chemistry, flame chemistry, gas laser plasma chemistry, and radiation chemistry and biology.

Consideration of the behavior of negative ions in the atmosphere is essential in accounting for effects such as the reflection of radio waves at the lower ionosphere (4) and the fate of atmospheric pollutants (5). The ionosphere is a region of high free electron concentration extending from 60 to 450 kilometers above the earth's surface. Fluctuations, either local or temporal, in the free electron concentration in this region have profound effects on the reflectivity to radiofrequencies exhibited by the region. Consequently, the formation and destruction of negative ions with the concomitant loss or gain of free electrons must be characterized to account for the observed radiofrequency reflectivity.

Negative ion chemistry in the lower atmosphere, the stratosphere (15-60 kilometers) and the troposphere (0-15 kilometers), is pertinent to air pollution chemistry and had been suggested as a sink for chlorofluorocarbons released into the atmosphere. Recent studies have discredited this suggestion as the reactions of the hydrated negative ions which predominate at the lower altitudes with chlorofluorocarbons have been shown to proceed slowly (6).

The study of ions in flames is of current interest (7) and has been of interest since Moreau's early studies of negative ion transport in flames (8). The complexity of the negative ion composition of flames is illustrated by the number of negative ions in significant concentration in a simple, clean, methane-oxygen flame in which no fewer than twelve negative ions have been identified (9). Not only the characterization of flames by the study of the ion distribution, which remains an active area of research (10), but also the use of flames in spectroscopy rely upon the clarification of negative ion-flame chemistry.

The accelerated search for laser media with output in the ultraviolet and vacuum ultraviolet wavelength regions (11) requires knowledge of electron-neutral interactions and negative ion formation. Typically, short wavelength lasers have employed some variation of a fast-risetime, high-energy electron discharge pumping scheme (12). The excited neutrals and positive ions formed during discharge have been included in models of laser performance (13). A recent investigation has extended consideration to negative ions produced by the attachment of secondary electrons to $F_2$ and $NF_3$, the alternate sources of fluorine in XeF laser gas mixtures (14). In addition, the mobility of $Cl^-$ in Xe, a factor in evaluating the XeCl excimer mixtures, has been investigated (15) and it has been suggested that the molecular bromine anion contributes to XeBr* excimer formation in electron discharge pumped mixtures through reaction with $Xe^+$ (16).

Negative ions are of interest in radiation and nuclear chemistry. Biologically active free radicals, excited states,and negative ions are generated by radiation incident on biological matter (17). The development of nuclear pumped lasers and gas-core reactors employing $UF_6$ as the fuel/medium requires that the negative ion formation of this compound of relatively large electron affinity be evaluated (18).

## Electron Affinity

The electron affinity of the corresponding neutral is the most fundamental property associated with a negative ion. The electron affinity is defined as the change in the total energy of the system upon the addition of an electron. The change in the system energy may be positive or negative. Conventionally, stabilization of the system corresponds to a positive sense for the electron affinity.

Negative electron affinities are associated with unstable systems which may, however, exhibit resonances related to the formation of a transient negative ion state (19).

For an atomic negative ion, the given definition of electron affinity is complete. A complication arises for molecular negative ions due to the change in the nuclear configuration associated with the addition of the electron. Two distinct types of electron affinities are conceivable. The energy difference associated with the ground state neutral and ground state ion both with zero internal energy and both at their respective equilibrium geometries is referred to as the adiabatic electron affinity. A more readily observable energy difference, the vertical electron affinity, corresponds to the change in energy between the neutral and negative ion ground electronic states at the equilibrium nuclear configuration of the neutral. In general, the term vertical electron affinity is used for all values of observed electron affinities for which either the negative ion or the neutral possess internal excitation. Herein lies the basic problem in the interpretation of experimental measurements of molecular electron affinities, the difficulty encountered in the evaluation of the internal energy of the initial and final states. In general, experimental techniques measure vertical electron affinities which provide upper or lower limits to the adiabatic or thermodynamic electron affinity based upon some estimate of the internal excitation. Several reviews (20-23) of the techniques applied in the evaluation of electron affinities of molecular species have appeared including the recent article by Janousek and Brauman which provides an excellent overview of the topics discussed here.

## Experimental Techniques

Two types of charge transfer techniques have proven useful in the study of electron affinities: exothermic charge transfer (CT) and endothermic charge transfer (ECT). Exothermic charge transfer yields limits on a molecular electron affinity by observation of the direction of spontaneous charge transfer between negative ions and target neutrals. More accurate values of the limits for the electron affinity may be surmised if the exothermicity of the charge transfer reaction can be estimated (24). Endothermic charge transfer employs the energy of translation to induce a nominally endothermic charge transfer (25). This technique enables the energy dependence of the cross-section above threshold to be determined. Collisional ionization is a related scheme in which both of the initial reactants are neutrals. Collision-induced, ion-pair formation lends itself to the evaluation of the product negative ion electron affinity provided the positive ion's ionization potential is independently known (26). These techniques are limited by the residual uncertainties in the distribution of the excess energy between translation and internal modes and the detailed distribution of the internal energy for systems with more than one degree of internal freedom.

A variety of photodetachment techniques for obtaining electron affinities have been developed. These include fixed (27) and variable (28) frequency photoelectron spectrometry and variable frequency crossed beam (29) and drift tube (30) photodetachment techniques. The rapid development of variable wavelength, wide-wavelength-tuning-range lasers of excellent monochromaticity has greatly assisted the application of photodetachment schemes. The major characteristic distinguishing the different photodetachment techniques is the detailed means by which the process is instigated and detected. The fixed frequency photoelectric experiment employs an argon ion ($Ar^+$) laser (488.0 nm) to eject electrons from a beam of negative ions. The photoelectrons are energy analyzed over a defined angular collection aperture to obtain the photoelectron spectrum. Variable frequency photoelectron spectrometry measures the production of photoelectrons as a function of the irradiation wavelength. Beam and drift tube photodetachment employ either neutral beam or residual ion beam detection rather than direct analysis of the ejected electrons. The important advantage of a drift tube experiment is the reasonable assurance that an ion has a thermal internal energy distribution prior to photoexcitation.

Ion cyclotron resonance (ICR) techniques for the study of photoinduced processes of ions merge the advantage of drift tube thermalization with controlled, low energy, electron-impact production of negative ions to minimize ion internal excitation (31-32). The pulsed ICR technique is capable of characterizing effects of ion internal excitation by varying the time available for the collisional de-excitation prior to photoexcitation (33).

## Theoretical Techniques

Evaluation of the experimental measurement of electron affinities has been hampered by the absence of reliable, theoretical predictions of the electron affinity and by the inability to predict the features of a photodetachment spectrum. Means of estimating electron affinities and evaluating cross-section behavior have been developed and may be classified as semiempirical, ab initio, and collision theory techniques. Semiempirical results deal solely with the prediction of electron affinities. Pritchard (34) gave a very complete historical summary of semiempirical estimation of electron affinities based on observed lattice energies and thermodynamic arguments. Person (35) suggested a semiempirical scheme based upon the charge-transfer frequency of donor-acceptor complexes (36) and its relation to the vertical electron affinity of the acceptor and derived good results for several diatomic halogen molecules. Recently, a means of estimating molecular electron affinities from the constituent atoms' electron affinities and positions in the Periodic Table has been proposed (37).

Theoretical determinations of electron affinities have employed either direct or indirect schemes (38). Indirect methods consist of individual calculations for the potential energy of the neutral and negative ion states. The potential energy curves generated are then used to obtain values for the adiabatic and vertical electron affinities. These methods are constrained by the necessity of very high precision in the individual state energies since the electron affinities are given as the difference of two large values, yet are quite small with respect to the total energies of either state. In addition, it is not trivial to insure that the calculations for both states employing a common calculation technique, Hartree-Fock, CI, or perturbation theory, are carried out to the same order when the number of electrons is changed by one. Finally, the electron affinity is normally of the order of the correlation energy (39), the energy associated with the assumption of an average potential due to all of the electrons with the exception of the electron whose energy state is calculated. This average potential is an assumption basic to all Hartree-Fock schemes and limits the value of this particular scheme for electron affinity determination. CI accounts for correlation effects by including a number of electronic configurations into the energy calculations (40). Generally, the validity of any indirect method depends upon the system as well as the technique.

Several variations of a direct method for calculating potential energy differences between electronic states at a selected nuclear configuration have recently been developed (38). These techniques eliminate the inaccuracies of the indirect procedures. The method begins with a calculation of the neutral potential energy curve. An operator simulating the addition or removal of an electron is then applied to a specific point on the potential energy surface. This determines the ion energy. For vertical and adiabatic electron affinity estimation, this method appears promising. It is feasible, although computationally extensive, to generate the detailed anion potential surfaces necessary to predict spectral behavior for the transitions.

Photodetachment spectral analysis consists of modeling the energy dependence of the cross-section at threshold. The rigorous mathematical basis for the threshold behavior has been delineated by Wigner (41). An excellent, detailed derivation of the theory has been published by Lane and Thomas (42) and the extension of the formalism to a coordinate system applicable to diatomics is well documented (43). The details of the theory and derivation will not be of significance here; however, the results will be applied in analysis of the observed spectral behavior.

## Outline of the Dissertation

This dissertation presents a description of photodetachment studies executed on molecular negative ions. These investigations were carried out using a pulsed ion cyclotron resonance mass spectrometer combined with a pulsed, flashlamp-pumped dye laser. A data collection and analysis system was interfaced to the experiment to simplify and accelerate data reduction. Chapter II describes the theory of ion cyclotron resonance as it pertains to ion containment and detection. Chapter III addresses the details of the experimental procedure and set-up. Chapter IV presents the results for the diatomic halogen anions investigated, $Cl_2^-$, $Br_2^-$, and $BrCl^-$. Chapter V presents the results for the enolate anion of acetophenone. A summary of the results and assessment of the technique for the study of molecular anions is put forward in Chapter VI.

Appendix I documents alterations made to the microcomputer to enhance its data handling performance. Appendix II itemizes the control registers for the software data collection and analysis. Appendix III contains the microcomputer programs written to implement the data collection. Appendix IV describes the sample preparations and handling techniques for the parent compounds. Appendix V contains the calculated potential energy curves and Franck-Condon analysis for $Cl_2 - Cl_2^-$.

# CHAPTER II
# THEORY OF ION CYCLOTRON RESONANCE

The study of photo-induced processes of gas phase ions necessitates a well-defined region of observation and the minimization of non photo-induced ion losses. In addition, a sensitive method of sufficient resolution is required for the detection of ions of varying mass-to-charge ratios. The classical motion of a charged particle in electric and magnetic fields is applied to the spatial restriction and the detection of ions.

## Ion Motion in Static Fields

An isolated, charged particle in motion located in a magnetic field interacts with the field classically. This interaction of charged particle and magnetic field constrains the particle motion in the plane perpendicular to the field. For a uniform and static magnetic field, the interaction of the particle and the field results in the gyration of the particle about the magnetic field lines. The field-induced motion is characterized by the frequency of the rotation, $\omega$, given as (44)

$$\omega = qB/m \tag{1}$$

where q is the charge on the particle, m is the particle mass, B is the magnitude of the magnetic field strength and $\omega$ is the natural cyclotron frequency. Although the component of the initial particle velocity perpendicular to the field, $v_{0_\perp}$, must be nonzero for this interaction, significantly, the frequency of gyration is independent of the actual magnitude of the velocity component. Therefore, ions of identical charge-to-mass ratios circulate about the magnetic field lines at a single natural cyclotron frequency regardless of the distribution of velocity components, $v_{0_\perp}$. The component, $v_{0_\perp}$, remains significant since the radius of gyration, r, retains a functional dependence on $v_{0_\perp}$

$$r = \frac{mv_{0_\perp}}{qB} = \frac{v_{0_\perp}}{\omega} \quad . \tag{2}$$

The motion of a charged particle in the presence of uniform and static electric and magnetic fields, $\underline{E}$ and $\underline{B}$, respectively, is governed by the Lorentz force law,

$$\underline{F} = q(\underline{E} + \underline{v} \times \underline{B}) \tag{3}$$

where $\underline{v}$ is the particle velocity. This equation is readily soluble for the assumed field conditions for the equations of motion of the particle (44). For the simplified field conditions in which $\underline{E}$ and $\underline{B}$ are mutually perpendicular, the equations of motion dictate a trochoidal path, the superposition of the cyclotron motion and the drift of the center of the cyclotron orbit perpendicular to both fields (Figure 1). The separation of the complex trajectory of the particle into the cyclotron and drift components is a useful modification for the analysis and visualization of ion motion in complicated electrostatic fields. The center of the cyclotron motion is referred to as the "guiding center" and the separation of motions is called the "guiding center" or "drift" approximation (45).

Figure 1. Trochoidal Trajectory of a Charged Particle in Uniform and Static Crossed Electric and Magnetic Fields. A nonzero component of particle velocity in the y-direction is presumed in the generation of the trochoidal path.

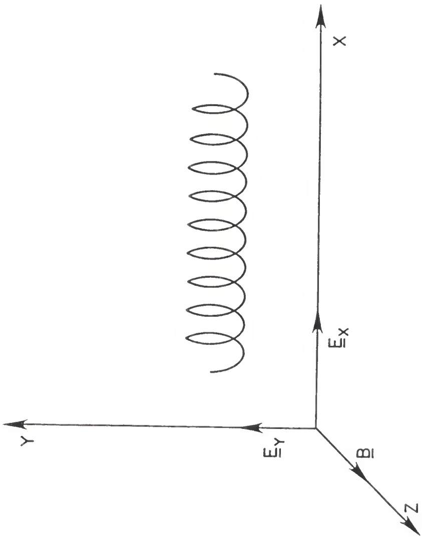
X
$\underline{E}_X$
Y
$\underline{E}_Y$
$\underline{B}$
Z

Three-dimensional ion containment is not accomplished with the simple field conditions thus far treated. In neither of the cases considered has the motion of the particle parallel to the magnetic field lines been restricted. Also, the transverse electric field induces a particle drift producing a channel for ion loss perpendicular to both the electric and magnetic fields. Consequently, a configuration of fields eliminating these ion loss channels must be selected.

The trapped ion cell developed by McIver produces an electrostatic potential for which the equipotential lines close on themselves in the plane perpendicular to the magnetic field in addition to forming an electrostatic potential well parallel to the magnetic field axis (46). The cell geometry and definition of coordinate axes are indicated in Figure 2, which also indicates the direction of the magnetic field for subsequent discussion. The cell consists of six electrically independent plates. For effective negative ion trapping, the upper (U), lower (L), and end (E) plates are held at +1.0 volt, while the trapping (T) plate potentials are -1.5 volts. In the case of positive ion trapping, the polarity of each plate potential is reversed. The solution of Laplace's Equation for a cell identical to that shown in Figure 2 has provided an expression for the three-dimensional potential produced in the cell interior (47). An analytic approximation to this expression valid near the center of the cell yields a quadrupolar electric field

$$\underline{E} = \frac{2(V_T - V_0)}{a^2} \left(\alpha x \, \underline{i} + \lambda y \, \underline{j} - \beta z \, \underline{k}\right) \qquad (4)$$

Figure 2. Trapped Ion Cyclotron Resonance Cell Schematic. Components of the trapped ion cell which influence the geometry of the electrostatic cell potential are $T_c$ and $T_f$, the collector and filament trapping plates, respectively; U, the upper plate; L, the lower plate; $E_1$ and $E_2$, equivalent, open end plates.

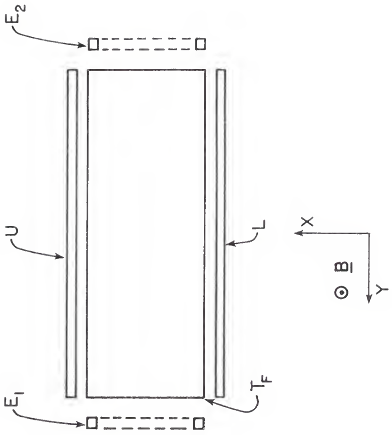
$E_2$
U
L
X
$\underline{B}$
Y
$E_1$
$T_F$

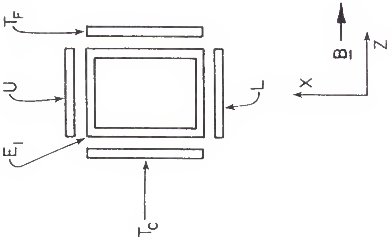
$T_F$
U
$E_1$
L
X
$\underline{B}$
Z
$T_C$

where a is the cell width, $V_T$ is the trapping plate potential, $V_0$ is the upper and lower plate potential and $\alpha$, $\lambda$ and $\beta$ are constants related to the actual dimensions of the cell. The restriction of ion motion is evident when the guiding center motion is evaluated for the approximately quadrupolar cell potential.

The expression for the drift velocity of the guiding center, $\underline{v}_d$, is

$$\underline{v}_d = \underline{E} \times \underline{B} \;/\; B^2. \tag{5}$$

With the magnetic field direction as defined (Figure 2), the drift velocity in component form becomes

$$v_{d_x} = E_y/B = [2\lambda(V_T - V_0)/a^2B]y$$

and

$$v_{d_y} = -E_x/B = [-2\alpha(V_T - V_0)/a^2B]x \; . \tag{6}$$

Clearly, the drift velocity vector in any plane of constant z lies in the plane and is perpendicular to the electric field vector, $\underline{E}$.

Since $\underline{E}$ is everywhere perpendicular to the equipotential lines, ion drift occurs along the closed equipotential lines of the electrostatic field. The frequency of the drift along the elliptical equipotential lines is derived from the solution of the equations of motion in the quadrupolar field as (47)

$$\Omega = \frac{2(V_T - V_0)\ (\alpha\lambda)^{\frac{1}{2}}}{a^2B} \; . \tag{7}$$

Therefore, in the trapped ion cell, the circulation of the guiding centers about elliptical paths defined by the electrostatic equipotential lines at frequency $\Omega$ eliminates the mechanism of drift loss of ions.

The remaining component of the electric field, $\underline{E}_z$, is of the form (47)

$$\underline{E}_z = -Kz\ \underline{k} \tag{8}$$

where

$$K = 2(V_T - V_0)\beta/a^2.$$

Substitution of this expression into the z-component of the Lorentz force law (2) yields the equation for simple harmonic motion of a charged particle along the magnetic field lines

$$\dot{v}_z = -\omega_T{}^2 z \tag{9}$$

where $\omega_T = (qK/m)^{\frac{1}{2}}$. Oscillatory motion along the z axis is imposed upon ions whose initial total energy, kinetic and potential, is less than the trapping potential well. A side-effect of the electrostatic restriction of the ions in the z-direction is a shift in the observed cyclotron frequency from the natural cyclotron frequency, $\omega$. The effective cyclotron frequency, $\omega_c$, is (47)

$$\omega_c = (\omega^2 - \omega_T{}^2)^{\frac{1}{2}} = \{\omega^2 - [\frac{2(V_T - V_0)}{a^2 B}\beta]^2\}^{\frac{1}{2}}. \tag{10}$$

Clearly, alteration of the trapping potentials results in a shift of the cyclotron frequency unless compensated with an appropriate alteration of the magnetic field strength.

Typical values of the ion motion parameters for an ion of mass number 70 and unit negative charge in a magnetic field of 0.70 Telsa with the standard plate potentials are

| | |
|---|---|
| Natural cyclotron frequency, $\omega/2\pi$ | 153.6 kHz |
| Radius of cyclotron orbit, r | 0.2 mm |
| Drift frequency, $\Omega/2\pi$ | 214 Hz |
| Drift velocity, $v_d$ | 0.27 m/sec |
| Trapping frequency, $\omega_T/2\pi$ | 24.4 kHz |
| Observed cyclotron frequency, $\omega_c/2\pi$ | 152 kHz |

where $v_x=v_y=v_z$ is 2 x $10^2$ m/sec. The motion of the ion proceeds as follows: during the period of one complete oscillation of the guiding center along the magnetic field line ($T\omega_T \sim 40\ \mu s$) the ion will have completed six rotations about the guiding center ($T_\omega \sim 6\mu s$) and the guiding center will have drifted along an electrostatic equipotential line and perpendicular to the magnetic field axis a distance of approximately 0.01 mm.

## Ion Motion in an RF Electric Field

An rf electric field takes the form

$$\underline{E}_1(t) = E_1 \sin(\omega_1 t)\ \underline{i} \tag{11}$$

for a field linearly polarized in the x-direction. A linearly polarized rf field may be decomposed into counterrotating circularly polarized fields

$$\underline{E}^+_1(t) = \frac{E_1}{2} \sin(\omega_1 t)\ \underline{i} + \frac{E_1}{2} \cos(\omega_1 t)\ \underline{j}$$

and

$$\underline{E}^-_1(t) = \frac{E_1}{2} \sin(\omega_1 t)\ \underline{i} - \frac{E_1}{2} \cos(\omega_1 t)\ \underline{j} \tag{12}$$

Restricting consideration to the circularly polarized component of the same sense as the ion motion, $\underline{E}^{+}_{1}(t)$ (48), the force equation in component form becomes

$$\frac{du_x}{dt} = \frac{qE_1}{2m} \sin(\omega_1 t) + \omega_c u_y$$

$$\frac{du_y}{dt} = \frac{qE_1}{2m} \cos(\omega_1 t) - \omega_c u_x \tag{13}$$

Transforming and solving these equations yields the velocity components driven by the rf electric field in a static magnetic field

$$u_x(t) = \frac{qE_1}{2m(\omega_1 - \omega_c)} [\cos(\omega_c t) - \cos(\omega_1 t)]$$

$$u_y(t) = \frac{-qE_1}{2m(\omega_1 - \omega_c)} [\sin(\omega_c t) - \sin(\omega_1 t)]. \tag{14}$$

The time dependent expression for the energy of the motion, $\mathcal{E}$ (49), attributable to the combined rf electric and static magnetic field is

$$\frac{d\mathcal{E}}{dt} = q\underline{u}\cdot\underline{E} = \frac{q^2 E_1^{\,2}}{4m(\omega_1 - \omega_c)} \{[\cos(\omega_c t) - \cos(\omega_1 t)] \sin(\omega_1 t) - [\sin(\omega_c t) - \sin(\omega_1 t)] \cos(\omega_1 t)\}. \tag{15}$$

Equating the instantaneous kinetic energy, $d\mathcal{E}/dt$, to the spontaneous power absorption, $A(t)$, and simplifying the trigonometric terms produces an expression for $A(t)$

$$A(t) = d\mathcal{E}/dt = \frac{q^2 E_1^{\,2}}{4m(\omega_1 - \omega_c)} \sin(\omega_1 - \omega_c)t. \tag{16}$$

This general expression for instantaneous power absorption may be evaluated for the conditions of ion resonance and extended rf irradiation to determine the average power absorption per resonant ion.

Substituting into the expression for the kinetic energy, $E=\frac{1}{2}mv^2$, yields the particle kinetic energy due to rf excitation

$$E = \frac{q^2E_1{}^2}{2m(\omega_1 - \omega_c)^2} \sin^2(\frac{\omega 1 - \omega c}{2})\, t. \qquad (17)$$

The instantaneous power absorption is then readily converted to the average power absorption, $A(\omega_1)$, over the period of irradiation, $T$,

$$A(\omega_1) = \frac{1}{T} \frac{q^2E_1{}^2}{4m(\omega_1 - \omega_c)^2} [1-\cos(\omega_1 - \omega_c)T]. \qquad (18)$$

Finally, the behavior of these quantities at resonance $(\omega_1 = \omega_c)$ can be evaluated

$$\begin{aligned} A(t) &= (dE/dt) = \frac{q^2E_1{}^2t}{4m} \\ E &= \frac{q^2E_1{}^2t^2}{8m} \\ A(\omega_c) &= \frac{q^2E_1{}^2T}{8m} . \end{aligned} \qquad (19)$$

The rf electric field directly influences the cyclotron motion of the ion about the magnetic field lines. The nature of the interaction becomes evident when the time dependent radius of the cyclotron motion in the field is derived

$$r(t) = \frac{cE_1}{B} \quad \frac{\sin\, (\omega_1 - \omega_c)t}{2} / \, (\omega_1 - \omega_c). \qquad (20)$$

At resonance ($\omega_1=\omega_c$) Equation 20 reduces to

$$r = \frac{cE_1}{2B}\,t. \tag{21}$$

The radius of gyration of an ion in resonance increases linearly with the irradiation time and with the electric field amplitude. At higher magnetic fields the resonant ion radius is smaller for the same rf irradiation conditions. The radius of a nonresonant ion is seen to be varying with time but is bounded as a result of the phase mismatch between the resonant frequency of the ion and the driving rf field (Figure 3).

The motion of a collection of ions with a distribution of velocities has been determined from the equations for single particle motion (47). In the trapped ion cell, ions are formed through the interaction of a pulsed electron beam directed along the z-axis with a sample gas in thermal equilibrium. Assuming that there is no gradient of electron energy along the electron beam (generally invalid) and that the electron pulse is long with respect to the period for simple harmonic motion along the z-axis (generally true), then the ions can be assumed to be uniformly distributed along the z-axis. The uniform distribution of guiding centers along the z-axis drifts along equipotential field lines. If an electron beam of circular cross-section is assumed the initial distribution of guiding centers is circular in the xy-plane. The geometry of the initial distribution is altered due to the variation in ellipticity of the paths followed by individual ions as a function of the distance from the z-axis

Figure 3. Time-Dependent Radii for Non-Resonant Particles. For $(\frac{\omega_1-\omega_c}{2\pi})$ = 1 Hz (---), $r_{max}$ is equal to $r + \frac{cE}{B}$ and $r_{min}$ is equal to $r-\frac{cE}{B}$. For $(\frac{\omega_1-\omega_c}{2\pi})$ = 2 Hz (——), $r_{max}$ is equal to $r + \frac{cE}{4B}$ and $r_{min}$ is equal to $r-\frac{cE}{4B}$.

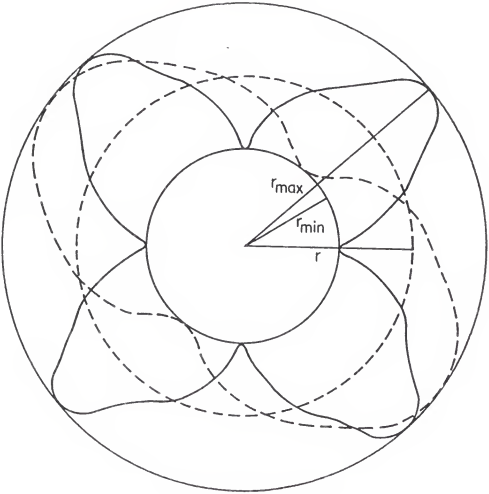
$r_{max}$
$r_{min}$
$r$

at the drift frequency, $\Omega$. This produces an oscillation of the population of guiding centers between a circular distribution and an elliptical distribution at twice the drift frequency, which for the numerical example above corresponds to 428 Hz. However, the duration of the electron beam pulse, ~25 ms, is longer than the period of the guiding center drift oscillation, ~2.3 ms, and the ions will be uniformly distributed along the elliptical orbits if ion formation is constant during the electron beam pulse. Therefore, ions formed at any instant exhibit a shifting population distribution but the total collection of ions is uniformly distributed along elliptical drift lines.

## Ion Detection

Power absorption by an ion from an amplitude limited rf electric field is the basis of ion cyclotron resonance detection. Obviously the means for generating a suitably stable rf field and a means of detecting absorption of the field are required. Both of these functions can be accomplished with a marginal oscillator detector.

Marginal oscillator circuit applications in ion cyclotron resonance detection (50) are completely analogous to their earlier application in nuclear magnetic resonance (nmr) detection (51). Consequently, ion cyclotron resonance marginal oscillators have evolved with few modifications from nmr marginal oscillators. Two alterations of the basic marginal oscillator circuit serve to adapt it for use in a pulsed mode (52). First, the addition of a limiter in the feedback loop of the oscillator insures reliable low level operation as required for ion detection. Second, a gated amplifier serves to pulse the circuit output with the application of an externally derived gate pulse.

The analysis of marginal oscillator detection can be carried out in terms of the gated, limited feedback oscillator (Figure 4). The parallel, GLC (conductance-inductance-capacitance) tank circuit of the oscillator has a resonant frequency

$$\omega_0 = (LC)^{-\frac{1}{2}} \tag{22}$$

where L is the circuit inductance and C is the circuit and cell capacitance. The conductance, G, represents resistive losses in the circuit. The limiter supplies a constant amplitude signal, $V_0$, to the resonant circuit through the feedback resistor, $R_f$. At resonance, $\omega_0 C = (\omega_0 L)^{-1}$, hence the admittance is a pure conductance and the voltage across G, $V_G$, becomes

$$V_G = \left(\frac{G^{-1}}{G^{-1} + R_f}\right) \cdot V_0 = \frac{V_0}{1 + GR_f} \tag{23}$$

where $V_0$ is the rms voltage level from the limiter and $V_G$ is the rms voltage level across the resonant circuit. An infinitesimal change in conductance directly affects the rms voltage level of the resonant circuit

$$\frac{\Delta V_G}{\Delta G} = -\frac{V_0 R_f}{(1 + GR_f)^2} = -\frac{V_G R_f}{1 + GR_f} . \tag{24}$$

The power absorption ($\Delta A$) due to a change in the cell conductance is represented by the total derivative of the instantaneous power with respect to the conductance and the voltage across the conductance,

$$\Delta A = -V_G \cdot \Delta V_G \left(\frac{1 + GR_f}{R_f}\right). \tag{25}$$

Figure 4. GLC Circuit Emulation of ICR Detection. $V_o$ is the output of the limiter. $R_f$ is the amplifier feedback resistance. G, L, and C represent the conductance, inductance and capacitance of the ion cyclotron resonance cell.

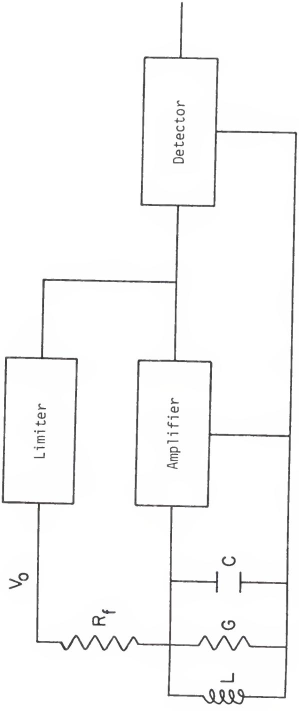
Detector
Limiter
Amplifier
$V_0$
$R_f$
G
C
L

The expression for the instantaneous power absorption of a resonant ion (Equation 19) is equated to Equation 25 and solved for $\Delta V_G$

$$\Delta V_G = - \frac{q^2 E_1{}^2 t}{4mV_G} \left(\frac{R_f}{1 + GR_f}\right). \tag{26}$$

The criterion for maximum power transfer is

$$G^{-1} = R_f \tag{27}$$

as would be anticipated. This solution is extended to n ions and the average value of $\Delta V_G$ for such an ensemble is

$$\Delta V_G = - \frac{nq^2 E_1{}^2 t}{4mV_G} \left(\frac{R_f}{1 + GR_f}\right). \tag{28}$$

Equation 28 contains the important aspects of the detection process. First, signal intensity is a direct measure of the number of resonant ions. Implicit is the assumption that the ion-field interaction is not interrupted by particle collisions, reactive or nonreactive, or by loss of ions due to containment leaks. In practice, t is short with respect to ion loss mechanism characteristic times and this expression is valid. Second, the signal intensity is inversely related to the mass of the ion. This complicating behavior must be considered in pulsed ICR mass spectrometry analyses. Third, the average voltage level change as derived has an ambiguous dependence on the rf field strength. An alternate expression clarifies this dependence

$$\Delta V_G = - \frac{nq^2 t}{ma^2} V_G \left(\frac{R_f}{1 + GR_f}\right). \tag{29}$$

Thus, the voltage change due to absorption is linearly related to the voltage across the circuit and inversely proportional to the square of the plate separation, a, across which the rf field is applied.

In practical pulsed ICR, the transient voltage level change is integrated over the period of the rf irradiation. The resulting amplitude may be sampled and held for display or transfer. Integration alters the dependence of the signal on the irradiation period so that the integrator output level is now described by

$$\Delta V_G = - \frac{nq^2 E_1{}^2 t^2}{8mV_G} \left(\frac{R_f}{1 + GR_f}\right)$$

or (30)

$$\Delta V_G = - \frac{nq^2 V_G t^2}{2ma} \left(\frac{R_f}{1 + GR_f}\right)$$

when the instantaneous change in the voltage level is linear over the period of integration. The negative sign in the numerator of Equations 26-30 is removed by inversion of the signal voltage level in the post-detection electronics.

# CHAPTER III
# EXPERIMENTAL APPARATUS

The pulsed ion cyclotron resonance experiments presented in this dissertation required the interfacing of electronic, optical, and vaccum components. The central component of any ion cyclotron resonance experiment is the ion cell. The electronics apply required, properly timed pulses and excitations to the ion cell and detect the influence of the contained ions on an applied rf field. The vacuum system provides a suitable environment at the cell for the production, maintenance, and detection of ions. Since the experiments described involve radiative transitions of ions, a suitable radiation source must be coupled to the ion containment region through the vacuum hardware and ion cell. In addition, the radiation source must be controlled by an appropriate trigger so as to operate synchronously with the potentials and excitations employed in the ion detection process.

## Trapping Cell

The trapped ion analyzer cell (Figure 5) requires six dc potentials in conjunction with the uniform, static magnetic field to produce an effective ion trap. The dc potential polarities are dictated by the polarity of the ion. The trapping plate potentials are the same polarity as the ion, while end, lower, and upper plates are of opposite polarity. Typically the dc potentials are

Figure 5. Trapped Ion Cyclotron Resonance Cell. Six dc plate potentials produce the necessary electrostatic potential at the cell interior. Upper and lower plates both have multiple roles. The upper plate is used for $\omega_2$ excitation and quenching of ions. The lower plate is the marginal oscillator input/detect plate. The grid, filament and collector comprise the electron beam generation system.

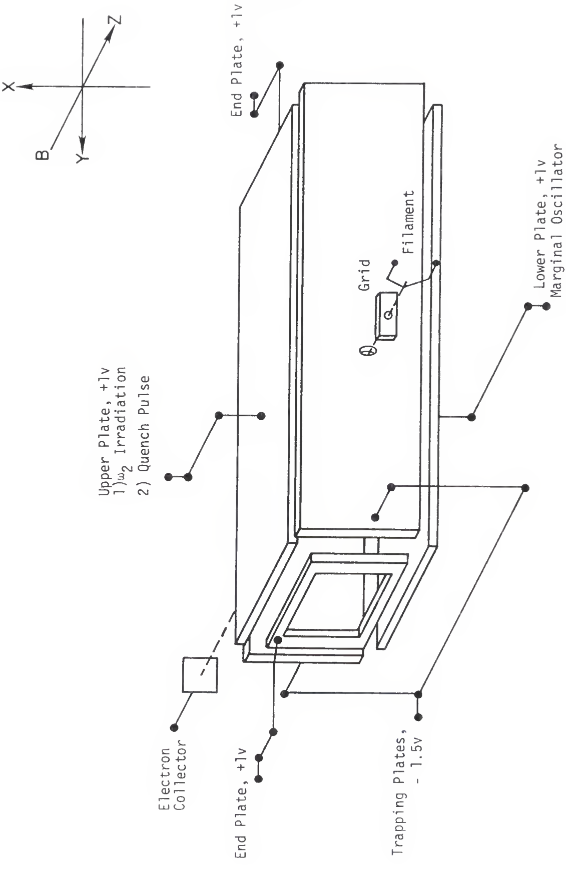
X
Y
Z
B
End Plate, +1v
Upper Plate, +1v
1) $\omega_2$ Irradiation
2) Quench Pulse
Grid
Filament
Lower Plate, +1v
Marginal Oscillator
Electron
Collector
End Plate, +1v
Trapping Plates,
- 1.5v

symmetric. Absolute voltage levels of one volt for the end, upper, and lower plates with trapping plate potentials of one and one-half volts are sufficient for effective trapping.

The cell dc potentials are taken from the regulated five-volt power supply of the digital pulse electronics (53) (Figure 6). A 500 Ω, ten-turn variable resistance connected across the +5 volt and -5 volt busses defines the dc level. The dc lines are buffered to the appropriate cell plates to insure that the dc power supply loading is minimal.

Filament and grid dc potentials are also produced in the digital pulse electronics package (53). The voltage range is 0 to -100 volts for each. The filament current is provided by a Kepco 1000-0.2 (M) Filament Power Supply (54).

The electron current through the cell is monitored at a positively biased collector plate. Current-to-voltage conversion and amplification produce a measurement suitable for display on an oscilloscope. A collector output voltage of 1 volt corresponds to an electron current of 1 microamp. Typical electron currents are on the order of 0.01 microamps.

## Vacuum Apparatus

The vacuum apparatus is illustrated schematically in Figure 7. The main vacuum can and low vacuum and high vacuum manifolds are constructed of stainless steel. A variety of gasket materials are used in the manifold connections. A gold wire gasket is used at the main vacuum can to high vacuum manifold connection. Copper gaskets are used at manifold-pump connections and nickel gaskets are used for

Figure 6. Schematic Diagram of the Digital Pulse Electronics. Cell interconnections are shown with respect to the dc level pick-offs and the varying rf fields. Pulse destinations are as indicated from the main control unit to the ancillary detection, collection and control equipment.

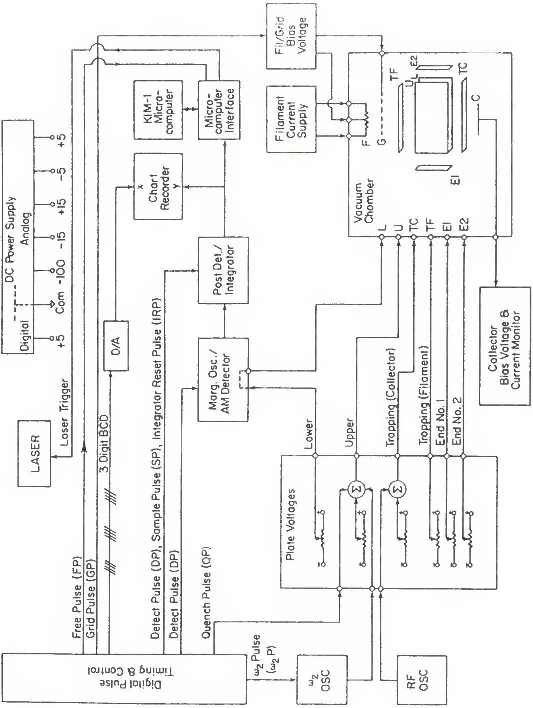
DC Power Supply
Digital
Analog
+5
Com
-100
-15
+15
-5
+5
LASER
Laser Trigger
D/A
3 Digit BCD
x
Chart Recorder
y
KIM-1 Micro-computer
Micro-computer Interface
Post Det./ Integrator
Marg. Osc./ AM Detector
Fil/Grid Bias Voltage
Filament Current Supply
Vacuum Chamber
F
G
TF
U
L
E2
TC
C
E1
L
U
TC
TF
E1
E2
Collector Bias Voltage & Current Monitor
Plate Voltages
Σ
Σ
Lower
Upper
Trapping (Collector)
Trapping (Filament)
End No. 1
End No. 2
Free Pulse (FP)
Grid Pulse (GP)
Detect Pulse (DP), Sample Pulse (SP), Integrator Reset Pulse (IRP)
Detect Pulse (DP)
Quench Pulse (QP)
Digital Pulse Timing & Control
$\omega_2$ Pulse ($\omega_2$ P)
$\omega_2$ OSC
RF OSC

Figure 7. Vacuum System Schematic.
The vacuum can which provides the proper environment for the ICR cell (N) has separate inlet manifold and high vacuum manifold to facilitate mixing of gases and control of gas flows.

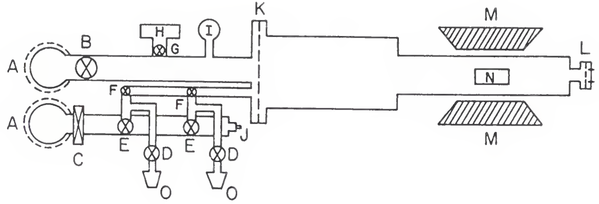

| | |
|---|---|
| A. | Two-inch oil diffusion pumps with liquid nitrogen traps |
| B. | High vacuum manifold cut off valve |
| C. | Low vacuum manifold cut off valve |
| D. | Inlet valve |
| E. | Inlet - low vacuum manifold cutoff valve |
| F. | Leak valve |
| G. | Vac ion cut off valve |
| H. | Vac ion pump |
| I | Ionization gauge |
| J. | Discharge gauge |
| K. | Gold wire gasket seal |
| L. | Laser window assembly |
| M. | Magnet pole faces |
| N. | Ion cell |
| O. | Tapered joints |

ionization gauge joints. In addition, valves B and G contain polyimide O-rings and valve C a Viton A seal. Two-inch oil diffusion pumps (A) (CVC Model PM-120) (55) with appropriate backing pumps maintain the vacuum of the two independent vacuum manifolds. The ultimate pressure attained in the high vacuum manifold is (1-3) x $10^{-8}$ Torr as measured at the Bayard-Alpert ionization gauge (I). Pressure of the inlet manifold is determined with a cold cathode discharge gauge (J). Typical inlet manifold pressures are (0.1-1.0) x $10^{-5}$ Torr. The sample is leaked from the inlet manifold to the main vacuum can through sapphire seal leak valves (F) (56). The titanium sublimation pump (H) (55) maintains the vacuum in the high vacuum manifold during periods of inactivity.

The location of the trapped ion cell (N) and the V-3400 low impedance electromagnet (57) pole faces (M) are shown for clarity. An antireflectivity-coated optical glass window (L) was mounted on the end of the main vacuum can by modifying a standard flange.

## Optical Apparatus

A standard Candela dye laser system comprised of an ED-100U head assembly, CL-100 flashlamp, a dye cavity with antireflectivity-coated optical windows, and a variable high voltage (25 kV maximum) power supply was employed in the photo-experiments (58). The ED-100U head produces a high energy discharge through the Xe flashlamp of the CL-100 flashlamp assembly upon sparkgap triggering. The pressurized (5-7 PSI dry $N_2$) sparkgap can be triggered manually or electronically.

Circuitry was constructed to transform a 1 ms TTL level pulse into the 150 volt, 1.5 μs sparkgap firing pulse to permit synchronous control by a TTL pulse sequence (59).

The dye reservoir volume and circulation speed are sufficient to insure that the dye cavity is flushed with fresh dye for each laser shot. A Micropump Model 10-85-316-865 pump circulates the dye solutions (60). Dye lines of polypropylene tubing are employed to minimize dye degradation due to leaching of impurities from the lines (61). A Pall liquid filtration system was added to the dye circulation system to remove particles which scatter light and reduce the efficiency of the dye laser (62).

Dye solutions were made up to a total volume of two liters in 100% ethanol obtained from chemical stores. The procedure for mixing the dye solutionswas to start with an initially highly concentrated solution and dilute the solution with ethanol until the output was maximized. This resulted in dye solution concentrations on the order of $10^{-4}$ to $10^{-5}$ molar. Laser dyes which were used in the photo-experiments,as well as dyes which were tested but did not lase with sufficient intensity or lased only over a very restricted wavelength range, are listed in Table 1. Nomenclature for the dyes is that of Exciton, the primary supplier of dyes used in this study (63). The position of the dye laser cavity relative to the main vacuum can and subsidiary optical components is illustrated in Figure 8.

Wavelength selection was achieved by incorporating a blazed relection grating in autocollimation as one end of the optical

Table 1. Laser Dyes and Observed Lasing Wavelength Regions

| Dye | Observed Useful Wavelength Range (nm) |
|---|---|
| LD 423 | No activity |
| LD 440 | No activity |
| LD 450 | No activity |
| LD 460 | 445-465 |
| LD 473 | Extremely weak |
| LD 480 | 470-485 |
| LD 490 | 470-510 |
| Coumarin 540 | 510-550 |
| Fluorol 555 | No activity |
| Rhodamine 6G | 575-605 |

Figure 8. Dye Laser Apparatus and Orientation. The primary components of the dye laser system are: the optical cavity (OC); Xe flashlamp (FL); antireflectivity coated windows (ARW); high voltage discharge power supply and capacitor (HV). Wavelength selection is accomplished with a diffraction grating (G), mounted on a base (B) which is rotated by a motor-driven (GDM) lever arm (LA). Wavelength determination is accomplished with a beam splitter (BS) and monochromator (GM). A window (W) permits the laser cavity extension to the end mirror (M) in the cell(C).

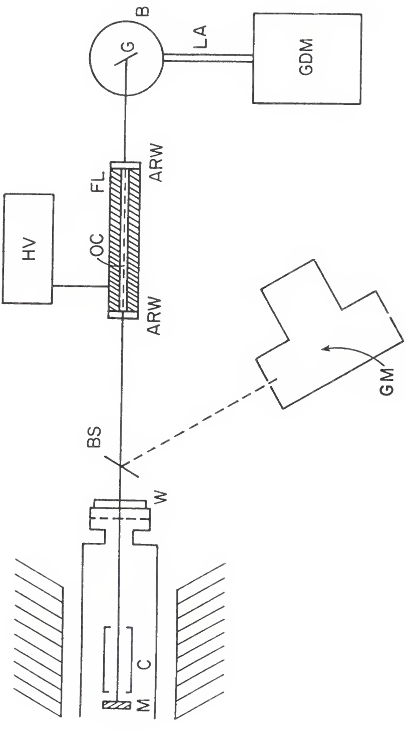
M
C
W
BS
GM
ARW
OC
HV
FL
ARW
G
B
LA
GDM

resonator. All gratings used were blazed at 500 nm. Either a 1200 line/mm PTR (64) or Bausch and Lomb grating (65) was employed for these studies. The general characteristics of these gratings are presented in Table 2. In a few studies a 600 line/mm grating obtained from Edmund Scientific (66) was also used. The grating selected was mounted on a Burleigh SG-101 Star Gimbal Mount and SG-305 Mount Base (67). This assembly was fixed to a rotating base driven by a motor-turned lead screw/lever arm assembly.

At the ion cell, the laser cavity optical element was a copper mirror attached physically to and contacting electrically the end plate of the trapped ion cell. Visual inspection of this mirror indicated that it was of low quality and the surface was in poor condition. Replacement of the copper mirror with a reconditioned 90% reflecting Al mirror did not markedly improve the laser output.

Wavelength selection is determined solely by the dispersive cavity element, the diffraction grating. Since the grating drive was uncalibrated, a beamsplitter on the optical axis split a fraction of the incident light to a monochromator for spectral analysis. An American Instrument Company Model 1-8401 monochromator (68) and and Instruments SA J-Y H20 0.5 meter monochromator (69) were used. Both were periodically calibrated versus Hg lines and the 632.8 nm line of a HeNe laser.

Following wavelength determination at a particular grating angle, a GenTec ED 200 Joulemeter (70) was positioned to intercept the fraction of the beam split to the monochromator. The joulemeter

Table 2. Grating Characteristics as a Function of Wavelength for a 1200 line/mm Grating in Autocollimation

| λ(nm) | Littrow Angle, β(deg) | Angular Dispersion (μrad/nm) | Inverse Linear Dispersion* nm/mm |
|---|---|---|---|
| 300 | 10.4 | 1224 | 0.41 |
| 400 | 13.9 | 1237 | 0.40 |
| 500 | 17.5 | 1264 | 0.40 |
| 600 | 21.1 | 1286 | 0.39 |
| 700 | 24.8 | 1320 | 0.39 |

*Linear dispersion is calculated based upon an intracavity single-pass pathlength of two meters.

output and was read from an oscilloscope or transferred through properly buffered inputs (1 MΩ) to a data collection system.

The simplicity of the optical arrangement did not lead to fast and simple alignment, since one element of the laser cavity was contained inside the vacuum can and was not stationary with respect to the remaining laser cavity components. Alignment was aided by use of a Spectra Physics 155 HeNe Laser (71) which could be directed first to align the vacuum can laser cavity element relative to the oscillator cavity and then redirected to align the grating with respect to the oscillator cavity.

The dye laser head and high voltage power supply were contained in separate rf shield cages. This shielding eliminated rf interference with the marginal oscillator detector circuitry.

## Pulsed Electronics

A pulsed ion cyclotron resonance experiment requires a sequence of control pulses of variable delay and, in some instances, variable width to govern the timing of ion formation, ion detection, ion removal from the cell and when desired, ion irradiation. A digital synchronously-timed control system has been constructed for the generation of the requisite pulses (53) (Figure 9).

A typical pulse sequence is initiated by two internal pulses that are required to reset and clamp the counters and flip-flops (precondition pulse) and serve as the zero time reference (start pulse) for the working pulses: "grid", "detect", "sample", "integrator reset", "quench", "$\omega_2$", and "free" pulses. The grid,

Figure 9. A Typical Pulsed ICR Experiment Pulse Sequence. Breaks in the line indicate variability. The pulses are: precondition, PC; start, S; grid, G; $\omega_2$; free, F; detect, D; quench, Q. Not shown are the integrate, sample and integrate reset pulses. The integrate pulse coincides with D and the sample pulse is a 2ms pulse triggered at the falling edge of D. The integrate reset pulse is generated prior to detection.

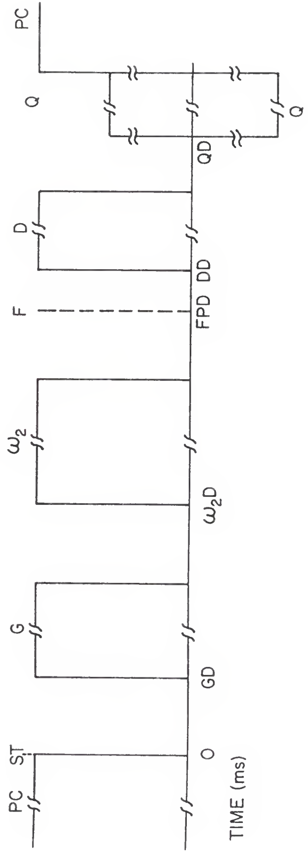
PC
ST
G
$\omega_2$
F
D
Q
PC
TIME (ms)
O
GD
$\omega_2$D
FPD
DD
QD
Q

detect, quench, and $\omega_2$ pulses are of variable delay and variable width and consequently each pulse has two assigned timing circuits. The emaining pulses, sample, integrator reset, and free are of variable delay but constant width and each requires only a single timing circuit. Delay timers for all pulses are referenced to the 25 μs start pulse. Pulse width timers begin counting at the end of their corresponding pulse delay. The delay timers may be collectively operated at one of three available clock frequencies. Clock frequencies of 10 kHz, 1 kHz, and 100 Hz may be selected to yield minimum pulse delays of 0.1 ms, 1 ms, and 10 ms, respectively. The pulse width timers are operated from a set clock frequency of 10 kHz and produce a minimum width pulse of 0.1 ms. Each pulse delay and width is selected by three-decade thumbwheel switches.

The grid pulse is the first working pulse generated following the start pulse. The grid pulse is amplified so that low is 0 volts and high is +10 volts. This pulse is mixed with a variable dc level and applied to the grid separating the rhenium filament from the electron beam entrance slit in the side plate of the trapped ion cell. The variable dc grid potential is set to be 5 volts more negative than the variable dc filament potential and the electrons, emitted at the filament, do not pass through the grid into the cell. During the grid pulse the potential of the grid is 5 volts more positive than the filament potential and electrons are accelerated into the cell.

The detect pulse serves several functions. First, it controls the marginal oscillator rf output to the lower plate of the cell through the gated amplifier in the limiter feedback circuit of the marginal oscillator as described by McIver (46). Second, in combination with a variable length, inverted pulse from a one-shot which itself is triggered by the rising edge of the detect pulse, the detect pulse produces an integrate pulse during which the integrator is active. The logical "AND"ing of the detect pulse and inverted one-shot pulse eliminates the initial spike observed in the marginal oscillator output due to mismatching in the marginal oscillator compensation circuitry (53). The falling edge of the detect pulse triggers a one-shot which produces a 2 ms sample pulse to activate the sample/hold circuit. Ion detection is a concerted action of the marginal oscillator, integrator, and sample/hold circuits. The detect pulse gates on the marginal oscillator and integrator and the ions are irradiated, the power absorption is determined and is converted to a voltage level at the integrator output. At the end of the detect (and integrate) pulse the 2 ms sample pulse is generated and the sample/hold circuit samples its input which is the output of the integrator. Finally, an independently generated integrator reset pulse resets the integrator prior to the next pulse sequence.

To insure that only ions produced during a single grid pulse are present during a detect, a quench pulse is applied to the upper plate to eject all ions from the cell prior to repetition of the pulse sequence. A pulse of either polarity will perturb the trapping field and remove the ions from the cell.

The $\omega_2$ pulse is used as a gate for an external gateable rf oscillator whose output is then applied to the upper cell plate for excitation of ions which are nonresonant at the selected magnetic field and marginal oscillator frequency. This excitation serves two purposes. At low voltage levels $\omega_2$ excitation increases the ion translational energy while trapping remains efficient. At high voltage levels $\omega_2$ excitation ejects the $\omega_2$ resonant ion from the cell (72).

The free pulse is a one millisecond width, variable delay pulse designed as a general, external trigger pulse. The free pulse operates on TTL logic levels. It has been used as the synchronous trigger for the flashlamp-pumped dye laser sparkgap discharge circuitry.

Initiation of a complete pulse sequence can be accomplished in three different modes: single cycle, fixed rate, or automatic operation. The single cycle mode results in one complete pulse sequence occurring whenever a front panel pushbutton is depressed. Fixed rate mode causes the complete pulse sequence to be repeated at a selected time interval which ranges from 20 milliseconds to 5 seconds in a 1-2-5 sequence. The automatic mode starts a pulse sequence 175 milliseconds after the quench pulse terminating the preceeding sequence.

A typical pulsed ion cyclotron resonance (PICR) experiment proceeds in the following manner. With no resonant ions, the previously set digital pulse sequence is performed to obtain a zero level for the marginal oscillator signal. Ions are then tuned into resonance by an appropriate adjustment of the magnetic field. Marginal oscillator and photodetector levels are recorded. The laser capacitor is charged and the trigger pulse, normally the free pulse or a microcomputer-generated pulse, is activated to fire the laser immediately prior to ion detection. The digital pulse sequence is repeated for the required number of laser shots. Marginal oscillator and photodetector data are recorded for each laser shot. The laser trigger is deactivated and with the ions still resonant the pulse sequence repeats until sufficient marginal oscillator level and photodetector level measurements have been obtained. Finally, the ions are tuned off resonance and the marginal oscillator zero level data is recorded for several pulse sequences. This scheme allows for the correction of zero baseline and resonant ion baseline drifts.

## Microcomputer

The resonant absorption of the output of the marginal oscillator is detected as a change in the analog voltage level of the marginal oscillator frequency envelope. To convert this analog signal to a digital signal suitable for analysis by a digital microcomputer a data conversion/collection system has been developed. The system is comprised of a microcomputer and an analog to digital (A/D) converter as well as input signal conditioning elements and programmable data routing components. The microcomputer architecture is addressed to the degree to which it has influenced the interface design and operation. The description of the interface is functional and non-specific with regard to chip designation. The operating system software is summarized by functional unit as it would be encountered in the course of normal operation. Analysis of the current status of the data conversion/collection system delineates its limitations and suggests refinements to attain 'key-on' operation. Experimental data was analyzed manually to verify the system performance.

## Microcomputer and Modifications

A KIM-1 microcomputer served as the control element for the data conversion/collection system (73). The KIM-1, a single-board, 6502-processor-based microcomputer, has integrated input/output hardware, hex keypad, system ROM (read-only memory) and 1K (1024 words) of RAM (random-access memory). The structure of the input/output hardware as to the available control and data lines requires further mention.

The KIM-1 can respond to an external event in a programmed fashion. This implies that the microcomputer acknowledge and correctly identify an external event. Recognition of an external event requires a combination of hardware and software. The level of the interrupt request line (IRQ) is altered synchronously with the external event and interrupts the processor upon completion of a logical machine step. Critical status registers are preserved by the IRQ software residing in ROM. Control is transferred to a program located through the interrupt request vectors (IV) which have been preprogrammed by user code to select the correct response to the external event. Once the external event has been correctly handled the critical registers are restored and operation is resumed from the point of interrupt.

An interrupt request is an externally generated request for service. The servicing of the interrupt involves data transfer to the microcomputer from the external device or vice versa. This transfer takes place across 15 input/output lines, divided into two ports, peripheral A data, PAD and peripheral B data, PBD. The 6502 architecture and operating system treat these ports as memory locations which can be written to or read. The direction of the data transfer is established by the status of the control ports, peripheral A data direction register, PADD, and peripheral B data direction register, PBDD. These registers are interpreted as collections of status bits which correspond directly to the PAD or PBD bits. A status bit value of 0 indicates that the corresponding peripheral device bit is to be read as an input, while a status bit set to 1 indicates that the bit is written to by the microprocessor. All combinations of inputs and outputs are permissible and buffering in both directions has been implemented on board.

A general appreciation of the input/output structure of the microcomputer is necessary for interfacing, in this case it is also necessary to be aware of the memory (RAM) architecture, due to the on-board modifications dictated by the limited memory available on the standard system. The 1024, 8-bit RAM words of the 6502 processor are constructed from eight 1-bit x 1024-location, memory chips. The address lines of all eight chips are tied together so that the same address is selected at each chip. The 1K of memory supplied by the KIM-1 is insufficient for complex control and data manipulation routines in addition to data storage. Consequently unused address lines were decoded and memory chips sufficient to increase the RAM to 2K were added. The details of this modification are in Appendix I.

## Microcomputer Interface Hardware

The limitations of the KIM-1 microcomputer's input/output architecture place constraints on interface design. The KIM-1 is restricted to digital input/output with a maximum of 8 bits transferred per input/output operation. Consequently, external analog signals to be transferred to the microcomputer memory must be converted to digital format. The KIM-1 is a TTL level microcomputer which requires that valid TTL levels be provided as inputs. These constraints are easily attended to; thus the interface design, although dependent on the KIM-1 input/output architecture and implementation, is more stringently defined by the nature of the external signals.

For a typical pulsed ion cyclotron resonance (PICR) experiment the values to be measured are zero baseline, the marginal oscillator output in the absence of resonant ions; ion baseline, the marginal oscillator output in the presence of resonant ions; laser level, the marginal oscillator output after laser irradiation of the resonant ions; laser energy values, the output of the photodetector with and without laser irradiation. Each of these signals is an analog voltage level and two separate channels to the A/D converter are required for the marginal oscillator and photodetector outputs. Since the A/D has a single analog input these signals are multiplexed to that input under software control. The sequence of control functions resulting in the input of converted marginal oscillator and photodetector levels may be summarized for a general, two-channel read.

The KIM-1 will be in a no operation (NOP) loop which can only be exited via an interrupt request or a keypad interrupt. An IRQ transfers control to programs addressed by the interrupt vectors, which contain either system start-up or program-defined values. Whatever the actual program location accessed, the scheme of the interrupt service requires a resetting of the interrupt vectors in preparation for an ensuing interrupt and the updating of running counters which identify the type and count of marginal oscillator and photodetector data on line. The transfer of the marginal oscillator or photodetector voltage via the A/D to the KIM is controlled through the microcomputer PAD (PA0-PA7) via four 3-bit, 8-bidirectional-channel multiplexers (MUX). PA0-PA3 are always configured as KIM-1 outputs. PA0 controls MUX inhibit lines and PA1-PA3 constitute a 3-bit, binary word which selects the MUX channels. The input to a MUX is transferred to the output on an inhibit low with the transfer direction determined by the PADD status bits. PA6 serves as the channel select line for the 1-bit, 2-channel (A/D input) MUX. A clocked latch intervenes to preserve the status of the select lines of the 2-channel MUX until it is reselected. PB0 is used as the software generated clock line for the clocked logic. (PB0 replaced PA4 which was defective on the KIM-1 used). A logical one on the 2-channel MUX select line transfers the photodetector level to the A/D input, a logical zero selects the MO level.

The free running A/D requires 25 milliseconds to convert the input to a stable digital output. A timed loop using the KIM-1 programmable counter allows for the conversion time. The 12-bit A/D output is read into the KIM-1 in three 4-bit parts through the four 8-bidirectional-channel MUX's. The data direction registers configure PB0 and PA5-PA7 as KIM-1 inputs. PA1-PA3 select the A/D channels. Channel one selects the least significant four bits of the conversion, channel two the next four significant bits, and channel three the four most significant bits. The conversion result is recombined and stored by the A/D read software.

The interface provides a pulse to the laser trigger electronics for program-defined counter states. In a preliminary version of the software a latch was set (1) during the read sequence prior to that for which the laser was to be fired. The latch output was AND'ed with the free pulse of the ensuing pulse sequence to provide the laser trigger pulse. The latch input was then reset (0) to prevent laser triggering by successive pulse sequences. This technique is cumbersome and a simplified scheme has been implemented in which the trigger pulse is generated by software immediately after the interrupt pulse is received. This scheme results in nontrivial simplification of the software.

The IRQ is provided by the free pulse for automatic triggering and by an debounced pushbutton for manual triggering. Both inputs are conditioned by a pair of Schmitt triggers, which feed into a one-shot pulse generator to produce a sharp, clean IRQ pulse at the microprocessor.

The output of the laser photodetector is buffered and amplified (x50) and the level held by a peak detector. The $\omega_2$ pulse is used as the peak detector reset and, consequently, must occur after the photodetector read is completed. For certainty, the $\omega_2$ pulse was positioned to occur immediately prior to the quench pulse.

## Microcomputer Software

Programs are coded in 6502 machine language. The architecture of the 6502 processor minimizes the volume of code, since operations are frequently performed on a single specialized memory location, the accumulator. Addressing codes are varied and specialized to transfer rapidly and efficiently selected data to and from the accumulator.

The software is designed to reduce the need for operator attention during a complete measurement sequence. The microcomputer is no longer merely a data router/interface controller. Data analysis codes are included to perform simple data reduction. The zero baseline average code averages the results of thirty-two (hex 20) zero baseline measurements. The ion baseline average code derives the average of eight ion baseline values symmetric about a laser shot sequence. Zero baseline correction of the ion baseline and laser level is coded. Similar functions, zero baseline measurement and correction of signal levels, are coded for the photodetector output. Full double precision (16-bit ÷ 16-bit) division is implemented. Vectored storage of intermediate results (raw data) to temporary storage areas and the relocation of reduced data prior to overlay of the temporary storage areas are provided to conserve memory. With the addition of simple data reduction codes the storage capacity required for a single complete sequence (thirty-two zero MO measurements, sixty-eight ion MO and photodetector measurements and sixteen laser MO and photodetector measurements) is reduced from four hundred bytes to sixty-four bytes.

Flowcharts outline the data conversion/collection and analysis software (Figures 10-14). A memory map showing the allocation of the expanded RAM is provided (Figure 15).

## Run Time Operation

Due to memory limitations some critical registers are not set by the initialization routine, these registers require keypad initialization. The status register (hex address 00F1) must be set to 00 to clear the interrupt request flag. No maskable interrupt (IRQ) can be acknowledged until the flag is cleared. Certain system interrupts are non-maskable and always acknowledged. The interrupt vector low (IVL, hex address 17FE) and interrupt vector high (IVH, hex address 17FF) are manually set to D0 and 08 respectively. The KIM-1 is thus configured to acknowledge an IRQ and to respond by calling the main control program (Figure 11). The status and interrupt vector registers must be reset for each complete measurement sequence. Three memory locations (hex addresses 0F, 10, and 11) contain the running sum of zero baseline values. These registers must also be zeroed at the start of a complete measurement sequence. The remaining registers require initialization prior to the first complete measurement sequence, but their status is then correctly maintained by the program for subsequent sequences. Zero page hex addresses 0C, 12, 14, 15, 16, 17, 40, 41 and 43 should be zeroed. Zero page hex

Figure 10. Operator/Microcomputer Interaction Flowchart. This flowchart describes the required operator attention. Programs are loaded from cassette tape and operation initializations are performed. Initial interrupt vector values are set and the microcomputer enters an NOP loop until interrupted. An end-of-experiment test determines the experiment status and then analyzes and stores the data in final form.

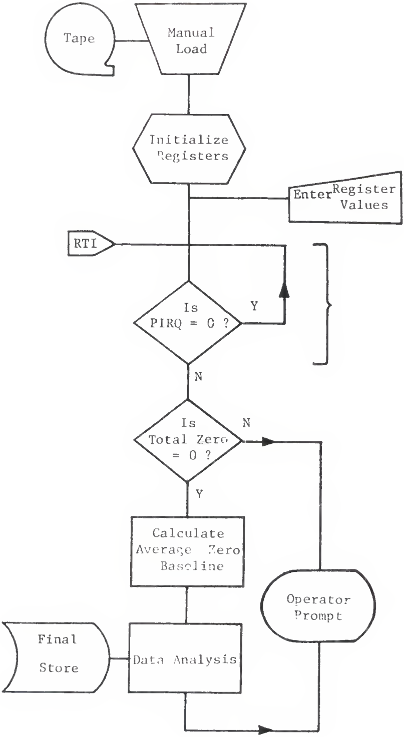
Tape
Manual Load
Initialize Registers
Enter Register Values
RTI
Is PIRQ = 0 ?
Y
N
Is Total Zero = 0 ?
N
Y
Calculate Average Zero Baseline
Operator Prompt
Final Store
Data Analysis

Figure 11. Main Program Branch Flowchart. The program flow about the primary decision is shown. Primary decision is the nature of the data to be obtained at the next interrupt. A test value of 0 corresponds to baseline data for the marginal oscillator (B). Test value 1 corresponds to ion baseline data for the marginal oscillator and the photodetector (C). Test value 2 corresponds to laser MO and photodetector data.

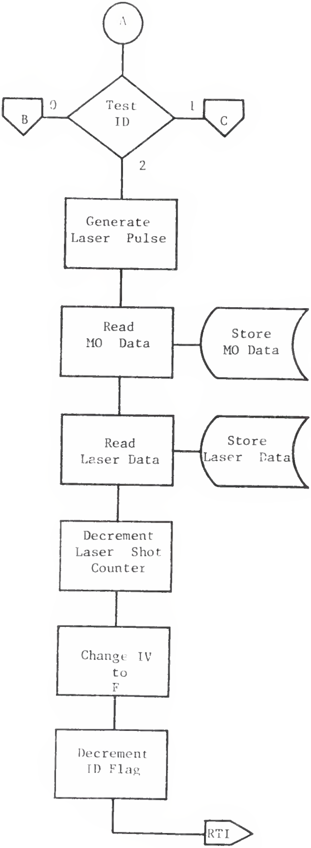
A
Test ID
0
B
1
C
2
Generate Laser Pulse
Read MO Data
Store MO Data
Read Laser Data
Store Laser Data
Decrement Laser Shot Counter
Change IV to F
Decrement ID Flag
RTI

Figure 12. Baseline MO Data Flowchart. The functions required for baseline data collection are indicated. A single decision is made to determine when ions should be tuned into resonance which when true prompts the operator.

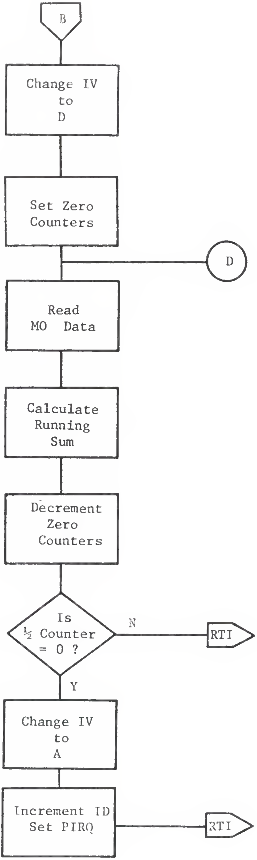
B
Change IV to D
Set Zero Counters
D
Read MO Data
Calculate Running Sum
Decrement Zero Counters
Is ½ Counter = 0 ?
N
RTI
Y
Change IV to A
Increment ID Set PIRQ
RTI

Figure 13. Resonant Baseline Data Flowchart. The procedure for taking baseline MO values with resonant ions while simultaneously taking zero photodetector values is diagrammed. Data overlap occurs for each four sets of measurements after the first eight baseline measurements are stored.

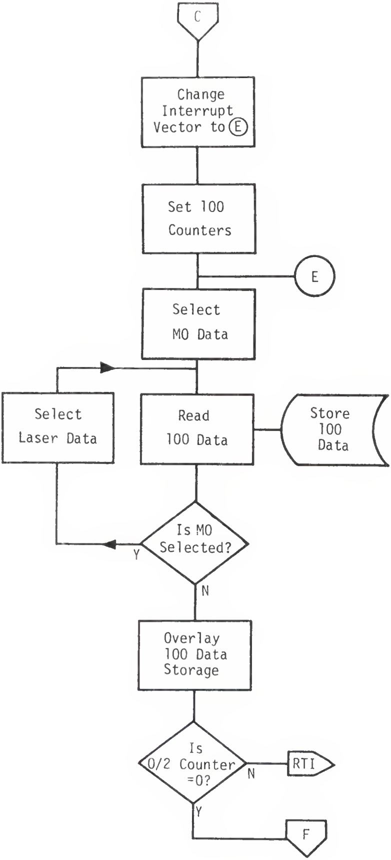
C
Change Interrupt Vector to E
Set 100 Counters
E
Select MO Data
Select Laser Data
Read 100 Data
Store 100 Data
Is MO Selected?
Y
N
Overlay 100 Data Storage
Is 0/2 Counter =0?
N
RTI
Y
F

Figure 14. Laser Status Flowchart. Determination of a laser firing is necessary for subsequent data reduction and memory overlap decision. In addition, the last laser shot of a sequence must be identified to reduce the data to final form.

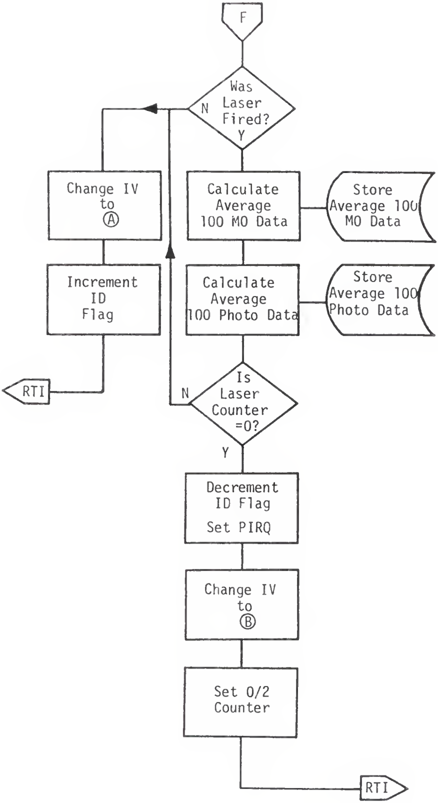
F
Was Laser Fired?
N
Y
Change IV to Ⓐ
Increment ID Flag
RTI
Calculate Average 100 MO Data
Store Average 100 MO Data
Calculate Average 100 Photo Data
Store Average 100 Photo Data
Is Laser Counter =0?
N
Y
Decrement ID Flag
Set PIRQ
Change IV to Ⓑ
Set 0/2 Counter
RTI

Figure 15. Microcomputer RAM Memory Map. The major divisions indicate blocks of four pages, natural machine divisions of memory. The beginning and ending hex address for each logical software unit is provided. Note that the A/D subroutine is dispersed throughout the available memory.

| | |
|---|---|
| 0800 - 0851 | Initialization Subroutine |
| 0852 - 0868 | Obtain Data and A/D Delay Subroutine |
| 0869 - 088D | MUX Select Photodetector Subroutine |
| 088E - 08B4 | MUX Select MO Subroutine |
| 08B7 - 08CE | A/D Read Subroutine (Part II) |
| 08D0 - 09F0 | Main Control Program |
| 0A00 - 0A45 | A/D Read Subroutine (Part I) |
| 0A50 - 0A91 | Four Channel Storage Subroutine |
| 0A9A - 0AFC | Data Analysis and Storage Subroutine |
| 0B00 - 0B80 | Double Precision Divide Subroutine |
| 0B81 - 0B8F | A/D Read Subroutine (Part IV) |
| 0B90 - 0BB0 | Triple Precision Average Subroutine |
| 0BB1 - 0BE3 | Laser Trigger Subroutine |
| 0BE7 - 0BFF | A/D Read Subroutine (Part III) |

address 42 should be set to 02 and following the fourth complete sequence set to 03. The initialization routine resides at hex address 0800. To run the initialization routine, 0800 is keyed to the address display and GO is keyed. The remaining critical registers are set and the microcomputer enters the nc operation (NOP) loop until interrupted by an IRQ or keypad interrupt (Figure 10). The function of each register is given in Appendix II.

The first IRQ enters the main control program at A (Figure 11). The initial value of the ID register (hex address 0000) is 0, consequently the B branch (Figures 11 and 12) is taken. The interrupt vectors are altered to point to D to protect the zero baseline counters which are subsequently set. The zero MO level is read and the result summed into the initially zeroed registers 0F, 10 and 11. The zero baseline counters are decremented. If less than one half of the zero baseline readings have been taken there is a simple return from interrupt (RTI), returning the KIM-1 to the NOP loop. Subsequent interrupts enter the main control program at D until one half of the zero baseline measurements have been accumulated. Then, interrupt vectors are changed to point to A, the ID register is incremented and a programmable interrupt request (PIRQ) flag set, prior to an RTI. As before the RTI returns the system to the wait loop, however, since PIRQ is the test value of the loop, the system will "fall through" the loop. The test of the total zero baseline counter will be negative at this point. A branch to the read-only memory (ROM) operating system is taken which displays "0001 xx". This is the operator prompt to tune the ions into resonance and charge the laser capacitor "084E" is entered in the address field of the display and GO is depressed to clear the interrupt flag and to return the KIM to the wait loop.

The next IRQ enters the main control program at A. The ID register contains 01 and branch C is selected. The interrupt vectors are changed to point to E to protect the ion baseline counters. The 100 level counters are set and MO level is read exactly as before. The two byte result is stored via the y-indexed address mode. The appropriate value for the y-register is loaded from 0C. The base address is located in 0D. The PHOTO level is read and stored as for the MO level, however, the base address is first incremented by hex 10 so that the two types of data are mapped into different memory locations. The base address is restored to its original value after the PHOTO read/store in preparation for the next cycle. The program requests eight two-byte MO levels and eight two-byte PHOTO levels per laser shot for the determination of the respective averages. Once the averages have been evaluated and stored, the first four levels of each type may be over written. "AND"ing the y-register value with hex 0F prior to saving its value in 0C accomplishes the overlay. If the (100/2) level counter is nonzero a simple return from interrupt is taken. If the counter is zero, the software determines if the laser has been fired. If not, the interrupt vectors are altered to point to A and the ID register incremented (02) so that the next interrupt fires the laser. Figure 11 illustrates the laser firing sequence and is straightforward. MO and PHOTO levels are read as before and stored. The laser counter is decremented and ID register decremented (01). Interrupt vectors are set to E so that the (100/2) level counter is reset and a new sequence of 100 levels taken. If the laser has fired, average 100 MO and 100 PHOTO levels are calculated and stored. If the laser counter is nonzero, the interrupt vectors and ID register are set to fire the laser on the ensuing interrupt. For a zero laser counter, the interrupt vectors and (0/2) level counter are reset to read the required zero baseline levels commencing with the next interrupt. The ID register is set to zero and PIRQ set (01) to initiate an operator prompt. The display "0000 xx" requests the operator to tune the ions off resonance. When the (0/2) counter tests zero, an RTI occurs and since PIRQ is set a test of the total zero (0) counter is made. The total zero counter will be zero and the zero baseline average is determined.

Data analysis consists of the evaluation of

$$F^{-1} = \frac{MOL_{NL} - MOL_{BASE}}{MOL_{L} - MOL_{BASE}} \qquad (31)$$

and

$$LSRL = PDL_{L} - PDL_{NL} \qquad (32)$$

where MOL represents a marginal oscillator level, PDL a photodetector level, L refers to a laser shot sequence with ions, NL refers to an ion resonance sequence with no laser shot and BASE refers to no resonant ions or laser shot. Thus $F^{-1}$ is the inverse of the fractional remainder of the ion signal upon irradiation by a laser pulse with a power level related to LSRL, the measured laser level. These four bytes of data are stored for each laser shot and a prompt is generated to signal that the data collection system is prepared for a new sequence.

Implementation of the division in Equation 31 requires a 16 bit by 16-bit divide routine and a 12-bit shift routine to format properly the data for storage. These routines have been coded and incorporated into the analysis loop.

Programs are listed in Appendix III. Memory addresses, machine codes and mnemonic codes are included to facilitate use, alteration, adaptation and relocation of the various subroutines. Comments have been included to simplify the reading of the code.

## Derivation of the Expression for the Photodetachment Cross-Section

The probability of photodetaching a negative ion of photodetachment cross-section $\sigma(\lambda)$ at wavelength $\lambda$ of the incident radiation field of photon flux $\rho(\lambda)$ in time t is given by the expression

$$P(\lambda) = 1 - \exp\left[-kt \int \rho(\lambda)\,\sigma(\lambda)\,d\lambda\right] \tag{33}$$

where k is a constant related to the interaction region (74). For a pulsed radiation source with pulse duration t and energy per pulse, $E_\lambda$, the number of photons per pulse is

$$n_\lambda = \lambda E_\lambda / hc. \tag{34}$$

This quantity is directly related to the photon flux provided a, the radiation beam cross-sectional area, is known

$$\rho(\lambda) = \lambda E_\lambda / hcat. \tag{35}$$

If $N_o$ represents the number of anions detected prior to irradiation and N the number of anions detected following irradiation, then N and $N_o$ are related by

$$N_o - N = f\, N_o\, P(\lambda) \tag{36}$$

where f represents the probability that every detected anion is in the radiation field. Substituting for $P(\lambda)$ and rearranging and taking the logarithm of each side yields

$$kt \int \rho(\lambda)\, \sigma(\lambda)\, d\lambda = \ln \left[ 1 - \frac{N_o - N}{fNo} \right]^{-1} . \tag{37}$$

If the bandwidth of the source is narrow and constant with respect to the wavelength, then

$$kt \int \rho(\lambda)\, \sigma(\lambda)\, d\lambda \simeq Ckt\, \rho(\lambda)\, \sigma(\lambda) \tag{38}$$

where C represents the effect of the constant bandwidth, and $\rho(\lambda)$ and $\sigma(\lambda)$ are assumed to be slowly varying with respect to wavelength. Using the simplification and substituting for $\rho(\lambda)$, an expression for the photodetachment cross-section containing only experimentally observable quantities is obtained

$$k'\, \sigma(\lambda) = \frac{\ln \left[ 1 - \frac{N_o - N}{fNo} \right]^{-1}}{\lambda\, E_\lambda} \tag{39}$$

where $k' = Ck/hca$. Rearranging the argument of the logarithm term, the cross-section expression becomes

$$k' \sigma(\lambda) = \frac{\ln \left[ \frac{fNo}{fN_o - (N_o - N)} \right]}{\lambda\, E_\lambda} . \tag{40}$$

Clearly this expression exhibits the correct limiting dependence on f, for as f approaches one, indicating that all ions are within the radiation field, the argument of the logarithm becomes $N_0/N$. Finally, $k'\sigma(\lambda)$ can be written as

$$k'\,\sigma(\lambda) = \frac{\ln\left[\dfrac{f}{f-\Delta}\right]}{\lambda\, E_\lambda} \tag{41}$$

where $\Delta$ is the fractional decrease in the ion signal upon irradiation, $(N_0 - N)/N_0$.

A standard error analysis yields the expression for the relative error for $k'\sigma(\lambda)$,

$$\frac{W^2[k'\sigma(\lambda)]}{[k'\sigma(\lambda)]^2} = \left(\frac{N/N_0}{f-\Delta}\right)^2 \frac{W^2(N_0)/N_0^{\,2}}{\left[\ln\,(f/f-\Delta)\right]^2} + \left(\frac{N/N_0}{f-\Delta}\right)^2 \frac{W^2(N)/N^2}{\left[\ln(f/f-\Delta)\right]^2}$$
$$+ \left(\frac{\Delta}{f-\Delta}\right)^2 \frac{W^2(f)/f^2}{\left[\ln\,(f/f-\Delta)\right]^2} + \frac{W^2(\lambda)}{\lambda^2} + \frac{W^2(E_\lambda)}{E_\lambda^{\,2}} \tag{42}$$

where $W(x)$ represents the random error of variable x. The influence of each of the factors involved in the error terms is indicated in Table 3 for a range of $\Delta$ values. The magnitudes of the coefficients of the relative errors in Table 3 do not completely characterize the errors. The relative errors themselves must also be considered. $N_0$, $W(N_0)/N_0$, $W(f)/f$ and $W(E_\lambda)/E_\lambda$ are constant for a constant amplitude ion signal with a constant S/N ratio. The relative error associated with N, $W(N)/N$ increases with decreasing N, that is, for a constant S/N ratio increased ion attenuation leads to increased relative error in the determination of the residual ion concentration. ABC represents the coefficient squared for the relative error of $N_0$. For an ion

Table 3. Factors in the Relative Errors in the Cross-Section for a Range of Δ Values and f Equal to 1.0 and 0.75

| Δ | A | B | | C | | D | | E | ABC | | BD | |
|---|---|---|---|---|---|---|---|---|---|---|---|---|
| | $(N/N_o)^2$ | $\{\ln[f/(f-\Delta)]\}^{-2}$ | | $(f-\Delta)^{-2}$ | | $[\Delta/(f-\Delta)]^2$ | | $W^2(N)/N^2$ | | | | |
| | | 1.0 | 0.75 | 1.0 | 0.75 | 1.0 | 0.75 | | 1.0 | 0.75 | 1.0 | 0.75 |
| .99 | $1\times10^{-4}$ | 0.05 | -- | $10^4$ | -- | 9801 | -- | 1 | 0.05 | -- | 490 | -- |
| .9 | $1\times10^{-2}$ | 0.19 | -- | 100 | -- | 81.0 | -- | $1\times10^{-2}$ | 0.19 | -- | 15.4 | -- |
| .8 | $4\times10^{-2}$ | 0.39 | -- | 25 | -- | 16.0 | -- | $2.5\times10^{-3}$ | 0.39 | -- | 6.24 | -- |
| .7 | $9\times10^{-2}$ | 0.69 | 0.14 | 11.1 | 400 | 5.44 | 196 | $1.11\times10^{-3}$ | 0.69 | 3.24 | 3.75 | 27.4 |
| .6 | 0.16 | 1.19 | 0.39 | 6.25 | 44.4 | 2.25 | 16.0 | $6.25\times10^{-4}$ | 1.19 | 2.77 | 2.68 | 6.24 |
| .5 | 0.25 | 2.08 | 0.83 | 4.00 | 16.0 | 1.00 | 4.00 | $4\times10^{-4}$ | 2.08 | 3.33 | 2.08 | 3.32 |
| .4 | 0.36 | 3.83 | 1.72 | 2.78 | 8.16 | 0.44 | 1.31 | $2.78\times10^{-4}$ | 3.83 | 5.04 | 1.69 | 2.25 |
| .3 | 0.49 | 7.86 | 3.83 | 2.04 | 4.94 | 0.18 | 0.44 | $2.04\times10^{-4}$ | 7.86 | 9.26 | 1.41 | 1.69 |
| .2 | 0.64 | 20.08 | 10.4 | 1.56 | 3.31 | 0.06 | 0.13 | $1.56\times10^{-4}$ | 20.08 | 22.02 | 1.20 | 1.35 |
| .1 | 0.81 | 90.01 | 48.8 | 1.23 | 2.37 | 0.01 | 0.02 | $1.23\times10^{-4}$ | 90.01 | 93.15 | 0.90 | 0.98 |

signal-to-noise ratio of 100, the squared relative error is $10^{-4}$. Therefore, the error contribution due to the $N_0$ measurement is $10^{-4}$ times the tabulated value of ABC. The error in the N measurement is tabulated (column E, Table 3) for the same initial signal-to-noise ratio. ABCE represents the squared relative error. ABCE will always be greater than the $N_0$ relative error term. Furthermore, ABCE exhibits a minimum near $\Delta$ equal to 0.6. A reasonable value for W(f)/f is 0.05 (33). This large relative error is combined with its coefficient and summed with the other large error source, N measurement, to determine the optimum ion attenuation. This occurs at an approximate $\Delta$ of 0.3. W(N)/N and $W(E_\lambda)/E_\lambda$ can be estimated to be $6x10^{-4}$ and 0.03 respectively. At the optimum $\Delta$ for an ion signal-to-noise ratio of 100 and for the relative errors as described and f equal to 1, the predicted relative error in the cross-section is 0.08. The error at a given $\Delta$ is most sensitive to changes in $W(E_\lambda)E_\lambda$ and W(f)/f. If $W(E_\lambda)/E_\lambda$ were doubled, the cross-section relative error would increase to 0.095, similarly doubling W(f)/f results in a relative error of 0.13. Departure from the optimum $\Delta$ value results in less dramatic changes in the cross-section relative error at least for deviations less than +0.3

To optimize the photo-induced experiments, the signal intensity ($N_0$) and the signal-to-noise ratio must be optimized. Increased apparent intensity without increased signal-to-noise will not improve the relative errors. $E_\lambda$ should be accurately variable with a constant f value. For the best observed signal-to-noise ratio and W(f)/f of 0.10 to account for poor shot-to-shot beam quality, the anticipated relative error in the cross-section is 16%.

# CHAPTER IV
# EXPERIMENTAL RESULTS AND DISCUSSION OF THE HALOGEN ANION STUDIES

The ions discussed in this chapter are those for which observable ion intensities could be produced. $Cl_2^-$ and $Br_2^-$ were generated with sufficient intensities to assure reasonable signal-to-noise ratios for the photo-excitation studies. $BrCl^-$ was observed and the instrumental parameters pertinent to its formation were optimized, but under no operating conditions was the signal quality adequate to undertake photo-excitation measurements.

## Chlorine Molecular Anion
### Formation of $Cl_2^-$

The generation of $Cl_2^-$ was not straightforward. Four means of producing the chlorine molecular anion were attempted; two procedures were successful. Direct attachment of low-energy electrons to chlorine molecules was attempted over the nominal electron energy range, 0 to 10 eV, for chlorine sample pressures at the ion cell vacuum can ranging from $1\times10^{-4}$ to $1\times10^{-7}$ Torr. No molecular chlorine anion was observed for any combination of these parameters. At all experimental conditions, dissociative attachment yielding $Cl^-$ was seen to occur exclusively. Dissociative attachment of low-energy electrons to carbon tetrachloride was tested for $Cl_2^-$ production. As for chlorine, sample pressures and electron energies were varied to cover all combinations of these parameters. The observed dissociative attachment generated $Cl^-$ only; no $Cl_2^-$ was detected. A charge transfer to chlorine from a suitable precursor anion was investigated. Nitrite ion, $NO_2^-$, was readily produced from nitromethane, $CH_3NO_2$. Electron transfer was expected to occur for the interaction of $NO_2^-$ with a species of greater electron affinity. Optimization of the nitrite ion intensity, followed by the addition of chlorine yielded $Cl_2^-$ at levels acceptable for pursuing the photo-excitation study. Finally, $Cl_2^-$ was produced in low-energy (0 ev) electron impact with a sample of chlorotrifluoroethylene ($C_2F_3Cl$). The $Cl_2^-$ signal intensity was not as strong as that observed from the charge transfer process. The means selected for $Cl_2^-$ generation in the ensuing photo-excitation study was the electron transfer from nitrite ion to molecular chlorine.

Prior to undertaking the discussion of the photo-excitation study of the chlorine molecular anion, the precursor anion's negative ion mass spectrum and generation will be analyzed. The nitrite ion intensity was optimized with respect to all ICR and sample parameters. The range of the parameters and the resolution of the variation of each parameter are presented in Table 4. The negative ion mass spectrum of nitromethane contained a single peak at a mass-to-charge (m/e) ratio of 46 amu/e. The signal-to-noise ratio at the optimized system settings was approximately 40 to 1 (Figure 16). No other ions were detected over the mass-to-charge range, 5 to 105 amu/e. No secondary or precursor ions were identified. The

Table 4. Variation of ICR Operating Parameters During Studies to Maximize Formation of the Nitrite Ion from Nitromethane.

| Parameter | Range | Resolution |
|---|---|---|
| Electron Energy[a] | 1.8 - 18 eV | 2 eV |
| Sample Pressure[b] | $4\times10^{-7}$ - $1\times10^{-4}$ mm Hg | $1\times10^{-7}$ - $1\times10^{-5}$ mm Hg |
| Grid Pulse | 8 ms - 25 ms | 5 ms |
| Detect Delay | 0 - 300 ms | 1 ms |
| Detect Width[c] | 5 ms | Not varied |
| Marginal Oscillator Level | 50 - 100 mV | 10 mV |

[a] A true estimate of the electron energy is obtained by subtracting the trapping plate potential of 1.50 v.

[b] The background sample pressure was 2-4 x $10^{-7}$ mm Hg.

[c] Detect width and marginal oscillator level are related, however, over the range of marginal oscillator levels attempted detect width did not require change.

Figure 16. Negative Ion Mass Spectrum of Nitromethane. The mass range is 5 to 105 amu. Sample pressure was 1 x $10^{-5}$ Torr. Electron energy was 2.4 eV. Detect delay time was 40 ms. The peak occurs at a mass-to-charge ratio of 46 amu/e.

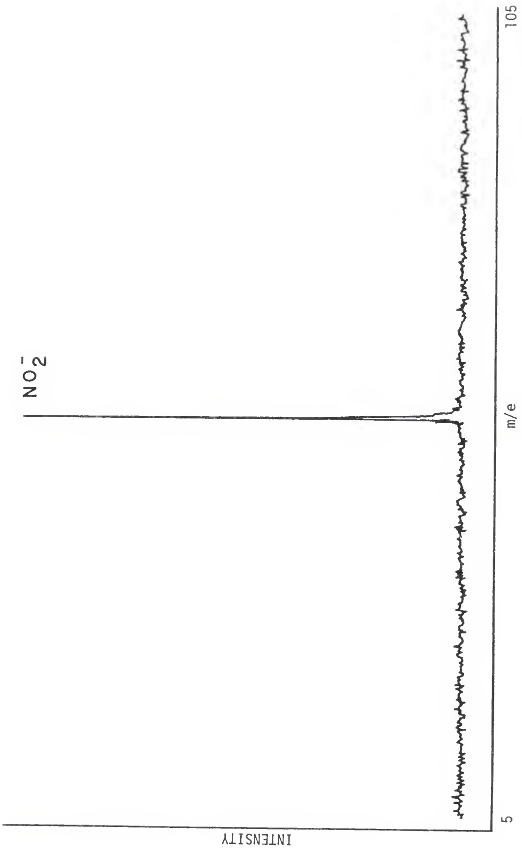
$NO_2^-$
m/e
5
105
INTENSITY

electron energy for peak nitrite ion intensity was 0.83 eV. Nitrite ion generation from nitromethane was deemed to be a suitable, clean choice as the precursor for the molecular anion of chlorine.

The chlorine molecular anion was generated and its signal intensity optimized in a manner that simplified the tuning procedure. Nitrite ions were detected and the intensity of the signal was maximized for a nitromethane pressure between $5x10^{-6}$ and $1x10^{-5}$ Torr. Chlorine was leaked to the cell through the second inlet manifold and jeweled leak valve. The $NO_2^-$ signal intensity was monitored as the chlorine was added. The nitrite ion intensity fell off rapidly with the introduction of chlorine. When the $NO_2^-$ intensity had decreased to less than 10% of its peak value, the chlorine pressure at the cell was stabilized. The magnetic field was set to bring the $Cl^-$ ion into resonance and once this signal was located the detect pulse delay was increased until the $Cl^-$ peak intensity had dropped to approximately 20% of the initially observed level. At this detect delay, the magnetic field was altered to bring the $Cl_2^-$ anion into resonance. In some instances, scans of the magnetic field about the nominal resonant magnetic field for $Cl_2^-$ proved necessary to locate the ion. The $Cl_2^-$ signal was maximized with respect to the ratio of components inlet to the ion cell region, the total sample pressure at the ion cell, and all of the tuning parameters of the spectrometer. A negative ion mass spectrum for a chlorine/nitromethane mixture (pressure ratio determined at the ionization gauge on the main vacuum manifold) is reproduced in Figure 17. The time dependences of the predominant negative ions, $NO_2^-$, $Cl_2^-$, and $Cl^-$, are indicated in the time-scanned spectra (Figure 18).

Figure 17. Negative Ion Mass Spectrum for a Chlorine/Nitromethane Mixture. The mass range is 10 to 100 amu. Total sample pressure of the 1 to 2 chlorine/nitromethane mixture was $2\times10^{-5}$ Torr. Electron energy was 2.5 eV. Detect delay time was 70 ms. The $Cl_2^-$ peak is weak at this detect delay, but increases with increasing detect delay.

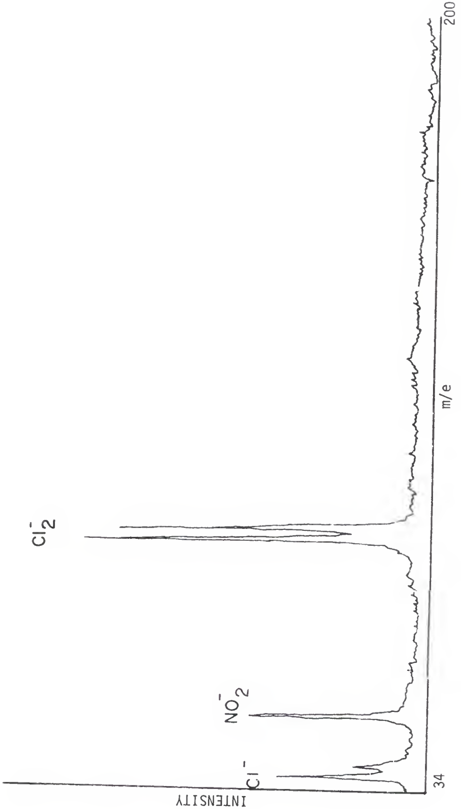
$Cl^-$
$NO_2^-$
$Cl_2^-$
INTENSITY
m/e
34
200

Figure 18. Time-dependent Mass Spectra of the Major Peaks of a Chlorine/Nitromethane Mixture. Three major peaks are observed $NO_2^-$, $Cl_2^-$ and $Cl^-$. $Cl^-$ is the most intense. $NO_2^-$ is observed only during the grid pulse when in the presence of chlorine. Time zero corresponds to the beginning of the grid pulse. The upper time limit is 350 ms.

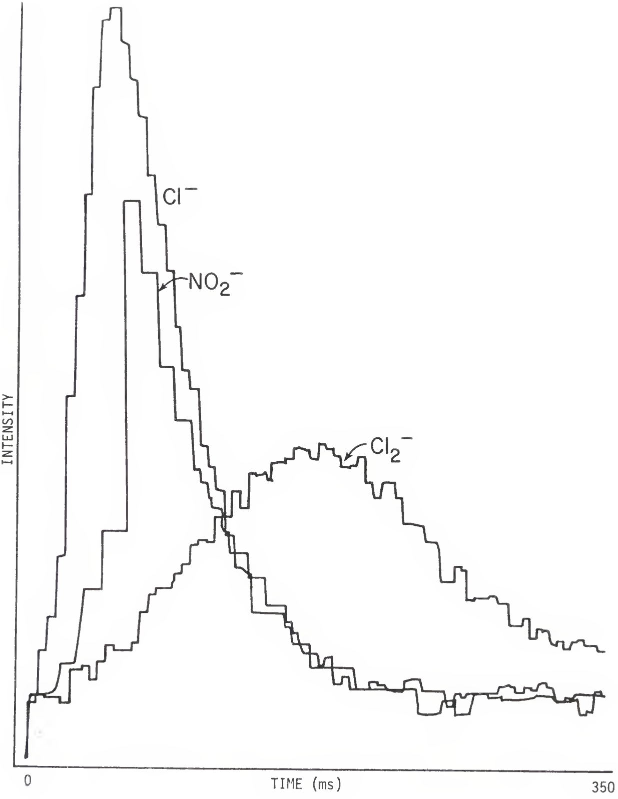
INTENSITY
TIME (ms)
0
350
$Cl^-$
$NO_2^-$
$Cl_2^-$

It was difficult to maintain stable $Cl_2^-$ signal levels. The total pressure at the ionization gauge drifted markedly. This variation was the result of the fluctuation of the chlorine delivery or the nitromethane delivery with equal frequency. After the sample pressures were continuously monitored and adjusted for periods of up to three hours, the drift was reduced and slowly varying $Cl_2^-$ signals were obtained.

There are discrepancies between the results of the molecular chlorine anion formation behavior observed in this study and previous studies. $Cl_2^-$ has been generated by electron attachment at total pressures as low as $4x10^{-7}$ Torr at electron energies of 1 to 2 eV (75). The resultant $Cl_2^-$ ions exhibited lifetimes up to one second in the cell of an ion cyclotron resonance mass spectrometer. This lifetime is significantly longer than those observed in this study; however, this may be attributed to the relatively high pressures used in this investigation (total pressure on the order of $10^{-5}$ Torr). Generation of $Cl_2^-$ from carbon tetrachloride has been reported with an appearance potential of 2.3 eV in a time-of-flight mass spectrometer (76). The inability to generate $Cl_2^-$ from $CCl_4$ in this study could not be attributed to a single instrumental parameter, but is likely the result of some combination of electron energy distribution aberrations, trapping imperfections, and relative detection sensitivity.

A number of investigations have been performed on $NO_2^-$ due to its possible atmospheric importance and the chance of overlap of its photodetachment spectrum with the solar radiation spectrum (77-84, 85, 86).

Experimental evaluations of the electron affinity of nitrogen dioxide are relevant to this study and are summarized in Table 5. Exact determination of the adiabatic electron affinity of nitromethane has been hampered by the significant structural differences between the ground states of the neutral and anion which lead to excited vibronic transitions (84, 87, 88a).

A long wavelength tail in the photodetachment spectrum of $NO_2^-$ led to a proposed peroxy isomer of lower electron affinity than the ground state anion (85). The existence of a low-energy isomer could have a significant impact on the subsequent spectral study of an ion formed by electron transfer from a mixture of the two isomers. Although the appearance of a long wavelength tail in the $NO_2^-$ photodetachment spectrum was corroborated (86), a recent study has been able to interpret the results of the previous works in terms of variations in the measured collisional de-excitation rates for vibrationally excited $NO_2^-$ by different bath gases (89). The appearance of the long wavelength tail in the photodetachment spectrum is best interpreted as the result of detachment from inefficiently quenched vibrationally-hot ions.

Although suggestion of an isomeric form of $NO_2^-$ has been discredited, the experimental results still indicate signficiant internal excitation for $NO_2^-$ produced by electron attachment to nitrogen dioxide. An alternate source of $NO_2^-$ for which the internal excitation could be minimized or at the very least permit the determination of an upper limit on the internal energy is essential in electron transfer generation of the chlorine anion. A strong

Table 5. Empirical Electron Affinities for $NO_2$ in eV.

| Electron Affinity | Method | Reference |
|---|---|---|
| 2.36 ± 0.10 | Tunable laser photodetachment<br>Hot cathode source beam | 85 |
| 2.8 (threshold) | Conventional source photodetachment<br>Ion cyclotron resonance | 86 |
| 2.29 ± 0.1 | Endothermic charge transfer | 79 |
| 2.30 ± 0.15 | Endothermic charge transfer | 80 |
| 2.38 ± 0.06 | Charge transfer | 78 |
| 2.7 ± 0.2 (threshold) | Conventional source photodetachment<br>Ion cyclotron resonance | 84 |
| 2.04 | Endothermic charge transfer | 81 |
| 3.1 | Photodetachment | 82 |
| 3.9 | Chemical ionization | 83 |

$NO_2^-$ peak at an appearance potential of 0.6 eV was found in the negative ion mass spectrum of nitromethane (90). $NO_2^-$ produced in this manner is anticipated to have a level of internal excitation that is essentially thermal since the appearance potential only slightly exceeds the minimum energy required for the process. This energy difference, the energy of bond rupture (DH (C-N) $\approx$ 73 kcal/mole) (91) minus the electron affinity of $NO_2$ (EA($NO_2$) = 2.38 ± 0.06 eV) (87), amounts to 0.8 eV. Since the potential for peak $NO_2^-$ ion intensity occurred at 0.83 eV in this study, the $NO_2^-$ ion is presumed to be vibrationally cool.

The experimental conditions for which the nitromethane negative ion mass spectrum was observed overlap those of previous investigations. In addition to the nitrite ion, $CN^-$ and $O^-$ have been observed in the nitromethane spectrum (90). The peak $CN^-$ and $O^-$ intensities are considerably less than the $NO_2^-$ peak intensity, on the order of one one-hundredth and one two-hundred-and fiftieth the $NO_2^-$ intensity, respectively. It is understandable that such low intensity ions should not be observed for the signal-to-noise evidenced in this study.

The electron transfer reaction

$$NO_2^- + Cl_2 \rightarrow Cl_2^- + NO_2 \qquad (43)$$

has been investigated (79). For $NO_2^-$ ions with 0.3 eV translational energy the rate constant for the reaction was determined to be 2.2 x $10^{-10}$ $cm^3$/molecule-second. At higher translational energies the cross section for this reaction dropped sharply indicating that it was exothermic. The reverse reaction was not observed ; however, a competing reaction

$$Cl_2^- + NO_2 \rightarrow NO_2Cl + Cl^- \qquad (44)$$

has been reported (78).

The generation of $Cl_2^-$ from chlorotrifluoroethylene was also observed. This behavior has been reported, but the mechanism for the formation was not determined (92). Investigation of this source of $Cl_2^-$ included a search for precursor and intermediate ions, however none were identified. The original investigators' conclusion that a pyrolytic reaction was occurring on a hot filament surface is a reasonable explanation of this behavior and is not contradicted by this study.

Halogens are known to be highly reactive, corrosive compounds. Reactions with pump oils, ion gauge cathodes, gaskets, etc. have hindered measurements of halogen properties. There is also empirical evidence confirmed by the experience of this study that passivation of the system is required prior to obtaining stable halogen ion signals (93, 94). This passivation time may be hours or days depending upon the vacuum containment system geometry, surface area and surface condition. Of particular significance is the effect of chlorine reactions at the surface of an electron filament which may alter the work function of the filament material and change the characteristics of the electron beam. This effect is pronounced for low-energy electrons and has been observed to result in the complete elimination of low-energy electrons from the distribution of electrons generated by a current heated filament (93). In addition, although certain aspects of the system may recover quickly, such as the proper functioning of leak valves, the effects due to surface reactions of a halogen at the electron filament and the ionization gauge cathode may be irreversible. This behavior certainly contributed to the experimental difficulties encountered in the generation and maintenance of a measurable halogen anion population.

## Photodetachment of $Cl_2^-$

In Figure 19 the raw data for the photodetachment of $Cl_2^-$ at two wavelengths are presented. The bandwidth of the laser output as measured at the monochromator was 0.4 nm. The x-axis is time and a typical run at a single wavelength required 15 to 20 minutes to complete. The experimental procedure and data reduction were as described in Chapter III. The detect delay time for chlorine anion photodetachment studies was selected with two factors in mind. First, that the detect delay be long enough that all of the precursor anions had reacted. Second, that the chlorine anion intensity be as near to the peak chlorine anion intensity as the first criterion would allow. Peak laser outputs varied strongly with dye, dye concentration, dye age, wavelength, and the high voltage setting for the laser discharge. The maximum laser output was about 100 millijoules (mj) and the lowest outputs that produced measurable changes

Figure 19. Photodetachment of $Cl_2^-$.

The photodetachment of an optimized $Cl_2^-$ ion signal at $\lambda$ = 478.5 nm(a) and $\lambda$ = 475 nm (b) is shown. The signal-to-noise is exceptional in this particular spectrum.

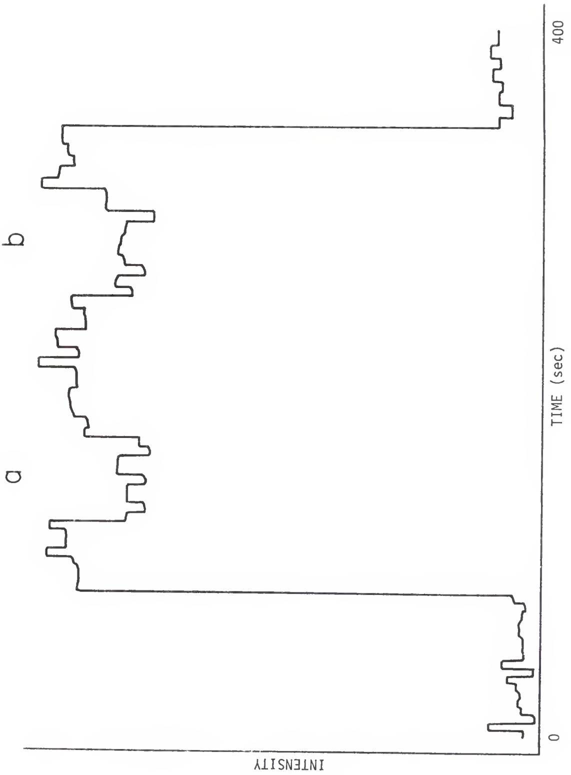
a
b
TIME (sec)
0
400
INTENSITY

in ion intensity were 10-15 mj for wavelengths corresponding to a maximum in the absorption spectrum of the ion.

In addition to observing the decrease in $Cl_2^-$ signal intensity upon irradiation, fragment/product ions were sought. In the case of $Cl^-$, the ion cyclotron resonance mass spectrometer could be tuned to the ion at a detect delay time at which the $Cl^-$ signal was measurable. The detect aperture was then returned to the time at which the $Cl_2^-$ reduction was observed; however, the $Cl^-$ resonance conditions were not altered. Subsequently, photo-produced $Cl^-$ or $Cl^-$ generated from some photo-produced intermediate could be measured. A photo-induced spectrum of $Cl^-$ is presented in Figure 20. Other product ions were sought as well. $CH_3NO_2Cl^-$, $NO_2Cl^-$, $NOCl^-$, $CH_3Cl^-$, and $CH_2Cl^-$ were possible product ions that were sought at each peak of $Cl_2^-$ photodestruction. Since these ions were not present in the original negative ion mass spectrum of the nitromethane/chlorine mixture, the procedure for determining their presence was more involved than those for $Cl^-$. While photoreduction of the $Cl_2^-$ signal intensity was taking place, a slow, magnetic field scan over 0.050 Tesla and centered at a possible product anion's nominal, resonant magnetic field strength was conducted. These measurements were performed for each postulated anion at each wavelength where a significant reduction in the $Cl_2^-$ intensity was observed. None of the proposed product anions with the exception of $Cl^-$ was observed.

The energy range covered in the photo-excitation experiments was limited to 0.39 eV (3170 $cm^{-1}$). The short wavelength limits

Figure 20. Photoproduction of $Cl^-$. This spectrum was generated as described in the text. The $Cl^-$ signal levels exceed that of the photodetachment $Cl_2^-$ due to the mass dependence of the detectivity and the photo production of $Cl^-$ from $Cl_2^-$ of varying isotopic character.

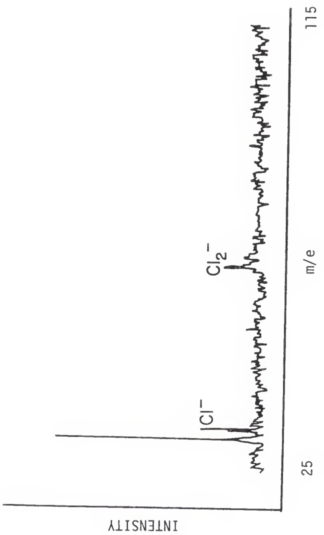
INTENSITY
Cl⁻
Cl₂⁻
25
m/e
115

were determined by inefficient lasing of the dye laser system toward blue wavelengths. The short-wavelength limit was 457 nm. Efficient dyes are available for wavelengths shorter than 457 nm, however, the particular Xe flashlamp employed does not effectively populate the upper state of the shorter wavelength dyes and lasing could not be achieved. The long-wavelength limit at 540 nm was the result of a gap in the lasing ranges of the available dyes. Fluorol 555 was obtained to extend the measurements into the red, however it did not lase (63). Measurements made to the red of the Fluorol 555 range ($\lambda > 565$ nm) resulted in no photo-reduction from 565 nm to 622 nm. The gap in the photo-excitation spectra between 500 nm and 510 nm occurs at a region where both LD 490 and Coumarin 540 dyes lased, but with poor beam quality and poor shot-to-shot repeatability of the beam profile.

The variation of the photodetachment cross-section with wavelength as restricted by the laser source considerations is presented in Figure 21. All data points were taken under identical spectrometer conditions: grid pulse delay, 1ms; grid pulse width, 30 ms; free pulse delay (laser trigger), 100 ms; detect pulse delay, 100 ms; marginal oscillator level, 50 to 60 mV; filament current, 2.5A; filament voltage, 4v; filament offset voltage, -2.4v; and grid offset voltage, -12.5v. Source pressures were held as constant as possible considering the stability difficulties described.
Each point on the spectrum represents an average of between four to ten runs at the individual wavelength corresponding to sixty to one hundred and fifty laser shots per point. The bulk of this data was

Figure 21. $Cl_2^-$ Photodetachment Cross-Section as a Function of Wavelength. The $Cl_2^-$ photodetachment spectrum is shown from 460 nm to 540 nm. Absolute cross-sections were not measured. The maximum photoreduction of $Cl_2^-$ observed over this wavelength range was approximately 80% in the blue region. Structure is evident in the cross-section.

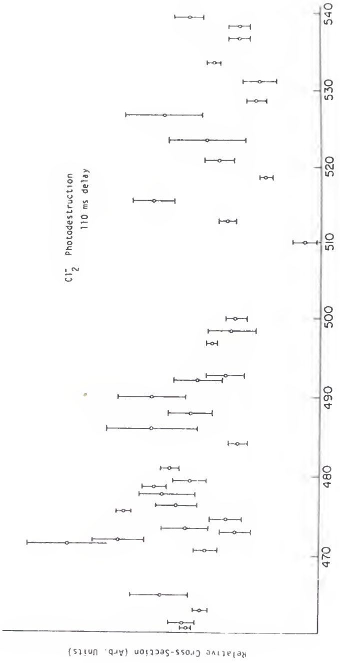
$Cl_2^-$ Photodestruction
110 ms delay
470
480
490
500
510
520
530
540
Relative Cross-Section (Arb. Units)

analyzed manually by the measurement of the ion signal intensities from the hardcopy spectrum generated at an x-y recorder. The individual laser shot intensities were measured visually with an oscilloscope and manually recorded for later correlation with the appropriate ion intensity value. A small amount of the data over the wavelength range from 470 nm to 490 nm was collected with the microcomputer-interface hardware. Microcomputer data collection decreased the actual data collection time and more significantly decreased the time required for data reduction. Typically, two hours were required to manually reduce the data of a single pass (15 laser shots) at a single wavelength. With the microcomputer interface this time was reduced to approximately ten to fifteen minutes depending upon the quality of the data. If the present microcomputer-interface were tied into a more powerful microcomputer, the data reduction time could be made significantly less and on-line analysis could be approached.

## Analysis of $Cl_2^-$ Results

Optically accessible electronic transitions of the halogen molecular anions are restricted to symmetry-allowed, single-electron transitions involving the valence molecular orbitals. The ground electronic state molecular anion configuration of the halogens may be written in the form

$$\ldots(\sigma_g ns)^2(\sigma_u ns)^2\ (\sigma_g np)^2\ (\pi_u np)^4\ (\pi_g np)^4\ (\sigma_u np)^1$$

where n equals 3 and 4 for chlorine and bromine, respectively. This notation is abbreviated to (2441) in which only pσ and pπ occupancies are explicitly given. This configuration (2441) yields a $^2\Sigma_u^+$ molecular electronic term (Hund's case b ). Consistent with the antibonding nature of the $\sigma_u$np electron, the chlorine anion exhibits an increased bond length (2.66A) and decreased vibrational frequency (260 cm$^{-1}$) (95) relative to the ground state of the neutral (1.988A, 565 cm$^{-1}$) (88b). No first-order spin-orbit coupling is expected for a $^2\Sigma_u^+$ state (88c).

The lowest, excited-state electeonic configurations correspond to single-electron excitations from the $\sigma_g$np, $\pi_u$np, or $\pi_g$np orbital to the $\sigma_u$np orbital. These states, (2432) $^2\Pi_g$, (2342) $^2\Pi_u$, and (1442) $^2\Sigma_g^+$ , are repulsive. Potential energy curves have been calculated both for the ground anionic state and the repulsive excited states for chlorine (95,96) and bromine (96). In addition, for chlorine the $^2\Pi_g \leftarrow {}^2\Sigma_u^+$ and $^2\Sigma_g^+ \leftarrow {}^2\Sigma_u^+$ electronic transitions have been observed in the gas phase (75,92), as well as in rare gas matrices (97), crystals (98), and glasses (99). The transition from the $^2\Sigma_u^+$ to the $^2\Sigma_u$ state is strongly forbidden and has not been observed. The $^2\Pi_g$ and $^2\Pi_u$states exhibit first-order, spin-orbit splitting; for chlorine the magnitude of the splitting is anticipated to be small (100).

The only state of neutral chlorine accessible with the wavelengths used in this study is the $X^1\Sigma_g^+$ground state. The next neutral state, 18310.5 cm$^{-1}$ above the ground state, is the $A^3\Pi_{0^+u}$ state (88d). This state lies at an energy significantly higher than can be reached with the current laser source and does not contribute further to the discussion of these results.

The spectrum for the photoreduction of $Cl_2^-$ exhibits significant, complex structure not observed in previous studies (75, 92, 97, 98, 99). Studies employing polarized incident radiation have identified the two transitions observed for chlorine anions as the $^2\Sigma_g^+ \leftarrow X^2\Sigma_u^+$ transition at approximately 365 nm and the $^2\Pi_g \leftarrow X^2\Sigma_u^+$ transition peaked at 750 nm (75,92,97). For chlorine the spin-orbit splitting of the $^2\Pi_g$ state was not observed (97). The photo-induced decrease of the $Cl_2^-$ intensity observed in this study cannot be explained in terms of transitions to the dissociative excited states of the anion. The wavelength range covered by this work corresponds to the region of the long wavelength tail of the ultraviolet transition (365 nm). In this range, the photodissociation of the molecular chlorine anion occurs with a lower probability and photodetachment processes from excited vibrational levels of the chlorine molecular anion may be observed.

## Computation of Franck-Condon Factors

The anticipated transitions are those occurring from a vibration-rotation manifold of the $^2\Sigma_u^+$ state of the anion to the vibration-rotation manifold of the neutral ground state $^1\Sigma_g^+$ . The relative intensities of the individual lines in such a spectrum depend upon the relative values of the Franck-Condon (FC) overlap factors, in conjunction with rotational parameters, for a constant electric dipole transition moment. FC factors may be obtained if accurate electronic potentials are known or can be generated for the two electronic states involved in the transition. Three types of potential energy curves are generally available: empirical, computational, and quantum mechanical. Empirical procedures rely on a parameterized model for the potential curve where spectroscopic constants determine the parameters. This method includes the Morse potential energy curve generation scheme (101) and several variations including the Hulbert-Hirschfelder potential function method (102). Quantum techniques involve numerical solution of the wave equation to some selected approximation over a range of nuclear configurations. A computational technique relies upon the spectroscopic constants for the generation of discrete molecular energy levels and upon the assumption of a functional form for the distribution of the levels. The most well-known computational method is the Rydberg-Klein-Rees (RKR) technique (103). The RKR potential is the best approximation to the true potential up to the term value for which the spectroscopic constants are unperturbed and valid. For this reason, the RKR technique with a Hulbert-Hirschfelder extension beyond the region of valid spectroscopic constants was used in this study.

The RKR method for potential curve construction is founded upon the Dunham phase integral (104, 105) and the Klein action integral (106, 105). The Dunham phase integral expresses the energy levels of a potential function with a single minimum. The expression for the phase integral is

$$\oint p\,dx = 2\int_{x_1}^{x_2} p\ dx = h\ (v+\tfrac{1}{2}) = I \qquad (45)$$

for p defined as the particle momentum. Where the effective potential can be represented as a potential without rotation and a centrifugal potential

$$U_K(R) = U(R) + \frac{K}{R^2} \qquad K = \frac{\hbar^2}{2\mu} J(J+1), \qquad (46)$$

the phase integral condition has the form

$$2\int_{R_1}^{R_2} [2\mu(E - U_K(R)]^{1/2} dR = I \qquad (47)$$

where E is the energy of the (v, J) term value, i.e.,

$$E(I,K) = hcF(v, J). \qquad (48)$$

The Klein action integral is written

$$S(V,K) = (2\pi^2\mu)^{-\frac{1}{2}} \int_0^{I'} [V-E(I,K)]^{\frac{1}{2}}\, dI \qquad (49)$$

where I' is determined by the stipulation

$$E(I',K) = V \qquad (50)$$

and V is the energy at the limit of the integration. The phase integral condition and Klein action integral may be combined and the intermediate expression evaluated to give a simple form of the action integral

$$S(V,K) = \tfrac{1}{2}\int_{R_1(V)}^{R_2(V)} (V- U_R(R_o)\ dR \qquad (51)$$

The potential derivatives with respect to V and K of the simplified form of the action integral are

$$f = \frac{\delta S}{\delta V} = \tfrac{1}{2}\ (R_2-R_1) \qquad (52)$$

$$g = \frac{\delta S}{\delta K} = \tfrac{1}{2}\ (\frac{1}{R_1} - \frac{1}{R_2}). \qquad (53)$$

These equations may be evaluated for $R_1$ and $R_2$, the classical turning points.

$$R_{1,2}\ (V) = (\frac{f}{g} + f^2)^{\frac{1}{2}} \mp f. \qquad (54)$$

Both f and g are determined as functions of V from the complex form of the Klein action integral

$$f(V) = (8\pi^2\mu)^{-\frac{1}{2}} \int_0^{I'} \frac{dI}{\sqrt{V-E(I,0)}} \qquad (55)$$

$$g(V) = \frac{(8\pi^2\mu c^2)^{\frac{1}{2}}}{h} \int_0^{I'} \frac{B_V(I)dI}{\sqrt{V-E(I,0)}} \qquad (56)$$

where $B_V(I) = B_e-\alpha_e(\frac{I}{h}) + \ .\ .\ .$ and other constants are defined as usual. The method evaluates numerically the f(V) and g(V) and determines the classical turning points.

The Hulbert-Hirschfelder (H-H) five-parameter empirical potential is a generalization of the Morse potential given by

$$U(R) - U(R_e) = a_1 \ (1-e^{-X})^2 + a_2 \ X^3 e^{-DX} + a_3 \ X^4 e^{-DX} \tag{57}$$

where

$$X = \frac{\omega_e (R-R_e)}{2 \ B_e^{\frac{1}{2}} D_e^{\frac{1}{2}} R_e} \tag{58}$$

and $a_1$, $a_2$, $a_3$ and D are fitting parameters which may be related to spectroscopic constants by means of Dunham's analysis (102). This potential function is used to extend the RKR potential curve so that vibrational wave functions may be determined up to the RKR limit. A Fortan RKR-HH potential energy function program (107) was used and calculations were performed on the Amdahl computer. The RKR-HH numerical potentials for $Cl_2$ and $Cl_2^-$ are given in Appendix V. The potentials are drawn in Figure 22. The input spectroscopic constants are listed in Tables 6 and 7.

The RKR potentials are the inputs to an FC factor program due to Zare and Cashion (107) which utilizes a solution of the radial Schrodinger wave equation by Cooley (108). Cooley's algorithm solves the second-order differential radial Schrodinger equation from a numerical input potential. The algorithm starts with limiting values for the wave function at the integration limits. From the upper limit, the wavefunction is integrated inward since the wavefunction's value at $r_{n-1}$ can be expressed as a function of $r_n$, $r_{n-1}$; $V_n$, $V_{n-1}$, the numerical potentials of $r_n$ and $r_{n-1}$; $P_n$; and E, a trial eigenvalue. An outward integration is performed similarly

Figure 22. Rydberg-Klein-Rees Potential Energy Curves for $Cl_2$ and $Cl_2^-$. The RKR curves for the anion-neutral pair are drawn on a single energy scale. The zero of energy corresponds to the minimum of the potential energy curve of the anion.

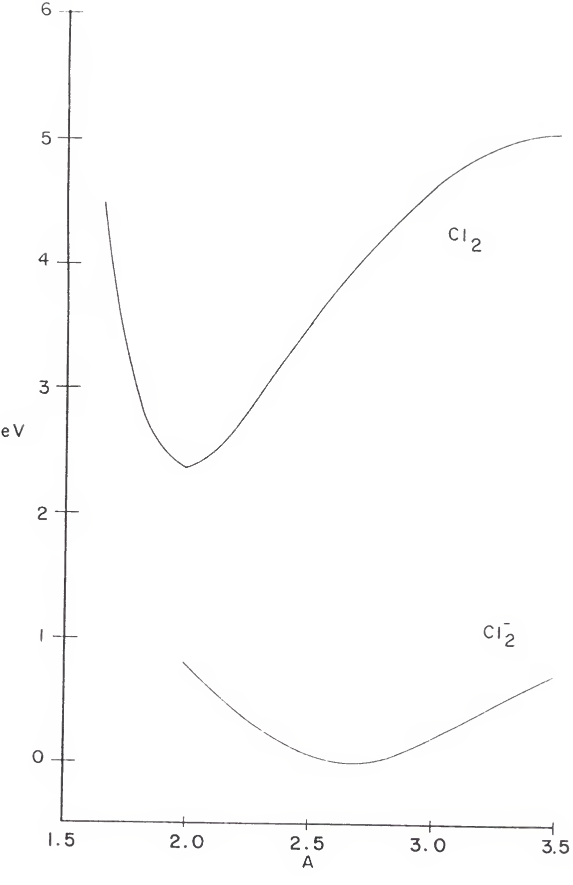
6
5
4
3
2
1
0
eV
$Cl_2$
$Cl_2^-$
1.5
2.0
2.5
3.0
3.5
A

Table 6. Spectroscopic Constants Used in the Determination of the Rydberg-Klein-Rees Potential Curve for $Cl_2$.

| | |
|---|---|
| $\omega_e$ | 559.75 $cm^{-1}$ |
| $\omega_e x_e$ | 2.694 $cm^{-1}$ |
| $B_e$ | 0.2442 $cm^{-1}$ |
| $\alpha_e$ | 1.516 x $10^{-3}$ $cm^{-1}$ |
| $D_o$ | 19997.14 $cm^{-1}$ |

Table 7. Spectroscopic Constants Used in the Determination of the Rydberg-Klein-Rees Potential Curve for $Cl_2^-$.

| | |
|---|---|
| $\omega_e$ | 260.0 $cm^{-1}$ |
| $\omega_e x_e$ | 1.50 $cm^{-1}$ |
| $B_e$ | 0.136 $cm^{-1}$ |
| $\alpha_e$ | 0.01 $cm^{-1}$ |
| $D_o$ | 10324.1 $cm^{-1}$ |

from the lower integration limit. This solution satisfies the wave equation at all points except for the single point where the inward and outward integrations overlap. This point is used to test for convergence with respect to variation of the trial eigenvalue. When the energy difference between the inward and outward wavefunctions is less than the selected convergence limit, the final wavefunction is obtained by a point normalization routine. The integrations are simplified if the potential is known at regularly spaced values of r, therefore, an eighth-order Lagrangian interpolation of the input RKR potentials is performed prior to wave function generation. The evaluation of the wave function integrations and the FC overlap integrals and other integrals take place over the range RMIN to RMAX. For the ground anionic state of chlorine and the chlorine neutral RMIN and RMAX were selected as 1.5A and 3.5A, respectively. These values are selected due to the constraints of the Lagrangian interpolation routine and the range of validity for the spectroscopic constants, and provide precise wavefunctions up to $v''_{max}=12$ for anion and $v'_{max}=20$ for the ground state neutral. The quantum numbers of the transitions (V*, V**), the term value, $T(cm^{-1})$, the Franck-Condon factor, Q, the wavelength of the transition, LAMBDA (A) and the FC factor times the cubic and fourth powers of the wave number, QT**3 and QT**4, as well as the r-centroid and r-squared-centroid and the sign of the overlap integral prior to squaring to obtain the FC factor, RC, R**2C and PHASE, respectively, are tabulated in Appendix V. The potential curves and Franck-Condon and associated integrals determined here were evaluated to assist in the interpretation of the structure present in the photodestruction spectrum of the molecular chlorine anion.

Table 8 contains the locations of the major peaks of the photoreduction spectrum of $Cl_2^-$ expressed in wavelength and wavenumbers. Based on the output of the FC factor program, vibronic transitions have been assigned to the observed transition energies. The results of the FC factor program are indicative of, but not conclusive evidence for, the assignment of the photoreduction of $Cl_2^-$ to a photodetachment process. The FC factor term values are accurate as far as the spectroscopic constants for each state retain validity. The spectroscopic constants for the $X^1\Sigma_g^+$ ground state of chlorine are well known for $v \leq 49$ (109, 88b). Therefore, exceptional accuracy in the term value is expected with respect to the neutral vibration-rotation manifold. The constants for the molecular anion are not well established and this hampers the peak assignments at higher vibrational quantum numbers of the anion (110, 111). Several of the assignments in Table 8 may be questionable, especially those at 471.5 nm ($V^*=20$, $V^{**}=13$) and 463 nm ($V^*=23$, $V^{**}=15$). However, at longer wavelengths the assigned transitions are obviously the best possible fit of the calculations to the experiment. The assigned FC factors, especially at the long wavelengths, are the only overlap factors of reasonable magnitude in the wavelength region. At shorter wavelengths more transitions could be contributing significant intensity to the observed spectrum.

Table 8. Correlation of the Observed Peaks ($\lambda$, $T_{exp}$) in the $Cl_2^-$ Photodetachment Spectrum with Calculated Transition Energies ($T_{calc}$) and Franck-Condon Factors

| $\lambda$ (nm) | $T_{exp}$ ($cm^{-1}$) | (V*, V**) | $T_{calc}$ ($cm^{-1}$) | Franck-Condon Overlap Factor |
|---|---|---|---|---|
| 539.5 | 18535 | (16,6) | 18527 | 0.4067 E-1 |
| 533.5 | 18744 | (15,6) | 18739 | 0.4757 E-1 |
| 527 | 18975 | (14,6) | 18954 | 0.4426 E-1 |
| 521 | 19193 | (13,6) | 19172 | 0.3429 E-1 |
| 516 | 19379 | (12,6)<br>(22,10) | 19393<br>19369 | 0.2265 E-1<br>0.1401 E-1 |
| 496 | 20161 | (11,7) | 20138 | 0.2645 E-1 |
| 490 | 20408 | (12,8) | 20430 | 0.4769 E-1 |
| 486 | 20576 | (16,10) | 20578 | 0.2682 E-1 |
| 482 | 20746 | (20,12) | 20751 | 0.2742 E-2 |
| 476 | 21008 | (14,10) | 21005 | 0.3784 E-2 |
| 473.5 | 21119 | (9,8) | 21110 | 0.1761 E-1 |
| 471.5 | 21208 | (20,13) | 21237 | 0.6497 E-1 |
| 463 | 21598 | (23,15) | 21610 | 0.1291 E-1 |

The interpretation of these results is complicated by the fact that no long progressions are present. From the (V*,V**) transitions (16,6), (15,6), (14,6), and (13,6) an average first difference of 219 $cm^{-1}$ is obtained as compared to an average first difference of 215 $cm^{-1}$ from the calculated term values. The average second difference from the experimentally determined term values is 4.5 $cm^{-1}$, but a positive and negative value are generated indicating that the wavelengths are not accurately enough determined to justify assigning any significance to this value.

Calculated Franck-Condon factors are not expected to predict the intensity pattern of the spectrum. This is due to the fact that the initial level populations cannot be controlled and only broad estimates of the energy available for internal excitation of the anion are known. For the accepted values of the electron affinities of nitrogen dioxide and of chlorine 2.38 ± 0.06 eV and 2.52 ± 0.17 eV, respectively, the maximum available energy for internal excitation from the electron transfer process alone is 0.37 eV (2985 $cm^{-1}$) which could account for anion excitation up to V** = 12.

One means for determining the internal energy of the molecular anion is through the observation of endothermic reactions of the anion (75). If the amount of endothermicity can be gauged, a limit on the anion's internal excitation may be set. This was attempted using the $Cl_2^-$ -$CH_3OH$ reaction. The experiment was complicated by the fact that there were only two gas inlets to the cell region. For $Cl_2^-$ formation, both inlets were already used. Consequently, a sample bulb containing nitromethane and methanol was made up and used in place of the nitromethane alone. The subsequent $Cl_2^-$ signal was reduced; however, this may be attributed to a decreased in [illegible] collision frequency between nitrite ions and chlorine and less efficient production of nitrite ion due to attenuation of the electron beam by methanol molecules rather than reaction of $Cl_2^-$ and $CH_3OH$. The technique could not be successfully applied in light of these instrumental limitations.

The spectrum of the $Cl_2^-$ photoreduction (Figure 19) does not exhibit the expected limiting wavelength dependence for the photodetachment cross-section near threshold at each transition (41, 42, 43). The onset behavior of the cross-section is predicted to be

$$\sigma(E) \propto k^{2l+1} (a_0 + a_1 k^2 + a_2 k^4 + \ldots) \qquad (59)$$

where $k$ is the magnitude of the linear momentum of the photoelectron and $l$ is the angular momentum quantum number of the ejected electron. For $Cl_2^-$ $l$ equals zero and a sharp onset is predicted at threshold. The absence of this behavior is due to masking by the enhancement of the cross-section near the sharp onset associated with each new vibrational resonance in the long wavelength tail regions.

The observation of $Cl^-$ production had led to the conclusion that photodissociation is the primary process observed in this wavelength region for $Cl_2^-$ (75, 92). This is definitely the case for the peak UV absorption centered at 365 nm. However, for vibrationally excited $Cl_2^-$ favorable Franck-Condon factors lead to photodetachment at longer wavelengths than predicted from the zero state energetics. Chlorine has been shown to react rapidly and efficiently with low energy electrons, the type produced by photodetachment (112, 113, 114). Consequently, even if photodetachment alone occurred, an increase in $Cl^-$ signal intensity is anticipated.

Table 9 lists the assigned transitions, wavelengths, term values, energy differences between the assigned transition and the (0,0) transition, and the adiabatic electron affinity of each peak. An average electron affinity of 2.3601 ± 0.0040 eV is determined based upon the peak assignments. This error reflects errors in the correct determination of the individual peak term values, but not the possibility of an incorrect numbering of the peaks. Due to the restricted range of the experiment, V** values could be off by +2 to -3 and V* values by +5 to -5 corresponding to a total error of +2164 $cm^{-1}$, -2576 $cm^{-1}$ (Table 10). Clearly, this error is a direct result of an incomplete spectrum of mediocre quality. Coverage of a wider spectral range would eliminate the questionable peak assignment and the higher precision error estimate would definitely apply.

## Bromine Molecular Anion

### Formation of $Br_2^-$

The molecular bromine anion, $Br_2^-$, was produced from $Cl_2^-$ by electron transfer. Direct formation of $Br_2^-$ by electron transfer fron nitrite ion was not observed. Direct electron attachment to bromine generated $Br^-$ by dissociative attachment. For a maximized $Br_2^-$ signal strength the ion cyclotron resonance mass spectrometer was first optimized for

Table 9. Adiabatic Electron Affinity Values for Chlorine Determined from the Assigment of the Photodetachment Spectrum Structure

|  | $T_{exp}$ | $(V^*,V^{**})$ | $T_{calc}(V^*,V^{**}) - T_{calc}(0,0)$ | Adiabatic Electron Affinity |  |
|---|---|---|---|---|---|
| (nm) | ($cm^{-1}$) |  | ($cm^{-1}$) | ($cm^{-1}$) | eV |
| 539.5 | 18535 | (16,6) | -505 | 19040 | 2.3606 |
| 533.5 | 18744 | (15,6) | -296 | 19404 | 2.3606 |
| 527.0 | 18975 | (14,6) | -81 | 19056 | 2.3626 |
| 521.0 | 19193 | (13,6) | 137 | 19056 | 2.3626 |
| 516.0 | 19379 | (12,6)<br>(22,10) | 358<br>334 | 19021<br>19045 | 2.3583<br>2.3612 |
| 496.0 | 20161 | (11,7) | 1103 | 19058 | 2.3628 |
| 490.0 | 20408 | (12,8) | 1395 | 19013 | 2.3573 |
| 486.0 | 20576 | (16,10) | 1543 | 19033 | 2.3597 |
| 482.0 | 20746 | (20,12) | 1716 | 19030 | 2.3594 |
| 476.0 | 21008 | (14,10) | 1973 | 19038 | 2.3604 |
| 473.5 | 21119 | (9,8) | 2076 | 19044 | 2.3611 |
| 471.5 | 21208 | (20,13) | 2173 | 19006 | 2.3564 |
| 463.0 | 21598 | (23,15) | 2563 | 19023 | 2.3585 |

Table 10. Comparison of Literature Values for the Electron Affinity of Chlorine.

| Electron Affinity (eV) | Technique | Reference |
|---|---|---|
| $2.36 \pm^{0.27}_{0.32}$ | Photodetachment | Present Work |
| 2.32 ± 0.1 | Endothermic Charge Transfer | 79 |
| 2.5 ± 0.5 | Chemionization | 115 |
| 2.52 ± 0.17 | Dissociative Electron Capture | 76 |
| 2.35 ± 0.15 | Exothermic Charge Transfer | 78 |
| 2.38 ± 0.1 | Endothermic Charge Transfer | 116 |

nitrite ion production from nitromethane, then a mixture of chlorine and bromine vapor was inlet and the $Cl_2^-$ signal intensity was maximized. Finally, the $Br_2^-$ signal was located and the system was tuned for the maximum $Br_2^-$ signal intensity. $Br_2^-$ signal satisfactory for subsequent photo-experiments was produced at a detect delay of 110 ms. The $NO_2^-$ and $Cl_2^-$ signal intensities had decreased to low levels at this detect delay time for the selected operating conditions. The negative ion mass spectrum of the chlorine/bromine-nitromethane mixture is presented in Figure 23. The intensity of the well-tuned $Br_2^-$ signal is approximately one-half the intensity of the optimum $Cl_2^-$ signal levels used in the $Cl_2^-$ photo-excitation study.

## Photodetachment of $Br_2^-$

The photo-excitation spectrum of $Br_2^-$ was investigated from 470 nm to 498 nm. At longer wavelengths (520-540 nm), the low ion signal intensity contributed to a reduced signal-to-noise ratio and this combined with the small cross-section for photo-excitation at longer wavelengths precluded cross-section measurements distinguishable from the background noise level. The photoreduction spectrum is presented in Figure 24. The dashed line spectrum shows more pronounced structure; this is due to more stable output and better wavelength coverage by the dye laser system for these points. The spectra show similar gross behavior. The determination of the cross-sections plotted was discussed in Chapter III.

## Analysis of $Br_2^-$ Results

RKR potentials and Franck-Condon overlap factors were not evaluated for the ${}^1\Sigma_g^+$ state of $Br_2$ and the ${}^2\Sigma_u^+$ state of $Br_2$,

Figure 23. The Negative Ion Mass Spectrum of a Mixture of Chlorine/Bromine and Nitromethane. The mass range is from 34 to 190 amu. Peaks are observed at mass-to-charge ratios of 35, 46, 70, 80, 129 and 160 amu/e. These correspond to $Cl^-$, $NO_2^-$, $Cl_2^-$, $Br^-$, $CH_2ClBr^-$ and $Br_2^-$ respectively.

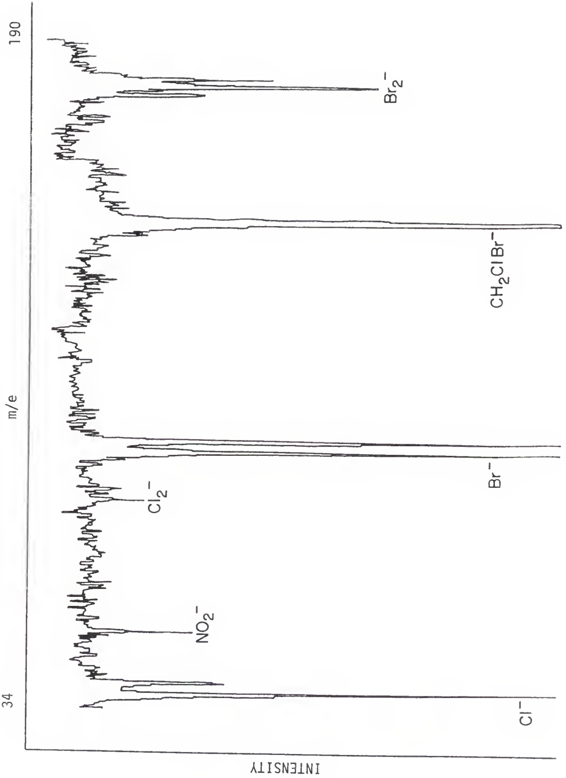
190
m/e
34
INTENSITY
$Br_2^-$
$CH_2ClBr^-$
$Br^-$
$Cl_2^-$
$NO_2^-$
$Cl^-$

Figure 24. Photodetachment Spectrum of $Br_2^-$. The optimized $Br_2^-$ signal photodetachment was observed from 470 nm to 500 nm. The structure apparent in the cross-section is not explained by the expected cross-section behavior near threshold.

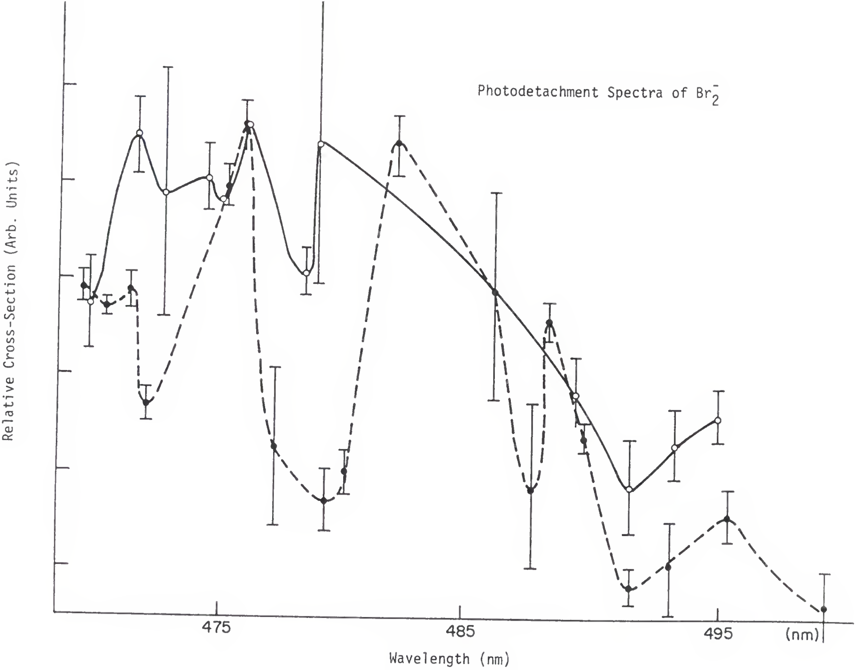

Photodetachment Spectra of $Br_2^-$

since the spectroscopic constants for the $Br_2^-$ $^2\Sigma_u^+$ anion state are not known with any degree of accuracy (96). Since the errors in the Franck-Condon overlap factors reach a level in the $Cl_2^-$ calculation that becomes significant at the high ($V^* = 12$) vibrational level of the ion and since higher internal excitation is expected for $Br_2^-$, the value of such a refined calculation is mitigated.

For the data with the greater number of experimental points in Figure 24, there are five identifiable peaks. The experimental wavelengths for these peaks and the corresponding term values are collected in Table 11. The first differences have been calculated and are also tabulated. The predicted $\omega_e$, the first-order anharmonic vibration constant, for the ground state anion is 160 $cm^{-1}$ (96). The separation between the peaks exceeds this energy. Furthermore, since $\omega_e x_e$ is small and positive (0.7 $cm^{-1}$) (96), the peak structure cannot be attributed to a vibrational distribution in the $^2\Sigma_u^+$ anion state. From the well-known spectroscopic constants for $Br_2$ ($^{79}Br$ $^{81}Br$), an estimate of the vibrational levels in the neutral ground state which would account for the empirically determined spacings can be obtained. Retaining only terms up to second-order in the anharmonic oscillator energy expression, an expression for the separation of vibrational levels in the ground state neutral ($\Delta G$) as a function of vibrational quantum number is obtained,

$$\Delta G = \omega_e - 2\omega_e x_e - 2\omega_e x_e v'' \tag{60}$$

where v" is the vibrational quantum number in the $^1\Sigma_g^+$ state of

Table 11. Experimental Wavelengths (λ) and Term Values ($T_{exp}$) and First Differences ($\Delta^1$) for the Observed Photoreduction of Bromine Molecular Negative Ions.

| λ(nm) | $T_{exp}$ ($cm^{-1}$) | $\Delta^1$($cm^{-1}$) |
|---|---|---|
| 495.4 ± 0.3 | $20186^{+12}_{-13}$ | |
| | | 281 |
| 488.6 | $20467^{+12}_{-13}$ | |
| | | 289 |
| 481.8 | $20756^{+13}_{-13}$ | |
| | | 266 |
| 475.7 | $21022^{+13}_{-14}$ | |
| | | 232 |
| 470.5 | $21254^{+14}_{-14}$ | |

bromine. Using $\omega_e$ and $\omega_e x_e$, 323.2 $cm^{-1}$ and 1.07 $cm^{-1}$, respectively (88d), this expression indicates that levels up to v' equal twenty must be involved in the transition.

No identifiable structure which can be associated with ground state anion excitation appears in the spectrum. This is due to the fact that high vibrational levels of the anion will produce closely spaced lines which remain unresolved here. From the correlation of the $Cl_2^-$ photoreduction spectrum with the term values generated by the FC overlap factor calculation it is apparent that the process for formation of $Cl_2^-$ from $NO_2^-$ (Equation 43) populates $Cl_2^-$ vibrational levels at least up to v''=16. This corresponds to 3752 $cm^{-1}$ of vibrational excitation of $Cl_2^-$. The nominal difference between the accepted electron affinities for nitrogen dioxide and chlorine can account for only one-third of this excitation. The excess excitation may result from two effects. First, for a vertical attachment process between the neutral and anion potential curves, highly excited vibrational levels of the anion are expected to be populated due to the large difference between the equilibrium bond lengths of the two states (88b). Second, electron-impact, vibrational excitation of chlorine neutral molecules may be competing with dissociative attachment. Then, attachment may occur to vibrationally hot neutrals with more favorable Franck-Condon overlap factors, but with a range of final state internal excitation (114). Assuming 3752 $cm^{-1}$ of excitation of $Br_2^-$, an estimated v'' of 23 is obtained. This corresponds to a vibrational energy spacing for the anion of approximately 108 $cm^{-1}$. This spacing would be observable under the resolution used here only under fortuitous circumstances. The lack of resolved structure which can be correlated with the internal state of the ion precludes an estimation of the adiabatic electron affinity for the bromine molecule.

## Bromine Monochloride Molecular Anion
## Formation of $BrCl^-$

Bromine monochloride negative ions were produced from the same mixtures of chlorine/bromine vapor-nitromethane used in the study of bromine photo-excitation. A mass spectrum with $BrCl^-$ at near peak intensity is shown in Figure 25. Clearly, the signal level of $BrCl^-$ was not satisfactory for photo-experiments considering the apparent errors in the cross-sections observed for $Cl_2^-$ and $Br_2^-$ which were produced and detected with much greater signal-to-noise characteristics.

Several attempts were made to increase the $BrCl^-$ intensity. Variation of the ratio of partial pressures of bromine and chlorine at the cell showed only deleterious effects when altered from a ratio of one. Steps were taken to insure that the initial mixture of bromine and chlorine was in equilibrium with bromine monochloride (117,118). This did not improve the $BrCl^-$ signal intensity.

## Analysis of $BrCl^-$ Results

$BrCl^-$ has been observed as a product of the reaction of $Cl_2^-$ with bromine. This reaction was reported earlier and a rate constant was determined ( 79). The value of this rate constant and that of competing reactions is presented in Table 12. Evidently $BrCl^-$ will be generated as a minor species regardless of the variation of neutral gas pressures.

Figure 25. Negative Ion Mass Spectrum with $BrCl^-$. A mixture of chlorine/bromine and nitromethane was inlet to the ICR and the conditions optimized for $BrCl^-$ production. The $BrCl^-$ signal intensity shown is the maximum observed and was insufficient for photo-studies.

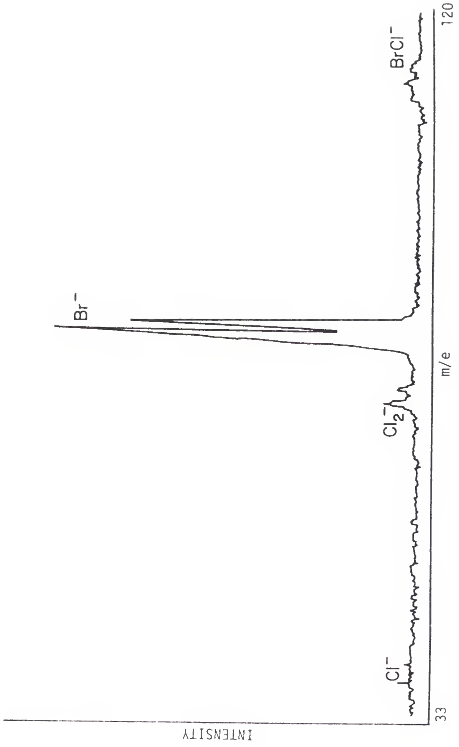
Cl⁻
Cl$_2^-$
Br⁻
BrCl⁻
33
m/e
120
INTENSITY

Table 12. Rate Coefficients for the Reaction of $Cl_2^-$ with $Br_2$.

| Reaction | Rate Coefficient (x $10^{-10}$ $cm^3$/molecule-sec) |
|---|---|
| $Cl_2^- + Br_2 \rightarrow Br_2^- + Cl_2$ | 1.8 |
| $\rightarrow Br_2Cl^- + Cl$ | 0.38 |
| $\rightarrow BrCl^- + BrCl$ | 0.16 |
| $\rightarrow BrCl_2^- + Br$ | 0.10 |

# CHAPTER V
# PHOTODETACHMENT STUDY OF THE ENOLATE ANION OF ACETOPHENONE

## Formation of the Enolate Anion

The enolate anion of acetophenone was produced by proton abstraction from the α-carbon of the neutral. This was accomplished via the acid-base reaction of acetophenone with a selected anion of greater gas phase basicity than the product enolate anion of acetophenone. Two anionic bases were used to abstract the proton, $OH^-$, produced from $H_2O$ by low energy electron impact and $F^-$, generated from $SO_2F_2$ also by electron impact.

The $OH^-$ anion is not produced directly upon electron impact with $H_2O$. Initially, $H^-$ is generated (119)

$$e^- + H_2O \longrightarrow H^- + OH. \qquad (61)$$

$H^-$ was not observed in this study since the minimum time-resolution of the pulsed ion cyclotron resonance mass spectrometer was insufficient to detect the extremely rapidly decaying parent ion. $H^-$ does react further with water (120)

$$H^- + H_2O \longrightarrow OH^- + H_2 \qquad (62)$$

producing $OH^-$. The $OH^-$anion was selected as the precursor anionic base for this study, because of the ease with which it could be produced, the simplicity of the negative ion mass spectrum of water and the large concentration of $OH^-$ which could be generated and trapped at the ion cell.

Electron attachment to sulfuryl fluoride produces $F^-$ in a single-step, dissociative attachment process. Nitrogen trifluoride also produces considerable $F^-$ upon electron impact, however, sulfuryl fluoride generates $F^-$ with markedly lower translational energy (121). For this reason, $F^-$ produced from surfuryl fluoride should produce fewer excited state secondary anions upon proton abstraction and $SO_2F_2$ was the source selected.

The enolate anion of acetophenone was efficiently produced using both anionic bases by the reaction

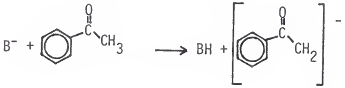

(63)

The enolate anion signal level for optimum conditions with $OH^-$ is reproduced in Figure 26. The negative ion mass spectrum of the acetophenone/base mixtures contained only the precursor anion and the acetophenone enolate anion (Figure 27).

## Photodetachment of the Enolate Anion

The photodetachment of the enolate anion of acetophenone was examined near threshold at differing delays between ion formation and ion irradiation and detection. The experimental conditions employed for the ion formation for each base are tabulated in Table 13. Laser irradiation preceded the detect pulse by 10 ms. The

Figure 26. Acetophenone Signal Intensity. The optimum acetophenone signal was obtained with $OH^-$ as the precursor for the spectrometer conditions: sample pressure, $2.0 \times 10^{-5}$ Torr, (1/10 mixture of acetophenone to $H_2O$), electron energy, 7.42 eV, detect delay, 170 msec, and detect width of 3.0 msec.

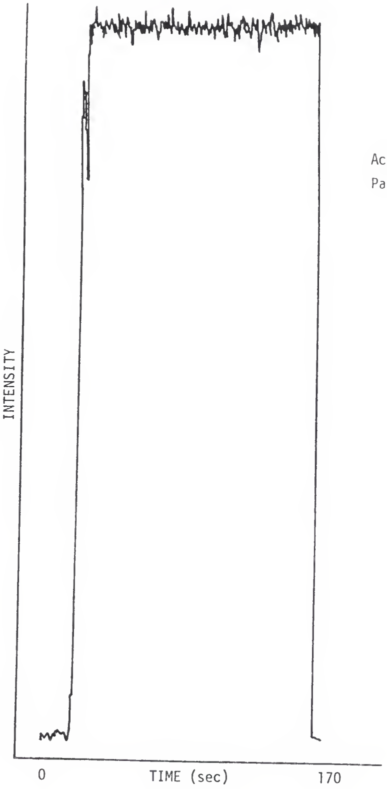

Acetophenone/$H_2O$
Partial Pressure Ratio 1/10

Figure 27. Photoreduction of the Enolate Anion. The most pronounced reduction of the acetophenone enolate anion signal level occurred at the peak of the first resonance. The anion reduction is about 70% at the maximum.

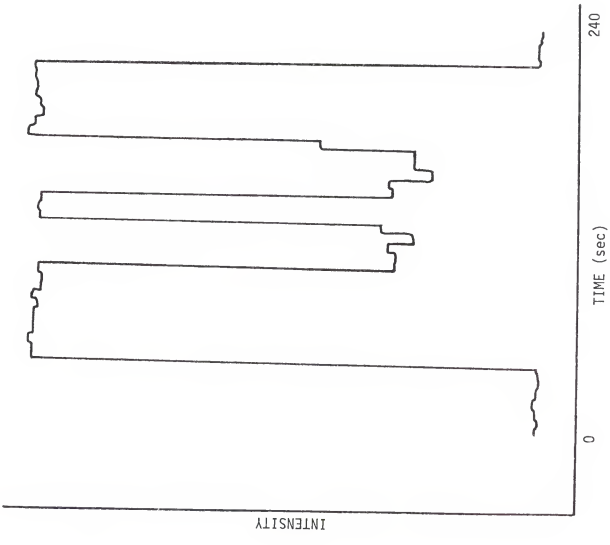
INTENSITY
TIME (sec)
0
240

Table 13. Values for Instrumental Parameters Pertinent to Acetophenone Anion Production and $OH^-$ and $F^-$ Precursor Anions.

| | $OH^-$ | $F^-$ |
|---|---|---|
| Filament Voltage | -7.22 V | -4.93 V |
| Filament Current | 1.5 A | 1.5 A |
| Trapping Plate Voltage | -1.75 V | -1.75 V |
| End, Upper, Lower Plate Voltage | +1.00 V | +1.00 V |
| Sample Pressure | $2x10^{-5}$ Torr | $3.5 \times 10^{-5}$ Torr |
| Partial Pressure Ratio (Acetophenone/Base) | 1/10 | 4/1 |
| Grid Pulse Width | 20 msec | 20 msec |
| Detect Delay | 150-200-250 msec | 100-200-250 msec |

observed photodetachment cross-section spectra are plotted in Figures 28-30 for the various detect delay times. The detect delays were limited at short and long times by the concentration of the acetophenone enolate anions. The anion signal peaked at 200 ms and was significantly lower below 150 ms and above 250 ms. The total pressure was maintained as accurately as possible throughout a photodetachment run to insure that the effects of collisions would not vary drastically. The photodetachment spectra indicate that the electron detachment process is not affected by collisions over the range that could be induced here.

## Analysis of the Acetophenone Enolate Anion Results

The photodetachment spectra of the acetophenone enolate anion indicate that a resonance occurs just above the threshold which is not affected by collisional de-excitation. The acetophenone anion has been studied and resonances have been observed throughout the near threshold region (121, 122). The analysis of these resonances indicated that they were attributable to electron-dipole resonances and not to different vibrational transitions between the anion and neutral states. These studies confirm this result as the first resonance above threshold is not influenced by delaying irradiation of the anion. The number of collisions is anticipated to vary by 35 to 40 over the range of detect delays at the pressures employed. The vibrational de-excitation is expected to be efficient, since the anion vibrational modes are not anticipated to be drastically

Figure 28. Photodetachment of Acetophenone at 150 ms Delay. Detect Delay time of 150 ms. Sample and spectrometer conditions as for Figure 26.

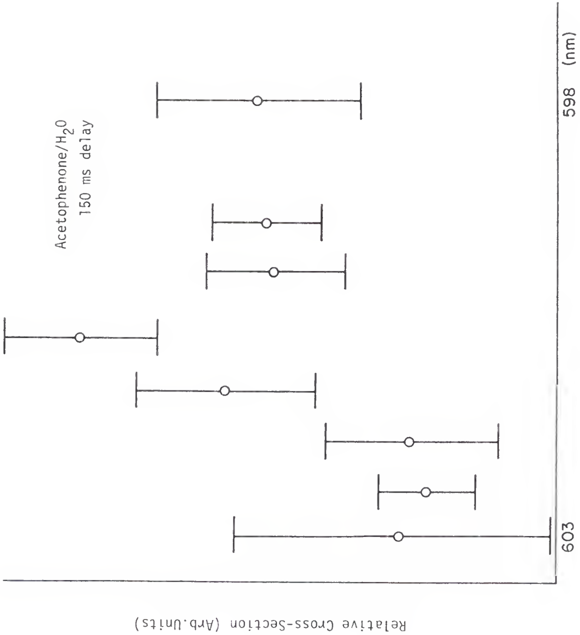
Acetophenone/$H_2O$
150 ms delay
598 (nm)
603
Relative Cross-Section (Arb.Units)

Figure 29. Photodetachment of Acetophenone at 200 ms Delay. Detect delay time of 200 ms. Sample and spectrometer conditions as for Figure 26.

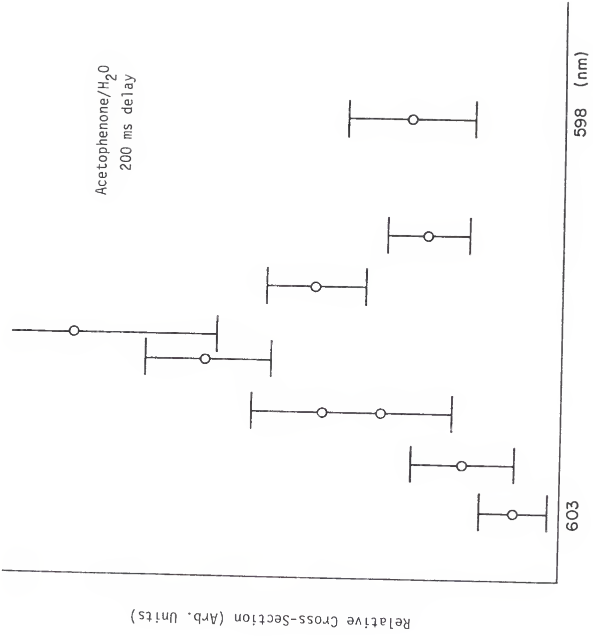
Acetophenone/$H_2O$
200 ms delay
603
598 (nm)
Relative Cross-Section (Arb. Units)

Figure 30. Photodetachment of Acetophenone at 250 ms Delay. Detect delay time of 250 ms. Sample and spectrometer conditions for Figure 26.

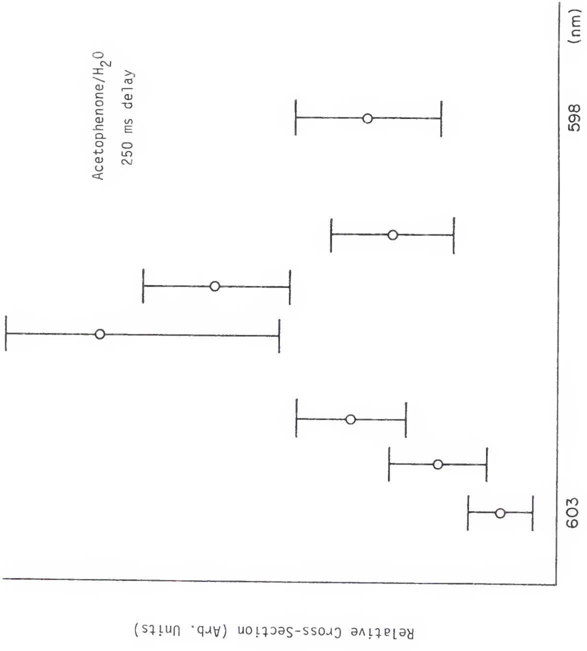
Acetophenone/$H_2O$
250 ms delay
603
598
(nm)
Relative Cross-Section (Arb. Units)

different from those of the neutral acetophenone. Consequently, it seems reasonable to agree with the previously reported results that the structure is due to electron-dipole resonances of the enolate anion. The electron affinity value taken from the wavelength at which a measurable reduction of the enolate anion occurs is 2.056 eV in excellent agreement with the reported value of 2.057 eV (122).

# CHAPTER VI
# SUMMARY

The investigation of negative ions has proved a complex, difficult , and perplexing problem. The rewards associated with performing such investigations have increased with the recognition of the significance of negative ions to a variety of scientific concerns. In this work, an ion cyclotron resonance mass spectrometer was employed as a negative ion source, containment device, and detector. Since the ions chosen for this study were known to exhibit small cross-sections for the transitions of interest, a tunable, flash-lamp-pumped dye laser system with a high output per pulse was employed. The possibility of time-resolved effects on negative ion spectra was investigated. In this study, no effects were observed but this in itself confirms the results of studies attributing structure to effects other than simple internal excitation.

This experimental technique allowed the observation of structure in the photodetachment cross-sections of the halogen molecular anions, $Cl_2^-$ and $Br_2^-$ . This structure was attributed to vibronic transitions between the ground state of the ankln and the neutral. The adiabatic electron affinity of chlorine is derived fron the assigned transitions, as 2.36 eV. This electron affinity has an error associated with the peak assignment of +0.27 and -0.32 eV. In the case of the bromine anion, the absence of structure due to the anion in the photodetachment cross-section of the bromine anion precludes the estimation of a reliable electron affinity. The experimental difficulties of operating with halogen compounds were marked and are reflected in the data; however, improvements in this area would necessitate an entirely different design of the apparatus.

For acetophenone, confirmation of the nature of the resonances near threshold was obtained. In addition, the electron affinity of the enolate anion was determined to be 2.056 eV in excellent agreement with earlier findings. This opens the possibility of differentiating between different sources of structure in photodetachment cross-section spectra.

The most significant result of this work has been the appearance of structure in the photodetachment of the chlorine anion. In order that this might be fully exploited the experimental design must be improved. The availability of high energy, excimer-pumped dye lasers is particularly significant. The optimization of the experiment is most critically dependent upon the level and quality of the source and the primitive dye laser system employed has been useful but is severely limited.

# APPENDIX I
# ON-BOARD MICROCOMPUTER HARDWARE MODIFICATIONS

The details of the modifications to the KIM-1 microcomputer are presented as a useful diagnostic. Memory chips (2102) are soldered on top of the on-board memory chips pin for pin with the exception of $\overline{CS}$, the chip select line, on each added memory chip (pin 13). The $\overline{CS}$ line of the eight 2102's comprising the additional 1K of RAM are tied together. The unmodified, on-board memory is selected by the K0 output of the KIM-1 8K decode chip (74 LS 145, pin 1) through the buffer/invertor (7404, pins 1 & 2). The direct K0 select is cut by clipping the input and output at the buffer/inverter, pins 1 & 2. A four-input NAND gate is mounted on top of the disabled 7404 with ground (pin 7) and power (pin 14) the only connections made to the NAND gate from the 7404 pins. K0 and K1 from the 8K decode chip are connected to the inputs of the four-input NAND gate. The K1 line must include a 560 $\Omega$ pull-up resistor tied to +5 volts. K0 is already supplied with an on-board pull-up resistor. The remaining NAND inputs are tied directly to the +5 volt line. The output of the four-input NAND gate is input to the 7400 AND gate. K1 is also connected to the chip select array of the add-on memory chips. Additional +5 volt supply and ground lines to the memory chips from the KIM-1 edge connector were added due to the increased current demands.

## APPENDIX II
## MICROCOMPUTER CONTROL REGISTERS

The control registers required for the data collection and analysis microcomputer system are given. Initial values are indicated.

| Hex Address | Description (Initial Value) |
|---|---|
| 00 | Main control register (00) |
| 01 | Number of zero levels (20) |
| 02 | Number of zero levels counter |
| 03 | One-half number of zero levels counter |
| 04 | Number of 100 levels per laser shot (08) |
| 05 | One-half number of 100's per laser shot |
| 06 | Number of laser shots (10) |
| 07 | Number of laser shots counter (10) |
| 08 | Index for average routines |
| 0A | Four-channel store base address (00) |
| 0C | Index storage for memory overlap (00) |
| 0D | Base address low for temporary storage (20) |
| 0E | Base address high for temporary storage (00) |
| 0F<br>10<br>11 | Storage for zero level (00) Running Sum |
| 12 | ID for the data to be averaged (00) |
| 14 | Index for final data store (00) |
| 15<br>16<br>17 | Dividend for three-byte average |
| 18 | Divisor for three-byte average |
| 19 | Programmable Interrupt Request (PIRQ) (00) |

| Hex Address | Description (Initial Value) |
|---|---|
| 1A | Index for four channel store |
| 1B | A/D high order byte |
| 1C | A/D low order byte |
| 40 | ID for data storage |
| 41 | Final data store low order address (00) |
| 42 | Final data store high order address (02) |
| 43 | Final data store index (00) |
| DB-DF | Registers for full 16-bit divide |

# APPENDIX III
# MICROCOMPUTER PROGRAMS

## Initialization Subroutine

```
Address   Label   Op Code   Mnemonic      Comment

0800      INIT    A9 00     LDA #00   ─┐
                  85 00     STA 00     │
                  85 1A     STA 1A     │
                  85 0A     STA 0A     │
                  85 0E     STA 0E     │
                  85 19     STA 19     │
                  A9 20     LDA #20    │
                  85 01     STA 01     │
0810              A9 08     LDA #08    ├──  Register Initialization
                  85 04     STA 04     │
                  A9 10     LDA # 10   │
                  85 06     STA 06     │
                  85 07     STA 07     │
                  A9 40     LDA #40    │
                  85 0D     STA 0D     │
                  A9 02     LDA #02    │
0820              85 0B     STA 0B    ─┘
          LOOP    A5 19     LDA 19    ─┐
                  F0 FC     BEQ FC     ├──  NOP Loop
                   78        SEI      ─┘
                  C6 19     DEC 19    ─┐
                  A5 02     LDA 02     │
                  D0 16     BNE 16     │
```

Appendix III. Microcomputer Programs (continued)

## Initialization Subroutine (continued)

```
Address   Label     Op Code    Mnemonic    Comment

                    A5 02      LDA 02      Determine if last zero has
                    D0 16      BNE 16      been taken
                    A5 0F      LDA 0F
                    85 15      STA 15
0831                A5 10      LDA 10
                    85 16      STA 16
                    A5 11      LDA 11      Perform zero average and
                    85 17      STA 17      Data Analysis
                    A5 01      LDA 01
                    85 18      STA 18
                    20 90 0B   JSR 0B90
0840                20 9A 0A   JSR 0A9A
          DISPLAY   A5 00      LDA 00
                    85 FA      STA FA
                    A9 00      LDA #00     Prompt Operator
                    85 FB      STA FB
                    4C 4F 1C   JMP 1C4F
                      58         CLI
084F                4C 22 08   JMP 0822
```

Appendix III. Microcomputer Programs (continued)

## Obtain Data and A/D Delay Subroutine

| Address | Label | Op Code | Mnemonic | Comment |
|---|---|---|---|---|
| 0852 | Ob & Del | 20 90 08 | JSR 0890 | Sets MUX to ICR Channel |
| | | 4C 5B 08 | JMP 985B | Jumps to Delay |
| | | 20 69 08 | JSR 0869 | Sets MUX to Photo Channel |
| | DELAY | A9 40 | LDA #40 | |
| | | 80 07 17 | STA 1707 | Sets Time for Delay & |
| 0860 | | 2C 97 17 | BIT 1707 | Checks for End of Delay Period |
| | | 10 FB | BPL 0860 | |
| | | 20 00 0A | JSR 0A00 | Jumps to Read A/D Subr. |
| 0868 | | 60 | RTS | |

Appendix III. Microcomputer Programs (continued)

## Multiplexer Select Photo Detector Subroutine

```
Address   Label       Op Code    Mnemonic     Comment

0869      MUX Photo   EA         NOP
                      EA         NOP
                      A9 5F      LDA #5F    ┐
                      8D 03 17   STA 1703   │
0870                  8D 01 17   STA 1701   ├─ Configure PADD's and PAD's
                      8D 00 17   STA 1700   │
                      8D 02 17   STA 1702   ┘
                      CE 00 17   DEC 1700      Drop inhibit
                      A9 53      LDA #5E    ┐
                      8D 02 17   STA 1702   │
0881                  A9 5F      LDA #5F    ├─ Toggle clock line PB0
                      8D 02 17   STA 1702   ┘
                      EE 00 17   INC 1700      Raise inhibit
                      A9 02      LDA #02    ┐
                      85 40      STA 40     ┘─ Set 'Type of Data' Flag
088D                  60         RTS
```

Appendix III. Microcomputer Programs (continued)

## Multiplexer Select Marginal Oscillator Subroutine

```
Address   Label     Op Code     Mnemonic
                                             Comment
088E      MUX MO    EA          NOP
                    EA          NOP
                    A9 5F       LDA #5F
                    8D 03 17    STA 1703
                    8D 01 17    STA 1701     Configure PADD's & PAD's
                    8D 02 17    STA 1702
                    A9 1F       LDA #1F
                    8D 00 17    STA 1700
                    CE 00 17    DEC 1700     Drop inhibit
                    A9 5E       LDA #5E
                    8D 02 17    STA 1702     Toggle clock line PB0
                    A9 5F       LDA #5F
                    8D 02 17    STA 1702
                    EE 00 17    INC 1700     Raise inhibit
                    A9 00       LDA #00
                    85 40       STA 40       Set 'Type of Data' Flag
08B4                60          RTS
```

Appendix III. Microcomputer Programs (continued)

Main Program

```
Address   Label    Op Code     Mnemonic     Comment
08D0      ID        A5 00      LDA 00    ┐
                    C9 01      CMP #01   │
                    90 08      BCC 08    │  Identifies the type of data
                    F0 08      BEQ 03    ├─ (zero, 100 or Laser) to be
                 4C 08 09      JMP 09DB  │  taken and routes accordingly
                 4C 1F 09      JMP 091F  ┘
          ZERO      A9 F1      LDA #F1   ┐  Sets interrupt vectors to
08E0             8D FE 17      STA 17FE  │  avoid ID & Zero for Zero
                    A9 08      LDA #08   ├─ points after the 1st, i.e.,
                 8D FF 17      STA 17FF  ┘  changes IV's to ZH, ZL
                    A5 01      LDA 01    ┐  Sets up running counters
                    85 02      STA 02    │  for total number of zeroes
                    A5 01      LOA 01    ├─ taken and half of total to
                      4A         LSR     │  be taken
                    85 03      STA 03    ┘
08F1      ZH, ZL 20 52 08      JSR 0852     Jumps to Obtain & Delay Subr.
                      18         CLC     ┐
                    A5 0F      LDA 0F    │
                    65 1C      ADC 1C    │
                    85 0F      STA 0F    │
                    A5 10      LDA 10    │
                    65 1B      ADC 1B    ├─ Maintains a running sum of
                    85 10      STA 10    │  Zero values
0901                A5 11      LDA 11    │
                    69 00      ADC #00   │
                    85 11      STA 11    ┘
```

Appendix III. Microcomputer Programs (continued)

Main Program (continued)

| Address | Label | Op Code | Mnemonic | Comment |
|---|---|---|---|---|
| | | C6 02 | DEC 02 | Decrements total and half total counters |
| | | C6 03 | DEC 03 | |
| | | F0 02 | BEQ 02 | If half total taken, skip return from interrupt and alter Interrupt Vectors (IV's) |
| | | 58 | CLI | |
| | | 40 | RTL | |
| | | E6 19 | INC 19 | Increment Int. Req. Flag |
| 0911 | ΔIV's | A9 D0 | LDA #D0 | Change Interrupt Vectors to ID |
| | | 8D FE 17 | STA 17FE | |
| | | A9 08 | LDA #08 | |
| | | 8D FF 17 | STA 17FF | |
| | | E6 00 | INC 00 | Increment ID Flag |
| | | 58 | CLI | |
| | | 40 | RTI | |
| 091F | | A9 2E | LDA #2E | Change Interrupt Vectors to 100 Data |
| 0921 | | 8D FE 17 | STA 17FE | |
| | | A9 09 | LDA #09 | |
| | | 8D FF 17 | STA 17FF | |
| | | A5 04 | LDA 04 | Sets Counter to one half of 100's per Laser Shot |
| | | 4A | LSR | |
| | | 85 05 | STA 05 | |
| 092E | | 20 52 08 | JSR 0852 | Jumps to Obt & Del |
| 0931 | | A4 0C | LDY 0C | Loads Y-register |
| | | A5 1C | LDA 1C | Stores LSB of 100 MO Data |
| | | 91 0D | STAy 0D | |

Appendix III. Microcomputer Programs (continued)

Main Program (continued)

| Address | Label | Op Code | Mnemonic | Comment |
|---|---|---|---|---|
| | | 88 | DEY | |
| | | 18 | CLC | |
| | | A9 10 | LDA #10 | Stores MSB of 100 and Data |
| 0940 | | 65 0D | ADC 0D | |
| | | 85 0D | STA 0D | |
| | | 20 58 08 | JSR 0858 | Jumps to 0b & Del |
| | | A5 1C | LDA 1C | Stores LSB of 100 Photo Data |
| | | 91 0D | STAy 0D | |
| | | C8 | INY | Stores MSB of 100 Photo Data |
| | | A5 1B | LDA 1B | |
| | | 91 0D | STAy 0D | |
| | | C8 | INY | |
| | | 38 | SEC | Changes Base Address to that for 100 MO Data |
| | | A5 0D | LDA 0D | |
| | | E9 10 | SBC #10 | |
| | | 85 0D | STA 0D | |
| | | 98 | TYA | Insures that Y-register ranges from 00 to 0F for overwrite of data |
| | | 29 0F | AND #0F | |
| | | 85 0C | STA 0C | |
| | | C6 05 | DEC 05 | Checks to derermine if one half of 100 data per laser pulse have been taken |
| | | F0 02 | BEQ 02 | |
| 0961 | | 58 | CLI | |
| | | 40 | RTI | |

Appendix III. Microcomputer Programs (continued)

Main Program (continued)

```
Address   Label   Op Code    Mnemonic         Comment

                  A5 07      LDA 07     ┐   Determines if any laser shots
                  C5 06      CMP 06     ├   have been taken, if so takes
                  90 20      BCC 0989   ┘   branch
0969                 EA        NOP
                     EA        NOP
                     EA        NOP
                     EA        NOP
                     EA        NOP
                     EA        NOP
                     EA        NOP
0970              4C 11 09   JMP 0911   —   Jumps to ΔIV's to ID
0973                 EA        NOP
                     EA        NOP
                  C6 00      DEC 00     —   Decrement ID Flag
                  C6 19      INC 19     —   Increment Interrupt Request Flag
                  A9 F1      LDA #F1    ┐
                  8D FE 17   STA 17FE   ├   Changes Interrupt Vector to ZH,ZL
                  A9 08      LDA #08    │
0980              8D FF 17   STA FF     ┘
                  A5 02      LDA 02     ┐
                  85 03      STA 03     ┘   Resets half zero counter
                     58        CLI
                     40        RTI
```

Appendix III. Microcomputer Programs (continued)

Main Program (continued)

```
Address    Label    Op Code     Mnemonic         Comment

0989                A9 00       LDA #00     ]
                    85 40       STA 40      ]-  Sets Laser/ICR flag to ICR
                    A5 04       LDA 04      ]
                    85 08       STA 08      ]-  Sets counter for 100 photo
0991                85 18       STA 18      ]   MO sums as well as division
                    A0 00       LDY #00
                     18          CLC
                    A5 15       LDA 15      ]
                    71 0D       ADCy 0D     |
                    85 15       STA 15      |
                     C8          INY        |
                    A5 16       LDA 16      |
                    71 0D       ADCy 0D     |
09A1                85 16       STA 16      |-  Sums the eight 100 MO Data
                    A9 00       LDA #00     |   per laser pulse
                    65 17       ADC 17      |
                    85 17       STA 17      |
                     C8          INY        |
                    C6 08       DEC 08      |
                    D0 E7       BNE E7      ]
                    20 90 0B    JSR 0B90        Jumps to 3-byte Avg.
09B1                20 50 0A    JSR 0A50        Jumps to STORE
                     18          CLC
```

Appendix III. Microcomputer Programs (continued)

Main Program (continued)

```
Address    Label    Op Code     Mnemonic    Comment

                    A9 10       LDA #10
                    64 0D       ADC 0D      Alters Base Address to that
09B9                85 0D       STA 0D      for Photo Data 100
                    A9 02       LDA #02
                    85 40       STA 40      Sets Laser/ICR Flag to Laser
                    E6 12       INC 12
09C1                A5 12       LDA 12      Sets Laser/MO Avg. Flag to
                    C9 01       CMP #01     Laser
                    F0 C6       BEQ C6      Returns to Avg. Laser
                    C6 12       DEC 12      Resets Laser/MO Avg. Flag to 0
                    C6 12       DEC 12
                    A5 0D       LDA 0D
                    E9 20       SBC #20
                    85 0D       STA 0D
09D1                A5 07       LDA 07
                    D0 03       BNE 03      Checks for final laser shot
                    4C 73 09    JMP 0973    Sets up for final four 100's
                    4C 69 09    JMP 0969    Jump to change IV's to ID
09DB                20 B1 0B    JSR 0BB1    Jump to Laser Trigger Subr.
                    20 52 08    JSR 0852
09E1                20 50 0A    JSR 0A50    Obtain and store laser M.O and
                    20 58 08    JSR 0858    Photo data
                    20 50 0A    JSR 0A50
```

Appendix III. Microcomputer Programs (continued)

Main Program (continued)

| Address | Label | Op Code | Mnemonic | Comment |
|---|---|---|---|---|
| | | EA | NOP | |
| | | EA | NOP | |
| | | EA | NOP | |
| | | EA | NOP | |
| | | C6 07 | DEC 07 | Decrement Laser Counter |
| 09F0 | | A9 1F | LDA #1F | |
| | | 8D FE 17 | STA 17F6 | |
| | | A9 09 | LDA #09 | Change IV's to 100 Data |
| | | 8D FF 17 | STA 17FF | |
| | | C6 00 | DEC 00 | Decrement ID Flag |
| | | 58 | CLI | |
| 09FD | | 40 | RTI | |

Appendix III. Microcomputer Programs

## A/D Subroutine

```
Address   Label      Op Code     Mnemonic      Comment

0A00      Read A/D   A9 0F       LDA #0F
                     80 01 17    STA 1701      Configure PADD and PBDD
                     A9 FE       LDA #FE
                     8D 03 17    STA 1703
                     A9 03       LDA #03
                     8D 00 17    STA 1700
                     CE 00 17    DEC 1700
                     AD 00 17    LDA 1700
                     85 1D       STA 1D        Read the Most Significant
                     AD 02 17    LDA 1702      Nibble
                     85 1E       STA 1E
                     EE 00 17    INC 1700
0A21                 4A          LSR
                     4A          LSR
                     4A          LSR
                     4A          LSR
                     4A          LSR
                     0A          ASL           Format the Most Significant
                     85 1D       STA 1D        Nibble
                     A9 01       LDA #01
                     25 1E       AND 1E
                     05 1D       ORA 1D
                     85 1B       STA 1B
```

Appendix III. Microcomputer Programs (continued)

A/D Subroutine (continued)

| Address | Label | Op Code | Mnemonic | Comment |
|---|---|---|---|---|
| | | A9 05 | LDA #05 | Read the Next Most Significant Nibble |
| | | 8D 00 17 | STA 1700 | |
| | | CE 00 17 | DEC 1700 | |
| | | AD 00 17 | LDA 1700 | |
| | | 85 1D | STA 1D | |
| 0A3E | | AD 02 17 | LDA 1702 | |
| | | 46 87 08 | JMP 0887 | |
| | | 85 1E | STA 1E | |
| | | EE 00 17 | INO 1700 | |
| | | A9 E0 | LDA #E0 | Format the Next Most Significant Nibble |
| | | 25 1D | AND 1D | |
| | | 85 1D | LDA 1E | |
| | | 0A | ASL | |
| | | 0A | ASL | |
| | | 0A | ASL | |
| | | 0A | ASL | |
| 08B7 | | 85 1E | STA 1E | |
| | | A9 10 | LDA #10 | |
| | | 25 1E | AND 1E | |
| | | 05 1D | AND 1E | |
| | | 85 1C | STA 1C | |

Appendix III. Microcomputer Programs (continued)

A/D Subroutine (continued)

| Address | Label | Op Code | Mnemonic | Comment |
|---|---|---|---|---|
| | | A9 07 | LDA #07 | Read the Least Significant Nibble |
| 08D6 | | 8D 00 17 | STA 1700 | |
| 0BE7 | | CE 00 17 | DEC 1700 | |
| | | AD 00 17 | LDA 1700 | |
| | | 85 1D | STA 1D | |
| | | AD 02 17 | LDA 1702 | |
| | | 85 1E | STA 1E | |
| | | EE 00 17 | INC 1700 | |
| | | A5 1D | LDA 1D | Format the Least Significant Nibble |
| | | 4A | LSR | |
| | | 4A | LSR | |
| | | 4A | LSR | |
| | | 4A | LSR | |
| | | 4C 81 0B | JMP 0B81 | |
| 0B81 | | 4A | LSR | |
| | | 0A | ASL | |
| | | 85 1D | STA 1D | |
| | | A9 01 | LDA #01 | |
| | | 25 1E | AND 1E | |
| | | 05 1D | ORA 1D | Combine the Two Least Significant Nibbles into the Low Order Byte |
| | | 05 1C | ORA 1C | |
| | | 85 1C | STA 1C | |
| | | 60 | RTS | |

Appendix III. Microcomputer Programs (continued)

Data Analysis Storage Subroutine

| Address | Label | Op Code | Mnemonic | Comment |
|---|---|---|---|---|
| 0A9A | | A6 14 | LDX 14 | |
| | | 38 | SEC | |
| | | B5 50 | LDAx 50 | Subtract Zero Baseline from Laser MO Levels |
| | | E5 1C | SBC 1C | |
| 0AA1 | | 85 DD | STA DD | |
| | | E8 | INX | |
| | | B5 50 | LDAx 50 | |
| | | E5 1B | SBC 1B | |
| | | 85 DC | STA DC | |
| | | CA | DEX | |
| | | 38 | SEC | |
| | | B5 70 | LDAx 70 | Subtract Zero Baseline from 100 MO Levels |
| | | E5 1C | SBC 1C | |
| 0AB0 | | 85 DF | STA DF | |
| | | E8 | INX | |
| | | B5 70 | LDAx 70 | |
| | | E5 1B | SBC 1B | |
| | | 85 DE | STA DE | |
| | | A9 04 | LDA #04 | Perform 16 bit Division and Reformat the Result |
| | | 85 DB | STA DB | |
| | | 86 14 | STX 14 | |
| | | 20 00 0B | JSR 0B00 | |
| 0AC2 | | 20 C2 03 | JSR 0302 | |
| | | EA | NOP | |
| | | EA | NOP | |

Appendix III. Microcomputer Programs (continued)

Data Analysis **Storage** Subroutine (continued)

| Address | Label | Op Code | Mnemonic | Comment |
|---|---|---|---|---|
| | | EA | NOP | |
| | | EA | NOP | |
| | | 7 EA's | NOP | |
| 0AD0 | | A6 14 | LDX 14 | Store the Result |
| | | 95 50 | STAx 50 | |
| | | CA | DEX | |
| | | A5 D2 | LDA D2 | |
| | | 95 50 | STA 50 | |
| | | 38 | SEC | |
| | | B5 90 | LDAx 90 | Subtract 100 Photodetector Level from Laser Photodetector Level |
| | | F5 B0 | SBCx B0 | |
| | | 95 70 | STAx 70 | |
| 0AE0 | | E8 | INX | |
| | | B5 90 | LDAx 90 | |
| | | F5 B0 | SBCx B0 | |
| | | 95 70 | STAx 70 | |
| | | E8 | INX | |
| | | E0 20 | CPX #20 | Test for Finish |
| | | 90 50 | BCC 0A9B | |
| | | A2 00 | LDX #00 | |
| 0AF0 | | B5 50 | LDAx 50 | |
| | | 91 41 | STA 41,Y | |

Appendix III. Microcomputer Programs (continued)

Data Analysis Storage Subroutine (continued)

| Address | Label | Op Code | Mnemonic | Comment |
|---|---|---|---|---|
| | | C8 | INY | |
| | | E8 | INX | |
| | | E0 40 | CPX #40 | Shift the results to the permanent storage area |
| | | 90 F6 | BCC F6 | |
| | | 84 43 | STY 43 | |
| 0AFC | | 60 | RTS | |

Appendix III. Microcomputer Programs (continued)

### Four/Channel Intermediate Storage Subroutine

| Address | Label | Op Code | Mnemonic | Comment |
|---|---|---|---|---|
| 0A50 | | 18 | CLC | Data Routing |
| | | A5 40 | LDA 40 | |
| | | 64 00 | ADC 00 | |
| | | 85 00 | STA 40 | |
| | | C9 03 | CMP #03 | |
| | | 90 10 | BCC 10 | |
| | | F0 07 | BEQ 07 | |
| | | A9 90 | LDA #90 | Set Laser Photodetector Vector |
| | | 85 0A | STA 0A | |
| 0A61 | | 4C 7A 0A | JMP 0A7A | |
| | | A9 B0 | LDA #B0 | Set 100 Photodetector Vector |
| | | 85 0A | STA 0A | |
| | | 4C 7A 0A | JMP 0A7A | |
| | | C9 02 | CMP #02 | Data Routing Flag |
| | | 90 07 | BCC 07 | |
| | | A9 50 | LDA #50 | Set Laser MO Vector |
| 0A71 | | 85 0A | STA 0A | |
| | | 4C 7A 0A | JMP 0A7A | |
| | | A9 70 | LDA #70 | Set 100 MO Vector |
| | | 85 0A | STA 0A | |

Appendix III. Microcomputer Programs (continued)

Four/Channel Intermediate Storage Subroutine (continued)

| Address | Label | Op Code | Mnemonic | Comment |
|---|---|---|---|---|
| 0A7A | | A4 1A | LDY 1A | |
| | | A5 1C | LDA 1C | |
| | | 91 0A | STAy 0A | |
| 0A80 | | C8 | INY | |
| | | A5 1B | LDA 1B | |
| | | 91 0A | STAy 0A | |
| | | A5 40 | LDA 40 | |
| | | C9 03 | CMD #03 | Vector Storage of Data |
| | | F0 02 | BEQ 02 | |
| | | 88 | DEY | |
| | | 88 | DEY | |
| | | C8 | INY | |
| | | 98 | TYA | |
| | | 85 1A | STA 1A | |
| 0A91 | | 60 | RTS | |

Appendix III. Microcomputer Programs (continued)

Triple Precision Average Subroutine

```
Address   Label   Op Code    Mnemonic    Comment

0B90              46 28      LSR 18      Test for Finish
                  B0 0A      BCS 0A
                  46 17      LSR 17      Divide by two
                  66 16      ROR 16
                  66 15      ROR 15
                    18         CLC       Repeat Division
                  4C 90 0B   JMP 0B90
                  A5 15      LDA 15      Store result and initialize
0BA0              85 1C      STA 1C      the Average Registers
                  A5 16      LDA 16
                  85 1B      STA 1B
                  A9 00      LDA #00
                  85 15      STA 15
                  85 16      STA 16
                  85 17      STA 17
                  85 18      STA 18
0BB0                60         RTS
```

Appendix III. Microcomputer Programs (continued)

## Laser Trigger Subroutine

| Address | Label | Op Code | Mnemonic | Comment |
|---|---|---|---|---|
| 0BB1 | | A9 9F | LDA #9F | Configure PADD and PBDD |
| | | 8D 01 17 | STA 1701 | |
| | | 8D 03 17 | STA 1703 | |
| | | 8D 02 17 | STA 1702 | Configure PAD and PBD |
| | | 8D 00 17 | STA 1700 | |
| | | CE 00 17 | DEC 1700 | Lower the Inhibit |
| | | A9 9E | LDA #9E | Hold clock line high |
| | | 8D 02 17 | STA 1702 | |
| | | A9 0E | LDA #0E | Hold pulse line low |
| | | 8D 00 17 | STA 1700 | |
| | | A9 7F | LDA #7F | Pulse Duration Loop |
| | | 8D 05 17 | STA 1705 | |
| | | 2C 07 17 | BIT 1707 | |
| | | 10 FB | BPL FB | |
| | | A9 8E | LDA #8E | Raise pulse line |
| | | 8D 11 17 | STA 1700 | |
| | | A9 9F | LDA #9F | Raise clock line |
| | | 8D 02 17 | STA 1702 | |
| | | EE 00 17 | INC 1700 | Raise inhibit |
| 0BE3 | | 60 | 60 | |

Appendix III. Microcomputer Programs (continued)

### Twelve Significant Bit Shift Subroutines

| Address | Label | Op Code | Mnemonic | Comment |
|---|---|---|---|---|
| 03C2 | Begin | A5 D3 | LDA D3 | Shifts the output of the Double Precision Divide Routine into the standard two byte format |
| | | D0 13 | BNE 13 | |
| 03C6 | D2 | A5 D2 | LDA D2 | |
| | | 30 1E | BMI 1E | |
| | | A9 00 | LDA #00 | |
| | | 85 D9 | STA D9 | |
| | | 06 D4 | RSL D4 | |
| | | 26 D5 | ROL D5 | |
| | | 26 D2 | ROL D2 | |
| | | E6 D8 | INC D8 | |
| | | 4C 06 03 | JMP 03C6 | |
| | D3 | A9 07 | LDA #07 | |
| | | 85 D9 | STA D9 | |
| | | 46 D3 | LSR D3 | |
| | | 66 D2 | ROR D2 | |
| | | 66 D5 | ROR D5 | |
| | | E6 D8 | INC D8 | |
| | | 4C C2 03 | JMP 03C2 | |
| | STO | 18 | CLC | |
| | | A5 D8 | LDA D8 | |
| | | 65 D9 | ADC D9 | |
| | | 85 D8 | STA D8 | |
| | | A5 D5 | LDA D5 | |
| | | 29 F0 | AND #F0 | |
| | | 05 D8 | ORA D8 | |
| | | 85 D5 | STA D5 | |
| | | 60 | RTS | |

Appendix III. Microcomputer Programs (continued)

## Double Precision Divide Subroutine

```
Address     Label     Op Code     Mnemonic              Comment

0B00                  A2 DA       LDX DA
                      A9 00       LDA 00
                      95 00       STA 00
                        CA          DEX
                      E0 D1       CPX D1
                      D0 F9       BNE 0B04                  DB 02    04    06    08
                        AA          TAX
                        36          SEC                 D3 D2 . D5 D4 D7 D6 D9 D8
                      26 D6       ROL D6                      ______________________
                      26 D7       ROL D7      DC   DD  | DE DF
                      A5 DC       LDA DC
                      30 10       BMI 0825
                      26 D6       ROL D6
                      A5 DC       LDA DC
                      D0 F0       BNE 0B11
                      A5 DD       LDA DD
                      D0 EC       BNE 0B11
                      A5 DE       LDA DE
                      B0 0E       BCS 2A37
                      C5 DC       CMP DC
                      90 35       BCC 0B62
                      F0 02       BEQ 0B31
                      B0 06       BCS 0B37
                      A5 DF       LDA DF
```

Appendix III. Microcomputer Programs (continued)

Double Precision Divide Subroutine (continued)

| Address | Label | Op Code | Mnemonic | Comment |
|---|---|---|---|---|
| | | C5 DD | CMP DD | |
| | | 70 2B | FCC 0B62 | |
| | | A5 DF | LDA DF | |
| | | E5 DD | SBC DD | |
| | | B0 0D | STA DF | |
| | | B0 0D | BCS 0B4C | |
| | | A5 DE | LDA BE | |
| | | E5 01 | SBC 01 | |
| | | 38 | SEC | |
| | | E5 DC | SBC DC | |
| | | 65 DE | STA DE | |
| | | 16 | CLC | |
| | | A5 DE | LDA DE | |
| | | 38 | SEC | |
| | | E5 DC | SBC DC | |
| | | 65 DE | STA DE | |
| | | 16 | CLC | |
| | | B5 D2 | LDA D2 | |
| | | 65 D6 | ADC D6 | |
| | | 95 D2 | STA D2 | |
| | | E6 | INX | |
| | | B5 D2 | LDA D2 | |
| | | 65 D7 | ADC D7 | |
| | | 95 D2 | STA D2 | |
| | | CA | DEX | |

Appendix III. Microcomputer Programs (continued)

Double Precision Divide Subroutine (continued)

| Address | Label | Op Code | Mnemonic | Comment |
|---|---|---|---|---|
| 0B62 | | 46 D7 | LSR D7 | |
| | | F0 05 | BEQ 0B6B | |
| | | 66 D6 | RCR D6 | |
| | | 4C 79 2A | JMP 0B79 | |
| | | 66 D6 | ROR D6 | |
| | | D0 0A | BNE 0B79 | |
| | | E6 | INX | |
| | | E6 | INX | |
| | | E4 DB | CPX DB | |
| | | F0 0B | BEQ 0B80 | |
| | | A9 80 | LDA 80 | |
| | | 65 D7 | STA D7 | |
| | | 06 DF | ASL DF | |
| | | 26 DE | ROL DE | |
| | | B8 | CLU | |
| | | 50 A5 | BVC 0B25 | |
| 0B80 | | 10 | RTS | |

## Appendix IV. Sample Preparation

Samples were prepared in standard pyrex bulbs fitted with ground glass or teflon vacuum stopcocks. All samples condensed at liquid nitrogen temperature (77K) and consequently could undergo freeze-pump-thaw cycles to remove volatile impurities. The sample bulbs were initially pumped down to 20 microns and filled on a glass vacuum line. Pressures were measured by a cold cathode gauge and an eight-inch Bourdon type differential pressure gauge. Final freeze-pump-thaw purification was performed on the ICR low vacuum manifold and was done prior to each use of the sample.

Acetophenone, nitromethane (Baker Chemical Co.) and water are liquids and were introduced as such into the sample bulbs. The vapor pressure of each was sufficient to maintain the necessary pressures at the jeweled leak valves and the ion cell. Bromine (Baker Chemical Co.) is liquid at room temperature; however, the sample was made up to the vapor pressure of bromine to facilitate mixing with chlorine at a constant ratio with sample use. Chlorine (Matheson) was obtained as 99% pure gas. No special preparation was involved other than freeze-pump-thaw purification. Sulfuryl fluoride (Matheson) was treated in the same manner.

In an attempt to increase the number of bromine monochloride anions generated, a mixture of bromine and chlorine was irradiated with a 450 watt quartz envelope Hg lamp to insure that an equilibrium mixture was being inlet to the ion generation region (117). A 50-50 mixture of bromine and chlorine was made up in the standard manner. The sample was then irradiated for 2 hours. As noted in the main text, no improvement in the $BrCl^-$ signal intensity was observed.

# APPENDIX V

# RKR POTENTIAL ENERGY CURVES AND FRANCK-CONDON FACTORS FOR $Cl_2$-$Cl_2^-$

## Appendix Va. Potential Energy Curves

```
********** MOLECULAR CHLORINE AND MOLECULAR CHLORINE ANION ***********
********** ************* F-C OVERLAP FACTORS ****************************

 THE FOLLOWING DATA PERTAIN TO THE LOWER STATE.   STATE NUMBER IS 10

FJ =   0.0

ZMU =   0.174768513D 02

DE =   0.202759762D 05

TE = -0.279222224D 03

LIM1 =     0.50000D 00

LIM2 =     0.50000D 01



 THE INPUT POTENTIAL POINTS AND ENERGIES ARE GIVEN BELOW.
          R                           PE

0.500000000D 00          0.514292116D 07
0.560477835D 00          0.347699831D 07
0.620955671D 00          0.307740324D 07
0.681433506D 00          0.237328646D 07
0.741911342D 00          0.183071620D 07
0.802389177D 00          0.141021963D 07
0.862867013D 00          0.108433834D 07
0.923344848D 00          0.931817873D 06
0.983822684D 00          0.636204600D 06
0.104430052D 01          0.484758759D 06
0.110477835D 01          0.367612970D 06
0.116525619D 01          0.277121080D 06
0.122573403D 01          0.207354564D 06
0.128621186D 01          0.153713200D 06
0.134668970D 01          0.112624212D 06
```

Appendix Va. Potential Energy Curves (con't)

| R | PE | R | PE |
|---|---|---|---|
| 0.1407167530D 01 | 0.2130955800D 05 | 0.1883100015D 01 | 0.1108715090D 04 |
| 0.1467645370D 01 | 0.5760792660D 05 | 0.1894086770D 01 | 0.8335724830D 03 |
| 0.1528123200D 01 | 0.3063311520D 05 | 0.1910063620D 01 | 0.5570737680D 03 |
| 0.1588601040D 01 | 0.2666998750D 05 | 0.1931647900D 01 | 0.2792222400D 03 |
| 0.1649078870D 01 | 0.1709027170D 05 | 0.1947449240D 01 | 0.1397901180D 03 |
| 0.1709556710D 01 | 0.1223356370D 05 | 0.1987539650D 01 | 0.0 |
| 0.1711966910D 01 | 0.1006303660D 05 | 0.2030558230D 01 | 0.1397901180D 03 |
| 0.1714430920D 01 | 0.9840874250D 04 | 0.2049295820D 01 | 0.2792222400D 03 |
| 0.1716950590D 01 | 0.9617088080D 04 | 0.2076776840D 01 | 0.5570737680D 03 |
| 0.1719528060D 01 | 0.9391689230D 04 | 0.2098682890D 01 | 0.8335724830D 03 |
| 0.1722165530D 01 | 0.9164683780D 04 | 0.2117731380D 01 | 0.1108715090D 04 |
| 0.1724865430D 01 | 0.8936037210D 04 | 0.2134973040D 01 | 0.1382497970D 04 |
| 0.1727630360D 01 | 0.8705924970D 04 | 0.2150945950D 01 | 0.1654917260D 04 |
| 0.1730463170D 01 | 0.8474182210D 04 | 0.2165969390D 01 | 0.1925968780D 04 |
| 0.1733366920D 01 | 0.8240878860D 04 | 0.2180251200D 01 | 0.2195648100D 04 |
| 0.1736344960D 01 | 0.8006024600D 04 | 0.2193935690D 01 | 0.2463950550D 04 |
| 0.1739400920D 01 | 0.7769628920D 04 | 0.2207127950D 01 | 0.2730871180D 04 |
| 0.1742538780D 01 | 0.7531701070D 04 | 0.2219907320D 01 | 0.2996404830D 04 |
| 0.1745762870D 01 | 0.7292250120D 04 | 0.2232335530D 01 | 0.3260546120D 04 |
| 0.1749077970D 01 | 0.7051284940D 04 | 0.2244461740D 01 | 0.3523289420D 04 |
| 0.1752489310D 01 | 0.6808814170D 04 | 0.2256325930D 01 | 0.3784628590D 04 |
| 0.1756002650D 01 | 0.6564846300D 04 | 0.2267961120D 01 | 0.4044558540D 04 |
| 0.1759624370D 01 | 0.6319389610D 04 | 0.2279395040D 01 | 0.4303072090D 04 |
| 0.1763361570D 01 | 0.6072452200D 04 | 0.2290651270D 01 | 0.4560163120D 04 |
| 0.1767222110D 01 | 0.5824041980D 04 | 0.2301750080D 01 | 0.4815825010D 04 |
| 0.1771214840D 01 | 0.5574166700D 04 | 0.2312709100D 01 | 0.5070050930D 04 |
| 0.1775349650D 01 | 0.5322833890D 04 | 0.2323543770D 01 | 0.5322833890D 04 |
| 0.1779637770D 01 | 0.5070050930D 04 | 0.2334267780D 01 | 0.5574166700D 04 |
| 0.1784091920D 01 | 0.4815825010D 04 | 0.2344893340D 01 | 0.5824041980D 04 |
| 0.1788726650D 01 | 0.4560163120D 04 | 0.2355431420D 01 | 0.6072452200D 04 |
| 0.1793558730D 01 | 0.4303072090D 04 | 0.2365891960D 01 | 0.6319389610D 04 |
| 0.1798607630D 01 | 0.4044558540D 04 | 0.2376284010D 01 | 0.6564846300D 04 |
| 0.1803896190D 01 | 0.3784628590D 04 | 0.2386615880D 01 | 0.6808814170D 04 |
| 0.1809451370D 01 | 0.3523289420D 04 | 0.2396895220D 01 | 0.7051284940D 04 |
| 0.1815305670D 01 | 0.3260546120D 04 | 0.2407129150D 01 | 0.7292250120D 04 |
| 0.1821498190D 01 | 0.2996404830D 04 | 0.2417324300D 01 | 0.7531701070D 04 |
| 0.1828077740D 01 | 0.2730871180D 04 | 0.2427486910D 01 | 0.7769628920D 04 |
| 0.1835105440D 01 | 0.2463950550D 04 | 0.2437622860D 01 | 0.8006024600D 04 |
| 0.1842660150D 01 | 0.2195648100D 04 | 0.2447737720D 01 | 0.8240878860D 04 |
| 0.1850846500D 01 | 0.1925968780D 04 | 0.2457836790D 01 | 0.8474182210D 04 |
| 0.1859806390D 01 | 0.1654917260D 04 | 0.2467925170D 01 | 0.8705924970D 04 |
| 0.1869753280D 01 | 0.1382497970D 04 | 0.2478007750D 01 | 0.8936037210D 04 |

Appendix Va. Potential Energy Curves (con't)

| R | PE | R | PE |
|---|---|---|---|
| 0.246808926D 01 | 0.915463575D 04 | 0.344934188D 01 | 0.213973513D 05 |
| 0.249317430D 01 | 0.979123428D 04 | 0.347395550D 01 | 0.214854223D 05 |
| 0.250826733D 01 | 0.981703803D 04 | 0.349856912D 01 | 0.215663214D 05 |
| 0.251837274D 01 | 0.994097425D 04 | 0.352318274D 01 | 0.216403609D 05 |
| 0.252349435D 01 | 0.100630366D 05 | 0.354779636D 01 | 0.217078461D 05 |
| 0.253863790D 01 | 0.102935637D 05 | 0.357240998D 01 | 0.217690755D 05 |
| 0.256325153D 01 | 0.108316568D 05 | 0.359702361D 01 | 0.218243403D 05 |
| 0.259786515D 01 | 0.113587953D 05 | 0.362163723D 01 | 0.218739242D 05 |
| 0.261247877D 01 | 0.118739283D 05 | 0.364625085D 01 | 0.219181035D 05 |
| 0.263709233D 01 | 0.123763797D 05 | 0.367086447D 01 | 0.219571469D 05 |
| 0.266170601D 01 | 0.128653850D 05 | 0.369547809D 01 | 0.219913150D 05 |
| 0.268631963D 01 | 0.133410855D 05 | 0.372009171D 01 | 0.220208608D 05 |
| 0.271093325D 01 | 0.138025159D 05 | 0.374470533D 01 | 0.220460293D 05 |
| 0.273554687D 01 | 0.142495961D 05 | 0.376931895D 01 | 0.220670577D 05 |
| 0.276016049D 01 | 0.146821229D 05 | 0.379393257D 01 | 0.220841753D 05 |
| 0.278477411D 01 | 0.150999627D 05 | 0.381854619D 01 | 0.220976037D 05 |
| 0.280938773D 01 | 0.155031443D 05 | 0.384315981D 01 | 0.221075566D 05 |
| 0.283400136D 01 | 0.158913546D 05 | 0.386777344D 01 | 0.221142400D 05 |
| 0.285861498D 01 | 0.162649282D 05 | 0.389238706D 01 | 0.221178525D 05 |
| 0.288322860D 01 | 0.166238469D 05 | 0.391700068D 01 | 0.221185848D 05 |
| 0.290784222D 01 | 0.169682325D 05 | 0.394161430D 01 | 0.221166206D 05 |
| 0.293245584D 01 | 0.172932425D 05 | 0.396622792D 01 | 0.221121362D 05 |
| 0.295706946D 01 | 0.176140661D 05 | 0.399084154D 01 | 0.221053007D 05 |
| 0.298168308D 01 | 0.179159206D 05 | 0.401545516D 01 | 0.220962764D 05 |
| 0.300629670D 01 | 0.182040475D 05 | 0.404006878D 01 | 0.220852194D 05 |
| 0.303091032D 01 | 0.184787099D 05 | 0.406468240D 01 | 0.220722756D 05 |
| 0.305552394D 01 | 0.187401888D 05 | 0.408929602D 01 | 0.220575900D 05 |
| 0.308013757D 01 | 0.189887811D 05 | 0.411390965D 01 | 0.220412973D 05 |
| 0.310475119D 01 | 0.192247968D 05 | 0.413852327D 01 | 0.220235272D 05 |
| 0.312936481D 01 | 0.194435568D 05 | 0.416313689D 01 | 0.220044032D 05 |
| 0.315397843D 01 | 0.196603910D 05 | 0.418775051D 01 | 0.219840429D 05 |
| 0.317859205D 01 | 0.198506362D 05 | 0.421236413D 01 | 0.219625583D 05 |
| 0.320320567D 01 | 0.200496343D 05 | 0.423697775D 01 | 0.219402560D 05 |
| 0.322781929D 01 | 0.202277312D 05 | 0.426159137D 01 | 0.219166370D 05 |
| 0.325243291D 01 | 0.203952751D 05 | 0.428620499D 01 | 0.218923973D 05 |
| 0.327704653D 01 | 0.205526152D 05 | 0.431081861D 01 | 0.218674279D 05 |
| 0.330166015D 01 | 0.207001004D 05 | 0.433543223D 01 | 0.218418150D 05 |
| 0.332627377D 01 | 0.208380788D 05 | 0.436004586D 01 | 0.218156359D 05 |
| 0.335088740D 01 | 0.209668960D 05 | 0.438465948D 01 | 0.217889797D 05 |
| 0.337550102D 01 | 0.210868949D 05 | 0.440927310D 01 | 0.217619071D 05 |
| 0.340011464D 01 | 0.211984148D 05 | 0.443388672D 01 | 0.217344904D 05 |
| 0.342472826D 01 | 0.213017903D 05 | | |

Appendix Va. Potential Energy Curves (con't)

| R | PE |
|---|---|
| 0.445850034D 01 | 0.217067943D 05 |
| 0.449311396D 01 | 0.216788793D 05 |
| 0.450772758D 01 | 0.216508024D 05 |
| 0.453234120D 01 | 0.216226168D 05 |
| 0.455695482D 01 | 0.215943726D 05 |
| 0.458156844D 01 | 0.215661165D 05 |
| 0.460618206D 01 | 0.215378921D 05 |
| 0.463079569D 01 | 0.215097399D 05 |
| 0.465540931D 01 | 0.214816977D 05 |
| 0.468002293D 01 | 0.214538005D 05 |
| 0.470463655D 01 | 0.214260807D 05 |
| 0.472925017D 01 | 0.213985684D 05 |
| 0.475386379D 01 | 0.213712909D 05 |
| 0.477847741D 01 | 0.213442738D 05 |
| 0.480309103D 01 | 0.213175401D 05 |
| 0.482770465D 01 | 0.212911111D 05 |
| 0.485231827D 01 | 0.212650059D 05 |
| 0.487693190D 01 | 0.212392421D 05 |
| 0.490154552D 01 | 0.212138352D 05 |
| 0.492615914D 01 | 0.211887993D 05 |
| 0.495077276D 01 | 0.211641469D 05 |
| 0.497538638D 01 | 0.211398891D 05 |
| 0.500000000D 01 | 0.211160354D 05 |

Appendix Va. Potential Energy Curves (con't)

```
********** MOLECULAR CHLORINE AND MOLECULAR CHLORINE ANION ***********
*********************** F-C OVERLAP FACTORS *************************

 THE FOLLOWING DATA PERTAIN TO THE UPPER STATE,  STATE NUMBER IS

FJ =   0.0

ZMJ =   0.174739986D 02

DE =   0.10453733D 05

TOE = -0.19164680D 05

LIMI =     0.15000D 01

LIM2 =     0.50000D 01



 THE INPUT POTENTIAL POINTS AND ENERGIES ARE GIVEN BELOW.
                                   DE
 0.150000000D 01        0.143627110D 06
 0.197929697D 01        0.653462994D 04
 0.198597415D 01        0.645000494D 04
 0.199266532D 01        0.636462994D 04
 0.199937190D 01        0.627850494D 04
 0.200609535D 01        0.619162994D 04
 0.201283721D 01        0.610400494D 04
 0.201959902D 01        0.601562994D 04
 0.202638239D 01        0.592650494D 04
 0.203318900D 01        0.583662994D 04
 0.204002056D 01        0.574600494D 04
 0.204687885D 01        0.565462994D 04
 0.205376574D 01        0.556250494D 04
 0.206068314D 01        0.546962994D 04
 0.206763707D 01        0.537600494D 04
```

Appendix Va. Potential Energy Curves (con't)

| R | PE | R | PE |
|---|---|---|---|
| 0.207461763D 01 | 0.528162994D 04 | 0.247519414D 01 | 0.640629938D 03 |
| 0.208163859D 01 | 0.518650494D 04 | 0.249475307D 01 | 0.514004938D 03 |
| 0.208869945D 01 | 0.509062994D 04 | 0.251698746D 01 | 0.386629938D 03 |
| 0.209580141D 01 | 0.499400494D 04 | 0.254343658D 01 | 0.258504938D 03 |
| 0.210294738D 01 | 0.489662994D 04 | 0.257808390D 01 | 0.129629938D 03 |
| 0.211014003D 01 | 0.479850494D 04 | 0.260274445D 01 | 0.649111877D 02 |
| 0.211738212D 01 | 0.469962994D 04 | 0.266302775D 01 | 0.0 |
| 0.212457663D 01 | 0.460000494D 04 | 0.272470729D 01 | 0.649111877D 02 |
| 0.213202655D 01 | 0.449962994D 04 | 0.275077036D 01 | 0.129629938D 03 |
| 0.213943550D 01 | 0.439850494D 04 | 0.278824204D 01 | 0.258504938D 03 |
| 0.214690668D 01 | 0.429662994D 04 | 0.281754156D 01 | 0.386629938D 03 |
| 0.215444391D 01 | 0.419400494D 04 | 0.284265279D 01 | 0.514004938D 03 |
| 0.216205117D 01 | 0.409062994D 04 | 0.286511538D 01 | 0.640629938D 03 |
| 0.216973270D 01 | 0.398650494D 04 | 0.288571739D 01 | 0.766504938D 03 |
| 0.217749306D 01 | 0.388162994D 04 | 0.290492617D 01 | 0.891629938D 03 |
| 0.218533713D 01 | 0.377600494D 04 | 0.292304574D 01 | 0.101600494D 04 |
| 0.219327017D 01 | 0.366962994D 04 | 0.294028701D 01 | 0.113962994D 04 |
| 0.220129793D 01 | 0.356250494D 04 | 0.295680336D 01 | 0.126250494D 04 |
| 0.220942625D 01 | 0.345462994D 04 | 0.297271053D 01 | 0.138462994D 04 |
| 0.221766212D 01 | 0.334600494D 04 | 0.298809835D 01 | 0.150600494D 04 |
| 0.222601265D 01 | 0.323662994D 04 | 0.300303828D 01 | 0.162662994D 04 |
| 0.223448578D 01 | 0.312650494D 04 | 0.301758825D 01 | 0.174650494D 04 |
| 0.224309019D 01 | 0.301562994D 04 | 0.303179604D 01 | 0.186562994D 04 |
| 0.225183542D 01 | 0.290400494D 04 | 0.304570152D 01 | 0.198400494D 04 |
| 0.226073204D 01 | 0.279162994D 04 | 0.305933883D 01 | 0.210162994D 04 |
| 0.226979175D 01 | 0.267850494D 04 | 0.307273667D 01 | 0.221850494D 04 |
| 0.227902761D 01 | 0.256462994D 04 | 0.308592021D 01 | 0.233462994D 04 |
| 0.228845426D 01 | 0.245000494D 04 | 0.309891131D 01 | 0.245000494D 04 |
| 0.229808819D 01 | 0.233462994D 04 | 0.311172921D 01 | 0.256462994D 04 |
| 0.230794811D 01 | 0.221850494D 04 | 0.312439095D 01 | 0.267850494D 04 |
| 0.231805530D 01 | 0.210162994D 04 | 0.313691170D 01 | 0.279162994D 04 |
| 0.232843452D 01 | 0.198400494D 04 | 0.314930511D 01 | 0.290400494D 04 |
| 0.233911407D 01 | 0.186562994D 04 | 0.316158344D 01 | 0.301562994D 04 |
| 0.235012738D 01 | 0.174650494D 04 | 0.317375785D 01 | 0.312650494D 04 |
| 0.236151355D 01 | 0.162662994D 04 | 0.318583849D 01 | 0.323662994D 04 |
| 0.237332107D 01 | 0.150600494D 04 | 0.319783466D 01 | 0.334600494D 04 |
| 0.238560624D 01 | 0.138462994D 04 | 0.320975491D 01 | 0.345462994D 04 |
| 0.239844045D 01 | 0.126250494D 04 | 0.322160713D 01 | 0.356250494D 04 |
| 0.241191311D 01 | 0.113962994D 04 | 0.323339865D 01 | 0.366962994D 04 |
| 0.242613952D 01 | 0.101600494D 04 | 0.324513627D 01 | 0.377600494D 04 |
| 0.244127264D 01 | 0.891629938D 03 | 0.325682635D 01 | 0.388162994D 04 |
| 0.245752297D 01 | 0.766504938D 03 | 0.326847086D 01 | 0.398650494D 04 |

## Appendix Va. Potential Energy Curves (con't)

| R | PE | R | PE |
|---|---|---|---|
| 0.328003740D 01 | 0.409062994D 04 | 0.380967576D 01 | 0.800610500D 04 |
| 0.329166926D 01 | 0.419400494D 04 | 0.382384629D 01 | 0.808149274D 04 |
| 0.330322546D 01 | 0.429662994D 04 | 0.383801681D 01 | 0.815509426D 04 |
| 0.331476273D 01 | 0.439850494D 04 | 0.385218734D 01 | 0.822691730D 04 |
| 0.332627961D 01 | 0.449962994D 04 | 0.386635787D 01 | 0.829696993D 04 |
| 0.333778641D 01 | 0.460000494D 04 | 0.388052839D 01 | 0.836526139D 04 |
| 0.334928528D 01 | 0.469962994D 04 | 0.389469892D 01 | 0.843180212D 04 |
| 0.336078019D 01 | 0.479850494D 04 | 0.390886945D 01 | 0.849660363D 04 |
| 0.337227495D 01 | 0.489662994D 04 | 0.392303997D 01 | 0.855967849D 04 |
| 0.338377327D 01 | 0.499400494D 04 | 0.393721050D 01 | 0.862104028D 04 |
| 0.339527872D 01 | 0.509062994D 04 | 0.395138103D 01 | 0.868070350D 04 |
| 0.340679475D 01 | 0.518650494D 04 | 0.396555155D 01 | 0.873868355D 04 |
| 0.341832475D 01 | 0.528162994D 04 | 0.397972208D 01 | 0.879499669D 04 |
| 0.342987200D 01 | 0.537600494D 04 | 0.399389261D 01 | 0.884965964D 04 |
| 0.344143970D 01 | 0.546962994D 04 | 0.400806313D 01 | 0.890269108D 04 |
| 0.345303107D 01 | 0.556250494D 04 | 0.402223366D 01 | 0.895410861D 04 |
| 0.346464901D 01 | 0.565462994D 04 | 0.403640419D 01 | 0.900393165D 04 |
| 0.347629673D 01 | 0.574600494D 04 | 0.405057471D 01 | 0.905217396D 04 |
| 0.348797716D 01 | 0.583662994D 04 | 0.406474524D 01 | 0.909887385D 04 |
| 0.349969325D 01 | 0.592650494D 04 | 0.407891577D 01 | 0.914403418D 04 |
| 0.351144797D 01 | 0.601562994D 04 | 0.409308629D 01 | 0.918768229 04 |
| 0.352324408D 01 | 0.610400494D 04 | 0.410725682D 01 | 0.922983995D 04 |
| 0.353508459D 01 | 0.619162994D 04 | 0.412142735D 01 | 0.927052941D 04 |
| 0.354697233D 01 | 0.627850494D 04 | 0.413559787D 01 | 0.930977320D 04 |
| 0.355891013D 01 | 0.636462994D 04 | 0.414976840D 01 | 0.934759428D 04 |
| 0.357090085D 01 | 0.645000494D 04 | 0.416393893D 01 | 0.938401587D 04 |
| 0.358294733D 01 | 0.653462994D 04 | 0.417810945D 01 | 0.941906143D 04 |
| 0.359711786D 01 | 0.665111461D 04 | 0.419227998D 01 | 0.945275489D 04 |
| 0.361128833D 01 | 0.676302927D 04 | 0.420645051D 01 | 0.948512006D 04 |
| 0.362545891D 01 | 0.687325415D 04 | 0.422062103D 01 | 0.951618115D 04 |
| 0.363962944D 01 | 0.698176902D 04 | 0.423479156D 01 | 0.954596248D 04 |
| 0.365379997D 01 | 0.708855588D 04 | 0.424896209D 01 | 0.957448851D 04 |
| 0.366797049D 01 | 0.719359900D 04 | 0.426313261D 01 | 0.960178378D 04 |
| 0.368214102D 01 | 0.724683479D 04 | 0.427730314D 01 | 0.962787293D 04 |
| 0.369631155D 01 | 0.733940174D 04 | 0.429147367D 01 | 0.965278066D 04 |
| 0.371048207D 01 | 0.742914033D 04 | 0.430564419D 01 | 0.967653169D 04 |
| 0.372465260D 01 | 0.751609299D 04 | 0.431981472D 01 | 0.969915076D 04 |
| 0.373882313D 01 | 0.760225401D 04 | 0.433398525D 01 | 0.972066258D 04 |
| 0.375299365D 01 | 0.768661945D 04 | 0.434815577D 01 | 0.974109186D 04 |
| 0.376716418D 01 | 0.776918713D 04 | 0.436232630D 01 | 0.976046323D 04 |
| 0.378133471D 01 | 0.784995649D 04 | 0.437649683D 01 | 0.977880127D 04 |
| 0.379550523D 01 | 0.792892859D 04 | 0.439066735D 01 | 0.979613048D 04 |

Appendix Va. Potential Energy Curves (con't)

| R | PE |
|---|---|
| 0.440423783D 01 | 0.981247522D 04 |
| 0.441900841D 01 | 0.982785978D 04 |
| 0.443317393D 01 | 0.984230827D 04 |
| 0.444734946D 01 | 0.985584468D 04 |
| 0.446151999D 01 | 0.986849283D 04 |
| 0.447569051D 01 | 0.988027635D 04 |
| 0.448986104D 01 | 0.989121870D 04 |
| 0.450403157D 01 | 0.990134312D 04 |
| 0.451820209D 01 | 0.991067266D 04 |
| 0.453237262D 01 | 0.991923013D 04 |
| 0.454654315D 01 | 0.992703811D 04 |
| 0.456071367D 01 | 0.993411894D 04 |
| 0.457488420D 01 | 0.994049473D 04 |
| 0.458905473D 01 | 0.994618730D 04 |
| 0.460322525D 01 | 0.995121822D 04 |
| 0.461739578D 01 | 0.995560879D 04 |
| 0.463156631D 01 | 0.995938002D 04 |
| 0.464573683D 01 | 0.996255265D 04 |
| 0.465990736D 01 | 0.996514712D 04 |
| 0.467407789D 01 | 0.996718358D 04 |
| 0.468824841D 01 | 0.996868186D 04 |
| 0.470241894D 01 | 0.996966153D 04 |
| 0.471658947D 01 | 0.997014180D 04 |
| 0.473075999D 01 | 0.997014160D 04 |
| 0.474493052D 01 | 0.996967955D 04 |
| 0.475910105D 01 | 0.996877394D 04 |
| 0.477327157D 01 | 0.996744273D 04 |
| 0.478744210D 01 | 0.996570359D 04 |
| 0.480161263D 01 | 0.996357385D 04 |
| 0.481578315D 01 | 0.996107051D 04 |
| 0.482995368D 01 | 0.995821026D 04 |
| 0.484412421D 01 | 0.995500946D 04 |
| 0.485829473D 01 | 0.995148415D 04 |
| 0.487246526D 01 | 0.994765004D 04 |
| 0.488663579D 01 | 0.994352252D 04 |
| 0.490080631D 01 | 0.993911664D 04 |
| 0.491497684D 01 | 0.993444715D 04 |
| 0.492914737D 01 | 0.992952846D 04 |
| 0.494331789D 01 | 0.992437468D 04 |
| 0.495748842D 01 | 0.991899957D 04 |
| 0.497165895D 01 | 0.991341660D 04 |
| 0.498582947D 01 | 0.990763890D 04 |

## Appendix Vb. Molecular Chlorine and Molecular Chlorine Anion Franck-Condon Overlap Factors

| V*,V** | T(cm-1) | Q | Lambda | QT**3 | QT**4 | RC | R**2C | Phase |
|---|---|---|---|---|---|---|---|---|
| 0, 3 | -20681.80 P | 0.1264D-12 | 4835.170 | 0.1119D 01 | 0.2312D 05 | 2.2809 | 5.2052 | + |
| 1, 3 | -20424.80 | 0.4630D-11 | 4896.010 | 0.3945D 02 | 0.8057D 06 | 2.2734 | 5.1712 | - |
| 2, 3 | -20170.80 | 0.8445D-10 | 4957.662 | 0.6930D 03 | 0.1398D 08 | 2.2660 | 5.1374 | + |
| 3, 3 | -19919.80 | 0.1021D-08 | 5020.132 | 0.8073D 04 | 0.1608D 09 | 2.2587 | 5.1045 | - |
| 4, 3 | -19671.80 | 0.9203D-08 | 5083.420 | 0.7006D 05 | 0.1378D 10 | 2.2515 | 5.0719 | + |
| 5, 3 | -19426.80 | 0.6582D-07 | 5147.529 | 0.4825D 06 | 0.9374D 10 | 2.2444 | 5.0397 | - |
| 6, 3 | -19184.80 | 0.3896D-06 | 5212.461 | 0.2744D 07 | 0.5264D 11 | 2.2373 | 5.0079 | + |
| 7, 3 | -18945.80 | 0.1946D-05 | 5278.216 | 0.1323D 08 | 0.2507D 12 | 2.2303 | 4.9765 | - |
| 8, 3 | -18709.80 | 0.8418D-05 | 5344.794 | 0.5513D 08 | 0.1032D 13 | 2.2234 | 4.9455 | + |
| 9, 3 | -18476.80 | 0.3192D-04 | 5412.194 | 0.2013D 09 | 0.3720D 13 | 2.2165 | 4.9149 | - |
| 10, 3 | -18246.80 | 0.1071D-03 | 5480.414 | 0.6509D 09 | 0.1188D 14 | 2.2097 | 4.8847 | + |
| 11, 3 | -18019.80 | 0.3209D-03 | 5549.452 | 0.1878D 10 | 0.3384D 14 | 2.2030 | 4.8548 | - |
| 12, 3 | -17795.80 | 0.8626D-03 | 5619.304 | 0.4861D 10 | 0.8651D 14 | 2.1963 | 4.8252 | + |
| 0, 4 | -21219.78 P | 0.1661D-11 | 4712.585 | 0.1587D 02 | 0.3368D 06 | 2.2965 | 5.2766 | + |
| 1, 4 | -20962.78 | 0.5600D-10 | 4770.360 | 0.5159D 03 | 0.1081D 08 | 2.2890 | 5.2423 | - |
| 2, 4 | -20708.78 | 0.9381D-09 | 4828.870 | 0.8332D 04 | 0.1725D 09 | 2.2817 | 5.2085 | + |
| 3, 4 | -20457.78 | 0.1040D-07 | 4888.116 | 0.8903D 05 | 0.1821D 10 | 2.2744 | 5.1753 | - |
| 4, 4 | -20209.78 | 0.8566D-07 | 4948.100 | 0.7071D 06 | 0.1429D 11 | 2.2672 | 5.1426 | + |
| 5, 4 | -19964.78 | 0.5585D-06 | 5008.821 | 0.4445D 07 | 0.8874D 11 | 2.2601 | 5.1103 | - |
| 6, 4 | -19722.78 | 0.2997D-05 | 5070.280 | 0.2300D 08 | 0.4535D 12 | 2.2531 | 5.0785 | + |
| 7, 4 | -19483.78 | 0.1359D-04 | 5132.475 | 0.1005D 09 | 0.1959D 13 | 2.2462 | 5.0472 | - |
| 8, 4 | -19247.78 | 0.5304D-04 | 5195.405 | 0.3782D 09 | 0.7280D 13 | 2.2393 | 5.0163 | + |
| 9, 4 | -19014.78 | 0.1905D-03 | 5259.067 | 0.1241D 10 | 0.2360D 14 | 2.2325 | 4.9858 | - |
| 10, 4 | -18784.78 | 0.5411D-03 | 5323.459 | 0.3587D 10 | 0.5738D 14 | 2.2258 | 4.9557 | + |
| 11, 4 | -18557.78 | 0.1438D-02 | 5388.576 | 0.9191D 10 | 0.1706D 15 | 2.2191 | 4.9260 | - |
| 12, 4 | -18333.78 | 0.3403D-02 | 5454.413 | 0.2097D 11 | 0.3845D 15 | 2.2125 | 4.8967 | + |
| 0, 5 | -21752.23 P | 0.1752D-10 | 4597.229 | 0.1303D 03 | 0.3922D 07 | 2.3119 | 5.3477 | + |
| 1, 5 | -21495.23 | 0.5422D-09 | 4652.194 | 0.5385D 04 | 0.1157D 09 | 2.3045 | 5.3131 | - |
| 2, 5 | -21241.23 | 0.8320D-08 | 4707.825 | 0.7974D 05 | 0.1694D 10 | 2.2971 | 5.2790 | + |
| 3, 5 | -20990.23 | 0.8427D-07 | 4764.121 | 0.7793D 06 | 0.1636D 11 | 2.2898 | 5.2456 | - |
| 4, 5 | -20742.23 | 0.6326D-06 | 4821.082 | 0.5645D 07 | 0.1171D 12 | 2.2826 | 5.2127 | + |
| 5, 5 | -20497.23 | 0.3747D-05 | 4878.707 | 0.3226D 08 | 0.5513D 12 | 2.2756 | 5.1803 | - |
| 6, 5 | -20255.23 | 0.1820D-04 | 4936.996 | 0.1512D 09 | 0.3063D 13 | 2.2686 | 5.1484 | + |
| 7, 5 | -20016.23 | 0.7437D-04 | 4995.945 | 0.5964D 09 | 0.1194D 14 | 2.2617 | 5.1170 | - |
| 8, 5 | -19780.23 | 0.2603D-03 | 5055.552 | 0.2014D 10 | 0.3984D 14 | 2.2548 | 5.0860 | + |
| 9, 5 | -19547.23 | 0.7899D-03 | 5115.814 | 0.5900D 10 | 0.1153D 15 | 2.2481 | 5.0555 | - |
| 10, 5 | -19317.23 | 0.2097D-02 | 5176.725 | 0.1511D 11 | 0.2920D 15 | 2.2414 | 5.0255 | + |
| 11, 5 | -19090.23 | 0.4893D-02 | 5238.281 | 0.3434D 11 | 0.6498D 15 | 2.2349 | 4.9959 | - |
| 12, 5 | -18866.23 | 0.1006D-01 | 5300.475 | 0.6758D 11 | 0.1275D 16 | 2.2284 | 4.9667 | + |

Appendix Vb. Molecular Chlorine and Molecular Clorine Anion Franck-Condon Overlap Factors (con't)

| V*,V** | T(cm$^{-1}$) | Q | Lambda | QT**3 | QT**4 | RC | R**2C | Phase |
|---|---|---|---|---|---|---|---|---|
| 0. 6 | -22279.12 | 0.1540D-09 | 4488.508 | 0.1703D 04 | 0.3794D 08 | 2.3273 | 5.4187 | + |
| 1. 6 | -22022.12 | 0.4357D-08 | 4540.869 | 0.4660D 05 | 0.1026D 10 | 2.3193 | 5.3837 | - |
| 2. 6 | -21768.12 | 0.6114D-07 | 4593.873 | 0.6306D 06 | 0.1373D 11 | 2.3124 | 5.3493 | + |
| 3. 6 | -21517.12 | 0.5639D-06 | 4647.463 | 0.5617D 07 | 0.1209D 12 | 2.3051 | 5.3155 | - |
| 4. 6 | -21269.12 | 0.3842D-05 | 4701.653 | 0.3697D 08 | 0.7862D 12 | 2.2979 | 5.2823 | + |
| 5. 6 | -21024.12 | 0.2058D-04 | 4756.442 | 0.1912D 09 | 0.4020D 13 | 2.2908 | 5.2497 | - |
| 6. 6 | -20782.12 | 0.8998D-04 | 4811.829 | 0.8076D 09 | 0.1678D 14 | 2.2838 | 5.2176 | + |
| 7. 6 | -20543.12 | 0.3293D-03 | 4867.810 | 0.2855D 10 | 0.5966D 14 | 2.2769 | 5.1860 | - |
| 8. 6 | -20307.12 | 0.1026D-02 | 4924.382 | 0.8593D 10 | 0.1745D 15 | 2.2701 | 5.1549 | + |
| 9. 6 | -20074.12 | 0.2752D-02 | 4981.539 | 0.2226D 11 | 0.4469D 15 | 2.2634 | 5.1244 | - |
| 10. 6 | -19844.12 | 0.6395D-02 | 5039.277 | 0.4998D 11 | 0.9917D 15 | 2.2568 | 5.0943 | + |
| 11. 6 | -19617.12 | 0.1292D-01 | 5097.589 | 0.9752D 11 | 0.1913D 16 | 2.2502 | 5.0646 | - |
| 12. 6 | -19393.12 | 0.2265D-01 | 5156.469 | 0.1652D 12 | 0.3204D 16 | 2.2438 | 5.0355 | + |
| 0. 7 | -22800.39 | 0.1158D-08 | 4385.891 | 0.1372D 05 | 0.3129D 09 | 2.3425 | 5.4898 | + |
| 1. 7 | -22543.39 | 0.2992D-07 | 4435.891 | 0.3428D 06 | 0.7729D 10 | 2.3349 | 5.4543 | - |
| 2. 7 | -22289.39 | 0.3815D-06 | 4486.440 | 0.4225D 07 | 0.9417D 11 | 2.3275 | 5.4194 | + |
| 3. 7 | -22039.39 | 0.3191D-05 | 4537.537 | 0.3415D 08 | 0.7527D 12 | 2.3202 | 5.3852 | - |
| 4. 7 | -21790.39 | 0.1964D-04 | 4589.180 | 0.2032D 09 | 0.4428D 13 | 2.3130 | 5.3517 | + |
| 5. 7 | -21545.39 | 0.9458D-04 | 4641.365 | 0.9460D 09 | 0.2038D 14 | 2.3059 | 5.3187 | - |
| 6. 7 | -21303.39 | 0.3699D-03 | 4694.089 | 0.3577D 10 | 0.7620D 14 | 2.2988 | 5.2863 | + |
| 7. 7 | -21064.39 | 0.1203D-02 | 4747.349 | 0.1125D 11 | 0.2369D 15 | 2.2919 | 5.2545 | - |
| 8. 7 | -20828.39 | 0.3306D-02 | 4801.140 | 0.2987D 11 | 0.6221D 15 | 2.2851 | 5.2232 | + |
| 9. 7 | -20595.39 | 0.7739D-02 | 4855.456 | 0.6761D 11 | 0.1392D 16 | 2.2784 | 5.1925 | - |
| 10. 7 | -20365.39 | 0.1550D-01 | 4910.292 | 0.1309D 12 | 0.2667D 16 | 2.2718 | 5.1622 | + |
| 11. 7 | -20138.39 | 0.2654D-01 | 4965.641 | 0.2167D 12 | 0.4365D 16 | 2.2653 | 5.1325 | - |
| 12. 7 | -19914.39 | 0.3853D-01 | 5021.495 | 0.3043D 12 | 0.6059D 16 | 2.2589 | 5.1032 | + |
| 0. 8 | -23315.99 | 0.7578D-08 | 4288.903 | 0.9605D 05 | 0.2240D 10 | 2.3577 | 5.5611 | + |
| 1. 8 | -23058.99 | 0.1780D-06 | 4336.704 | 0.2183D 07 | 0.5034D 11 | 2.3501 | 5.5250 | - |
| 2. 8 | -22804.99 | 0.2056D-05 | 4385.006 | 0.2439D 08 | 0.5561D 12 | 2.3425 | 5.4896 | + |
| 3. 8 | -22553.99 | 0.1552D-04 | 4433.805 | 0.1780D 09 | 0.4015D 13 | 2.3352 | 5.4549 | - |
| 4. 8 | -22305.99 | 0.8578D-04 | 4483.101 | 0.9521D 09 | 0.2124D 14 | 2.3279 | 5.4209 | + |
| 5. 8 | -22060.99 | 0.3690D-03 | 4532.889 | 0.3962D 10 | 0.8741D 14 | 2.3208 | 5.3875 | - |
| 6. 8 | -21818.99 | 0.1281D-02 | 4583.164 | 0.1330D 11 | 0.2902D 15 | 2.3137 | 5.3548 | + |
| 7. 8 | -21579.99 | 0.3665D-02 | 4633.923 | 0.3683D 11 | 0.7948D 15 | 2.3068 | 5.3226 | - |
| 8. 8 | -21343.99 | 0.8763D-02 | 4685.160 | 0.8521D 11 | 0.1819D 16 | 2.3000 | 5.2910 | + |
| 9. 8 | -21110.99 | 0.1761D-01 | 4736.870 | 0.1657D 12 | 0.3499D 16 | 2.2933 | 5.2600 | - |
| 10. 8 | -20880.99 | 0.2973D-01 | 4789.045 | 0.2707D 12 | 0.5651D 16 | 2.2867 | 5.2295 | + |
| 11. 8 | -20653.99 | 0.4174D-01 | 4841.680 | 0.3677D 12 | 0.7595D 16 | 2.2802 | 5.1995 | - |
| 12. 8 | -20429.99 | 0.4769D-01 | 4894.765 | 0.4066D 12 | 0.8308D 16 | 2.2738 | 5.1700 | + |

Appendix VD. Molecular Chlorine and Molecular Chlorine Anion Franck-Condon Overlap Factors (con't)

| V*,V** | T(cm$^{-1}$) | Q | Lamdba | QT**3 | QT**4 | RC | R**2C | Phase |
|---|---|---|---|---|---|---|---|---|
| 0, 9 | -23825.87 P | 0.4276D-07 | 4197.113 | [illegible] | 0.1411D 11 | 2.3727 | 5.6327 | + |
| 1, 9 | -23568.88 | 0.9327D-06 | 4242.264 | 0.1213D 08 | 0.2872D 12 | 2.3651 | 5.5969 | - |
| 2, 9 | -23314.88 | 0.9687D-05 | 4289.137 | 0.1228D 09 | 0.2862D 13 | 2.3575 | 5.5599 | + |
| 3, 9 | -23063.88 | 0.6558D-04 | 4335.785 | 0.8044D 09 | 0.1856D 14 | 2.3501 | 5.5247 | - |
| 4, 9 | -22815.88 | 0.3234D-03 | 4382.913 | 0.3841D 10 | 0.8764D 14 | 2.3427 | 5.4901 | + |
| 5, 9 | -22570.88 | 0.1232D-02 | 4430.485 | 0.1417D 11 | 0.3198D 15 | 2.3355 | 5.4563 | - |
| 6, 9 | -22328.88 | 0.3755D-02 | 4478.506 | 0.4180D 11 | 0.9334D 15 | 2.3285 | 5.4230 | + |
| 7, 9 | -22089.88 | 0.9333D-02 | 4526.961 | 0.1006D 12 | 0.2222D 16 | 2.3215 | 5.3905 | - |
| 8, 9 | -21853.88 | 0.1909D-01 | 4575.848 | 0.1992D 12 | 0.4353D 16 | 2.3146 | 5.3585 | + |
| 9, 9 | -21620.88 | 0.3215D-01 | 4625.160 | 0.3249D 12 | 0.7025D 16 | 2.3079 | 5.3271 | - |
| 10, 9 | -21390.88 | 0.4412D-01 | 4674.891 | 0.4318D 12 | 0.9237D 16 | 2.3013 | 5.2962 | + |
| 11, 9 | -21163.88 | 0.4800D-01 | 4725.033 | 0.4551D 12 | 0.9631D 16 | 2.2947 | 5.2658 | - |
| 12, 9 | -20939.88 | 0.3995D-01 | 4775.578 | 0.3577D 12 | 0.7489D 16 | 2.2883 | 5.2356 | + |
| 0,10 | -24325.99 P | 0.2254D-06 | 4110.153 | 0.3247D 07 | 0.7900D 11 | 2.3880 | 5.7045 | + |
| 1,10 | -24072.99 | 0.4314D-05 | 4154.033 | 0.6019D 08 | 0.1449D 13 | 2.3802 | 5.6673 | - |
| 2,10 | -23818.99 | 0.4024D-04 | 4198.330 | 0.5437D 09 | 0.1295D 14 | 2.3725 | 5.6305 | + |
| 3,10 | -23567.99 | 0.2427D-03 | 4243.043 | 0.3177D 10 | 0.7487D 14 | 2.3649 | 5.5946 | - |
| 4,10 | -23319.99 | 0.1058D-02 | 4288.166 | 0.1342D 11 | 0.3130D 15 | 2.3575 | 5.5554 | + |
| 5,10 | -23074.99 | 0.3535D-02 | 4333.696 | 0.4344D 11 | 0.1002D 16 | 2.3502 | 5.5250 | - |
| 6,10 | -22832.99 | 0.9333D-02 | 4379.627 | 0.1111D 12 | 0.2537D 16 | 2.3431 | 5.4912 | + |
| 7,10 | -22593.99 | 0.1978D-01 | 4425.955 | 0.2281D 12 | 0.5154D 16 | 2.3361 | 5.4581 | - |
| 8,10 | -22357.99 | 0.3376D-01 | 4472.674 | 0.3773D 12 | 0.8435D 16 | 2.3292 | 5.4256 | + |
| 9,10 | -22124.99 | 0.4599D-01 | 4519.776 | 0.4971D 12 | 0.1100D 17 | 2.3224 | 5.3937 | - |
| 10,10 | -21894.99 | 0.4815D-01 | 4567.254 | 0.5054D 12 | 0.1106D 17 | 2.3157 | 5.3623 | + |
| 11,10 | -21667.99 | 0.3608D-01 | 4615.102 | 0.3670D 12 | 0.7952D 16 | 2.3091 | 5.3312 | - |
| 12,10 | -21443.99 | 0.1554D-01 | 4663.311 | 0.1533D 12 | 0.3287D 16 | 2.3026 | 5.2999 | + |
| 0,11 | -24828.28 P | 0.1043D-05 | 4027.666 | 0.1596D 08 | 0.3962D 12 | 2.4032 | 5.7775 | + |
| 1,11 | -24571.28 | 0.1786D-04 | 4069.792 | 0.2649D 09 | 0.6509D 13 | 2.3952 | 5.7391 | - |
| 2,11 | -24317.28 | 0.1482D-03 | 4112.302 | 0.2131D 10 | 0.5182D 14 | 2.3874 | 5.7015 | + |
| 3,11 | -24066.28 | 0.7895D-03 | 4155.192 | 0.1102D 11 | 0.2648D 15 | 2.3798 | 5.6648 | - |
| 4,11 | -23818.28 | 0.3014D-02 | 4198.456 | 0.4073D 11 | 0.9701D 15 | 2.3723 | 5.6290 | + |
| 5,11 | -23573.28 | 0.8709D-02 | 4242.092 | 0.1141D 12 | 0.2689D 16 | 2.3649 | 5.5938 | - |
| 6,11 | -23331.28 | 0.1955D-01 | 4286.092 | 0.2445D 12 | 0.5797D 16 | 2.3576 | 5.5594 | + |
| 7,11 | -23092.28 | 0.3448D-01 | 4330.452 | 0.4246D 12 | 0.9805D 16 | 2.3505 | 5.5257 | - |
| 8,11 | -22856.28 | 0.4724D-01 | 4375.166 | 0.5641D 12 | 0.1289D 17 | 2.3435 | 5.4925 | + |
| 9,11 | -22623.28 | 0.4857D-01 | 4420.226 | 0.5524D 12 | 0.1272D 17 | 2.3367 | 5.4599 | - |
| 10,11 | -22393.28 | 0.3418D-01 | 4465.626 | 0.3838D 12 | 0.8595D 16 | 2.3299 | 5.4274 | + |
| 11,11 | -22166.28 | 0.1237D-01 | 4511.357 | 0.1347D 12 | 0.2986D 16 | 2.3230 | 5.3942 | - |
| 12,11 | -21942.28 | 0.1765D-03 | 4557.412 | 0.1864D 10 | 0.4090D 14 | 2.3132 | 5.3272 | + |
| 0,12 | -25320.57 P | 0.4358D-05 | 3949.342 | 0.7074D 08 | 0.1791D 13 | 2.4184 | 5.8516 | + |
| 1,12 | -25063.67 | 0.6633D-04 | 3989.838 | 0.1044D 10 | 0.2617D 14 | 2.4103 | 5.8115 | - |
| 2,12 | -24809.67 | 0.4857D-03 | 4030.646 | 0.7417D 10 | 0.1840D 15 | 2.4024 | 5.7730 | + |
| 3,12 | -24558.67 | 0.2263D-02 | 4071.381 | 0.3351D 11 | 0.8231D 15 | 2.3946 | 5.7355 | - |
| 4,12 | -24310.67 | 0.7464D-02 | 4113.420 | 0.1072D 12 | 0.2607D 16 | 2.3870 | 5.6989 | + |
| 5,12 | -24065.67 | 0.1833D-01 | 4155.29[illegible] | 0.2554D 12 | 0.6147D 16 | 2.3795 | 5.6628 | - |

Appendix VB. Molecular Chlorine and Molecular Chlorine Anion Franck-Condon Overlap Factors (con't)

| V*,V** | T(cm-1) | Q | Lambda | QT**3 | QT**4 | RC | R**2C | Phase |
|---|---|---|---|---|---|---|---|---|
| 6.12 | -23823.67 | 0.3417D-01 | 4197.509 | 0.4620D 12 | 0.1101D 17 | 2.3721 | 5.6276 | + |
| 7.12 | -23584.67 | 0.4819D-01 | 4240.042 | 0.6323D 12 | 0.1491D 17 | 2.3643 | 5.5931 | - |
| 8.12 | -23348.67 | 0.4960D-01 | 4282.896 | 0.6314D 12 | 0.1474D 17 | 2.3578 | 5.5590 | + |
| 9.12 | -23115.67 | 0.3360D-01 | 4326.067 | 0.4150D 12 | 0.9593D 16 | 2.3507 | 5.5261 | - |
| 10.12 | -22885.67 | 0.1056D-01 | 4369.547 | 0.1266D 12 | 0.2897D 16 | 2.3435 | 5.4920 | + |
| 11.12 | -22658.67 | 0.2391D-05 | 4413.321 | 0.2782D 08 | 0.6304D 12 | 2.3912 | 5.9219 | + |
| 12.12 | -22434.67 | 0.9917D-02 | 4457.386 | 0.1120D 12 | 0.2512D 16 | 2.3318 | 5.4401 | - |
| 0.13 | -25807.11 | 0.1653D-04 | 3874.901 | 0.2841D 09 | 0.7331D 13 | 2.4338 | 5.9252 | + |
| 1.13 | -25550.11 | 0.2218D-03 | 3913.873 | 0.3699D 10 | 0.9452D 14 | 2.4255 | 5.8847 | - |
| 2.13 | -25296.11 | 0.1419D-02 | 3953.177 | 0.2297D 11 | 0.5811D 15 | 2.4174 | 5.8452 | + |
| 3.13 | -25045.11 | 0.5708D-02 | 3992.795 | 0.8967D 11 | 0.2246D 16 | 2.4094 | 5.8065 | - |
| 4.13 | -24797.11 | 0.1599D-01 | 4032.723 | 0.2438D 12 | 0.6048D 16 | 2.4017 | 5.7692 | + |
| 5.13 | -24552.11 | 0.3259D-01 | 4072.970 | 0.4823D 12 | 0.1184D 17 | 2.3940 | 5.7321 | - |
| 6.13 | -24310.11 | 0.4859D-01 | 4113.515 | 0.6981D 12 | 0.1697D 17 | 2.3865 | 5.6959 | + |
| 7.13 | -24071.11 | 0.5140D-01 | 4154.359 | 0.7168D 12 | 0.1725D 17 | 2.3792 | 5.6603 | - |
| 8.13 | -23835.11 | 0.3462D-01 | 4195.492 | 0.4687D 12 | 0.1117D 17 | 2.3718 | 5.6247 | + |
| 9.13 | -23602.11 | 0.1004D-01 | 4236.909 | 0.1320D 12 | 0.3116D 16 | 2.3642 | 5.5867 | - |
| 10.13 | -23372.11 | 0.1054D-03 | 4278.604 | 0.1346D 10 | 0.3145D 14 | 2.3697 | 5.6468 | - |
| 11.13 | -23145.11 | 0.1223D-01 | 4320.567 | 0.1516D 12 | 0.3508D 16 | 2.3526 | 5.5371 | + |
| 12.13 | -22921.11 | 0.2706D-01 | 4362.791 | 0.3259D 12 | 0.7470D 16 | 2.3455 | 5.5013 | - |
| 0.14 | -26287.53 | 0.5709D-04 | 3804.085 | 0.1037D 10 | 0.2726D 14 | 2.4492 | 6.0024 | + |
| 1.14 | -26030.53 | 0.6690D-03 | 3841.643 | 0.1180D 11 | 0.3072D 15 | 2.4407 | 5.9567 | - |
| 2.14 | -25776.53 | 0.3696D-02 | 3879.499 | 0.6330D 11 | 0.1632D 16 | 2.4324 | 5.9180 | + |
| 3.14 | -25525.53 | 0.1263D-01 | 3917.647 | 0.2101D 12 | 0.5363D 16 | 2.4243 | 5.8784 | - |
| 4.14 | -25277.53 | 0.2940D-01 | 3956.083 | 0.4748D 12 | 0.1200D 17 | 2.4164 | 5.8396 | + |
| 5.14 | -25032.53 | 0.4799D-01 | 3994.802 | 0.7527D 12 | 0.1884D 17 | 2.4085 | 5.8016 | - |
| 6.14 | -24790.53 | 0.5385D-01 | 4033.799 | 0.8204D 12 | 0.2034D 17 | 2.4009 | 5.7642 | + |
| 7.14 | -24551.53 | 0.3749D-01 | 4073.066 | 0.5549D 12 | 0.1362D 17 | 2.3932 | 5.7263 | - |
| 8.14 | -24315.53 | 0.1090D-01 | 4112.598 | 0.1568D 12 | 0.3812D 15 | 2.3852 | 5.69[illegible] | + |
| 9.14 | -24082.53 | 0.1536D-03 | 4152.388 | 0.2145D 10 | 0.5166D 14 | 2.3914 | 5.7454 | + |
| 10.14 | -23852.53 | 0.1366D-01 | 4192.428 | 0.1854D 12 | 0.4421D 16 | 2.3736 | 5.6361 | - |
| 11.14 | -23625.53 | 0.2836D-01 | 4232.710 | 0.3740D 12 | 0.8837D 16 | 2.3661 | 5.5989 | + |
| 12.14 | -23401.53 | 0.2118D-01 | 4273.225 | 0.2715D 12 | 0.6352D 15 | 2.3590 | 5.5625 | - |
| 0.15 | -26761.85 | 0.1800D-03 | 3736.663 | 0.3450D 10 | 0.9233D 14 | 2.4647 | 6.0767 | + |
| 1.15 | -26504.85 | 0.1822D-02 | 3772.895 | 0.3392D 11 | 0.8990D 15 | 2.4550 | 6.0357 | - |
| 2.15 | -26250.85 | 0.8560D-02 | 3809.401 | 0.1548D 12 | 0.4065D 16 | 2.4475 | 5.9917 | + |
| 3.15 | -25999.85 | 0.2435D-01 | 3846.176 | 0.4280D 12 | 0.1113D 17 | 2.4392 | 5.9508 | - |
| 4.15 | -25751.85 | 0.4560D-01 | 3883.217 | 0.7787D 12 | 0.2005D 17 | 2.4311 | 5.9107 | + |
| 5.15 | -25506.85 | 0.5645D-01 | 3920.516 | 0.9369D 12 | 0.2390D 17 | 2.4231 | 5.8713 | - |
| 6.15 | -25264.85 | 0.4244D-01 | 3958.069 | 0.6844D 12 | 0.1729D 17 | 2.4151 | 5.8322 | + |
| 7.15 | -25025.85 | 0.1350D-01 | 3995.869 | 0.2117D 12 | 0.5297D 16 | 2.4067 | 5.7899 | - |
| 8.15 | -24789.85 | 0.5064D-04 | 4033.909 | 0.7715D 09 | 0.1913D 14 | 2.4264 | 5.9547 | - |
| 9.15 | -24556.85 | 0.1404D-01 | 4072.184 | 0.2079D 12 | 0.5106D 16 | 2.3943 | 5.7777 | + |
| 10.15 | -24326.85 | 0.2940D-01 | 4110.685 | 0.4233D 12 | 0.1030D 17 | 2.3870 | 5.6981 | - |
| 11.15 | -24099.85 | 0.2036D-01 | 4149.404 | 0.2850D 12 | 0.6869D 16 | 2.3795 | 5.65[illegible] | + |
| 12.15 | -23875.85 | 0.2216D-02 | 4188.333 | 0.3016D 11 | 0.7201D 15 | 2.3703 | 5.61[illegible] | - |

Appendix Vb. Molecular Chlorine and Molecular Chlorine Anion Franck-Condon Overlap Factors (con't)

| V*,V** | T(cm$^{-1}$) | Q | Lambda | QT**3 | QT**4 | RC | R**2C | Phase |
|---|---|---|---|---|---|---|---|---|
| 0,16 | -27230.01 | [illegible] | 3672.419 | 0.1047D 11 | 0.2852D 15 | 2.4803 | 6.1519 | + |
| 1,16 | -26973.01 | 0.44740D-02 | 3707.410 | 0.8780D 11 | 0.2368D 16 | 2.4715 | 6.1083 | - |
| 2,16 | -26719.01 | 0.17550D-01 | 3742.654 | 0.3349D 12 | 0.8947D 16 | 2.4624 | 6.0634 | + |
| 3,16 | -26468.01 | 0.40420D-01 | 3778.146 | 0.7495D 12 | 0.1984D 17 | 2.4542 | 6.0239 | - |
| 4,16 | -26220.01 | 0.58080D-01 | 3813.881 | 0.1047D 13 | 0.2744D 17 | 2.4459 | 5.9824 | + |
| 5,16 | -25975.01 | 0.49430D-01 | 3849.854 | 0.8662D 12 | 0.2250D 17 | 2.4375 | 5.9462 | - |
| 6,16 | -25733.01 | 0.18570D-01 | 3886.063 | 0.3164D 12 | 0.8141D 16 | 2.4288 | 5.8972 | + |
| 7,16 | -25494.01 | 0.46770D-04 | 3922.490 | 0.7750D 09 | 0.1976D 14 | 2.3905 | 5.6623 | - |
| 8,16 | -25259.01 | 0.13170D-01 | 3959.140 | 0.2122D 12 | 0.5359D 16 | 2.4167 | 5.8428 | - |
| 9,16 | -25025.01 | 0.30300D-01 | 3996.003 | 0.4748D 12 | 0.1186D 17 | 2.4083 | 5.8000 | + |
| 10,16 | -24795.01 | 0.20600D-01 | 4033.070 | 0.3141D 12 | 0.7787D 16 | 2.4003 | 5.7599 | - |
| 11,16 | -24568.01 | 0.16650D-02 | 4070.334 | 0.2469D 11 | 0.6065D 15 | 2.3895 | 5.7013 | + |
| 12,16 | -24344.01 | 0.60380D-02 | 4107.787 | 0.8711D 11 | 0.2121D 16 | 2.3994 | 5.7133 | + |
| 0,17 | -27691.92 | 0.13680D-02 | 3611.161 | 0.2905D 11 | 0.8044D 15 | 2.4963 | 6.2333 | + |
| 1,17 | -27434.92 | 0.98900D-02 | 3644.989 | 0.2042D 12 | 0.5602D 16 | 2.4871 | 6.1871 | - |
| 2,17 | -27180.92 | 0.31630D-01 | 3679.051 | 0.6352D 12 | 0.1727D 17 | 2.4781 | 6.1420 | + |
| 3,17 | -26929.92 | 0.56650D-01 | 3713.342 | 0.1106D 13 | 0.2980D 17 | 2.4693 | 6.0979 | - |
| 4,17 | -26681.92 | 0.57700D-01 | 3747.856 | 0.1096D 13 | 0.2924D 17 | 2.4606 | 6.0541 | + |
| 5,17 | -26436.92 | 0.27130D-01 | 3782.589 | 0.5014D 12 | 0.1325D 17 | 2.4516 | 6.0088 | - |
| 6,17 | -26194.92 | 0.97700D-03 | 3817.534 | 0.1756D 11 | 0.4600D 15 | 2.4366 | 5.9255 | + |
| 7,17 | -25955.92 | 0.10800D-01 | 3852.685 | 0.1889D 12 | 0.4903D 16 | 2.4392 | 5.9527 | + |
| 8,17 | -25719.92 | 0.30920D-01 | 3888.037 | 0.5261D 12 | 0.1353D 17 | 2.4300 | 5.9054 | - |
| 9,17 | -25486.92 | 0.22150D-01 | 3923.591 | 0.3668D 12 | 0.9348D 16 | 2.4215 | 5.8625 | + |
| 10,17 | -25256.92 | 0.16770D-02 | 3959.311 | 0.2702D 11 | 0.6826D 15 | 2.4097 | 5.7976 | - |
| 11,17 | -25029.92 | 0.69760D-02 | 3995.218 | 0.1094D 12 | 0.2738D 16 | 2.4105 | 5.8142 | - |
| 12,17 | -24805.92 | 0.22810D-01 | 4031.295 | 0.3482D 12 | 0.8636D 16 | 2.4016 | 5.7684 | + |
| 0,18 | -28147.52 | 0.32970D-02 | 3552.711 | 0.7353D 11 | 0.2070D 16 | 2.5124 | 6.3139 | + |
| 1,18 | -27890.52 | 0.19590D-01 | 3585.448 | 0.4250D 12 | 0.1185D 17 | 2.5029 | 6.2655 | - |
| 2,18 | -27636.52 | 0.49460D-01 | 3618.401 | 0.1044D 13 | 0.2886D 17 | 2.4936 | 6.2188 | + |
| 3,18 | -27385.52 | 0.64860D-01 | 3651.565 | 0.1332D 13 | 0.3648D 17 | 2.4844 | 6.1725 | - |
| 4,18 | -27137.52 | 0.40140D-01 | 3684.936 | 0.8023D 12 | 0.2177D 17 | 2.4752 | 6.1254 | + |
| 5,18 | -26892.52 | 0.46530D-02 | 3718.507 | 0.9055D 11 | 0.2434D 16 | 2.4635 | 6.0637 | - |
| 6,18 | -26650.52 | 0.68990D-02 | 3752.273 | 0.1306D 12 | 0.3480D 16 | 2.4629 | 6.0701 | - |
| 7,18 | -26411.52 | 0.30670D-01 | 3786.227 | 0.5655D 12 | 0.1492D 17 | 2.4524 | 6.0150 | + |
| 8,18 | -26175.52 | 0.25230D-01 | 3820.364 | 0.4525D 12 | 0.1184D 17 | 2.4434 | 5.9691 | - |
| 9,18 | -25942.52 | 0.23570D-02 | 3854.676 | 0.4116D 11 | 0.1068D 16 | 2.4313 | 5.9231 | + |
| 10,18 | -25712.52 | [illegible] | 3889.157 | 0.1125D 12 | 0.3091D 16 | 2.4322 | 5.9156 | + |
| 11,18 | -25485.52 | 0.23830D-01 | 3923.797 | 0.3944D 12 | 0.1005D 17 | 2.4226 | 5.8690 | - |

Appendix Vb. Molecular Chlorine and Molecular Chlorine Anion Franck-Condon Overlap Factors (con't)

| V*,V** | T(cm$^{-1}$) | Q | Lambda | QT**3 | QT**4 | RC | R**2C | Phase |
|---|---|---|---|---|---|---|---|---|
| [illegible] | [illegible] | 0.1431D-01 | 3458.[illegible]91 | 0.2733D 12 | 0.5907D 16 | 2.4141 | 5.8258 | + |
| 0.19 | -28596.70 | 0.7255D-02 | 3496.907 | 0.1697D 12 | 0.4852D 16 | 2.5288 | 6.3960 | + |
| 1.19 | -28339.70 | 0.3454D-01 | 3528.619 | 0.7861D 12 | 0.2228D 17 | 2.5199 | 6.3459 | - |
| 2.19 | -28095.70 | 0.6582D-01 | 3559.531 | 0.1458D 13 | 0.4096D 17 | 2.5093 | 6.2967 | + |
| 3.19 | -27834.70 | 0.5695D-01 | 3592.638 | 0.1228D 13 | 0.3419D 17 | 2.4996 | 6.2475 | - |
| 4.19 | -27586.70 | 0.1421D-01 | 3624.935 | 0.2982D 12 | 0.8227D 16 | 2.4890 | 6.1922 | + |
| 5.19 | -27341.70 | 0.2259D-02 | 3657.417 | 0.4616D 11 | 0.1262D 16 | 2.4898 | 6.2068 | + |
| 6.19 | -27099.70 | 0.2830D-01 | 3690.078 | 0.5633D 12 | 0.1526D 17 | 2.4757 | 6.1300 | - |
| 7.19 | -26860.70 | 0.2986D-01 | 3722.911 | 0.5786D 12 | 0.1554D 17 | 2.4661 | 6.0806 | + |
| 8.19 | -26624.70 | 0.4205D-02 | 3755.911 | 0.7937D 11 | 0.2113D 16 | 2.4542 | 6.0172 | - |
| 9.19 | -26391.70 | 0.6376D-02 | 3789.070 | 0.1117D 12 | 0.2948D 16 | 2.4544 | 6.0309 | - |
| 10.19 | -26161.70 | 0.2467D-01 | 3822.382 | 0.4417D 12 | 0.1156D 17 | 2.4442 | 5.9746 | + |
| 11.19 | -25934.70 | 0.1480D-01 | 3855.838 | 0.2582D 12 | 0.6696D 16 | 2.4350 | 5.9271 | - |
| 12.19 | -25710.70 | 0.9208D-05 | 3383.431 | 0.1395D 05 | 0.3587D 13 | 2.3309 | 5.2768 | + |
| 0.20 | -29039.39 | 0.1453D-01 | 3443.599 | 0.3554D 12 | 0.1033D 17 | 2.5453 | 6.4800 | + |
| 1.20 | -28782.39 | 0.5356D-01 | 3474.347 | 0.1279D 13 | 0.3683D 17 | 2.5351 | 6.4275 | - |
| 2.20 | -28528.39 | 0.7215D-01 | 3505.281 | 0.1675D 13 | 0.4779D 17 | 2.5250 | 6.3757 | + |
| 3.20 | -28277.39 | 0.3329D-01 | 3536.395 | 0.7527D 12 | 0.2129D 17 | 2.5146 | 6.3217 | - |
| 4.20 | -28029.39 | 0.7063D-04 | 3567.684 | 0.1555D 10 | 0.4359D 14 | 2.4644 | 6.0233 | + |
| 5.20 | -27784.39 | 0.2223D-01 | 3599.144 | 0.4725D 12 | 0.1313D 17 | 2.4999 | 6.2516 | + |
| 6.20 | -27542.39 | 0.3527D-01 | 3630.767 | 0.7370D 12 | 0.2030D 17 | 2.4896 | 6.1978 | - |
| 7.20 | -27303.39 | 0.9297D-02 | 3662.549 | 0.1689D 12 | 0.4611D 16 | 2.4783 | 6.1376 | + |
| 8.20 | -27067.39 | 0.3990D-02 | 3694.483 | 0.7913D 11 | 0.2142D 16 | 2.4789 | 6.1515 | + |
| 9.20 | -26834.39 | 0.2510D-01 | 3726.562 | 0.4950D 12 | 0.1301D 17 | 2.4665 | 6.0844 | - |
| 10.20 | -26604.39 | 0.1640D-01 | 3758.779 | 0.3087D 12 | 0.8214D 16 | 2.4567 | 6.0333 | + |
| 11.20 | -26377.39 | 0.9020D-05 | 3791.126 | 0.1655D 09 | 0.4366D 13 | 2.3402 | 5.3186 | - |
| 12.20 | -26153.39 | 0.1353D-01 | 3823.597 | 0.2420D 12 | 0.6328D 16 | 2.4453 | 5.9813 | - |

Appendix Vb. Molecular Chlorine and Molecular Chlorine Anion Franck-Condon Overlap Factors (con't)

| V*,V** | T(cm$^{-1}$) | Q | Lambda | QT**3 | QT**4 | RC | R**2C | Phase |
|---|---|---|---|---|---|---|---|---|
| 13. 0 | -15928.05 | 0.2692D-05 | 6278.232 | 0.1492D 08 | 0.2377D 12 | 2.1361 | 4.5655 | - |
| 14. 0 | -15710.05 | 0.1175D-04 | 6365.352 | 0.4558D 08 | 0.7160D 12 | 2.1289 | 4.5340 | + |
| 15. 0 | -15495.05 | 0.3463D-04 | 6453.674 | 0.1284D 09 | 0.1996D 13 | 2.1214 | 4.5025 | - |
| 16. 0 | -15283.05 | 0.5471D-04 | 6543.197 | 0.3381D 09 | 0.5167D 13 | 2.1140 | 4.4710 | + |
| 17. 0 | -15074.05 | 0.2412D-03 | 6633.917 | 0.8282D 09 | 0.1245D 14 | 2.1065 | 4.4394 | - |
| 18. 0 | -14869.05 | 0.5724D-03 | 6725.829 | 0.1895D 10 | 0.2802D 14 | 2.0990 | 4.4077 | + |
| 19. 0 | -14665.05 | 0.1275D-02 | 6818.931 | 0.4020D 10 | 0.5896D 14 | 2.0914 | 4.3758 | - |
| 20. 0 | -14465.05 | 0.2655D-02 | 6913.213 | 0.8035D 10 | 0.1162D 15 | 2.0837 | 4.3437 | + |
| 21. 0 | -14268.05 | 0.5187D-02 | 7008.664 | 0.1507D 11 | 0.2150D 15 | 2.0759 | 4.3112 | - |
| 22. 0 | -14074.05 | 0.9530D-02 | 7105.273 | 0.2657D 11 | 0.3739D 15 | 2.0680 | 4.2783 | + |
| 23. 0 | -13883.05 | 0.1654D-01 | 7203.025 | 0.4425D 11 | 0.6143D 15 | 2.0599 | 4.2448 | - |
| 24. 0 | -13695.05 | 0.2727D-01 | 7301.905 | 0.7004D 11 | 0.9592D 15 | 2.0515 | 4.2104 | + |
| 25. 0 | -13510.05 | 0.4290D-01 - | 7401.895 | 0.1053D 12 | 0.1429D 16 | 2.0429 | 4.1744 | - |
| 13. 1 | -16482.40 | 0.5636D-04 | 6067.077 | 0.2546D 09 | 0.4196D 13 | 2.1549 | 4.6455 | - |
| 14. 1 | -16264.40 | 0.1908D-03 | 6148.393 | 0.5919D 09 | 0.1125D 14 | 2.1479 | 4.6133 | + |
| 15. 1 | -16049.40 | 0.4182D-03 | 6230.762 | 0.1729D 10 | 0.2775D 14 | 2.1409 | 4.5851 | - |
| 16. 1 | -15837.40 | 0.1003D-02 | 6314.163 | 0.3983D 10 | 0.6307D 14 | 2.1339 | 4.5551 | + |
| 17. 1 | -15628.40 | 0.2219D-02 | 6398.603 | 0.8472D 10 | 0.1324D 15 | 2.1269 | 4.5253 | - |
| 18. 1 | -15422.41 | 0.4541D-02 | 6484.073 | 0.1666D 11 | 0.2569D 15 | 2.1199 | 4.4955 | + |
| 19. 1 | -15219.41 | 0.8590D-02 | 6570.559 | 0.3029D 11 | 0.4609D 15 | 2.1129 | 4.4659 | - |
| 20. 1 | -15019.41 | 0.1501D-01 | 6658.053 | 0.5086D 11 | 0.7638D 15 | 2.1060 | 4.4363 | + |
| 21. 1 | -14822.41 | 0.2419D-01 | 6746.543 | 0.7974D 11 | 0.1158D 16 | 2.0990 | 4.4070 | - |
| 22. 1 | -14628.41 | 0.3590D-01 | 6836.015 | 0.1124D 12 | 0.1644D 16 | 2.0921 | 4.3777 | + |
| 23. 1 | -14437.41 | 0.4892D-01 | 6926.452 | 0.1472D 12 | 0.2126D 16 | 2.0852 | 4.3486 | - |
| 24. 1 | -14249.41 | 0.6095D-01 | 7017.837 | 0.1703D 12 | 0.2513D 16 | 2.0783 | 4.3198 | + |
| 25. 1 | -14064.41 | 0.6840D-01 - | 7110.148 | 0.1903D 12 | 0.2676D 16 | 2.0715 | 4.2912 | - |
| 13. 2 | -17031.33 | 0.4299D-03 | 5871.533 | 0.2124D 10 | 0.3617D 14 | 2.1726 | 4.7221 | - |
| 14. 2 | -16813.33 | 0.1074D-02 | 5947.663 | 0.5104D 10 | 0.9582D 14 | 2.1659 | 4.6926 | + |
| 15. 2 | -16598.33 | 0.2448D-02 | 6024.704 | 0.1120D 11 | 0.1858D 15 | 2.1591 | 4.6634 | - |
| 16. 2 | -16386.33 | 0.5099D-02 | 6102.049 | 0.2244D 11 | 0.3676D 15 | 2.1524 | 4.6344 | + |
| 17. 2 | -16177.33 | 0.9783D-02 | 6181.491 | 0.4138D 11 | 0.6646D 15 | 2.1458 | 4.6056 | - |
| 18. 2 | -15971.33 | 0.1685D-01 | 6261.219 | 0.6863D 11 | 0.1096D 16 | 2.1392 | 4.5771 | + |
| 19. 2 | -15768.33 | 0.2661D-01 | 6341.825 | 0.1043D 12 | 0.1645D 16 | 2.1326 | 4.5489 | - |
| 20. 2 | -15568.33 | 0.3803D-01 | 6423.295 | 0.1435D 12 | 0.2234D 16 | 2.1261 | 4.5210 | + |
| 21. 2 | -15371.33 | 0.4879D-01 | 6505.613 | 0.1772D 12 | 0.2724D 16 | 2.1197 | 4.4935 | - |
| 22. 2 | -15177.33 | 0.5560D-01 | 6588.774 | 0.1943D 12 | 0.2945D 16 | 2.1134 | 4.4664 | + |
| 23. 2 | -14986.33 | 0.5482D-01 | 6672.743 | 0.1845D 12 | 0.2765D 16 | 2.1072 | 4.4400 | - |
| 24. 2 | -14798.33 | 0.4511D-01 | 6757.019 | 0.1462D 12 | 0.2163D 16 | 2.1013 | 4.4146 | + |
| 25. 2 | -14613.33 | 0.2792D-01 | 6843.067 | 0.8714D 11 | 0.1273D 16 | 2.0961 | 4.3915 | - |

Appendix Vb. Molecular Chlorine and Molecular Chlorine Anion Franck-Condon Overlap Factors (con't)

| V*,V** | T(cm$^{-1}$) | Q | Lamdba | QT**3 | QT**4 | RC | R**2C | Phase |
|---|---|---|---|---|---|---|---|---|
| 13, 3 | -17574.80 | 0.2088D-02 | 5639.965 | 0.1134D 11 | 0.1992D 15 | 2.1896 | 4.7959 | - |
| 14, 3 | -17356.80 | 0.4555D-02 | 5761.432 | 0.2387D 11 | 0.4143D 15 | 2.1830 | 4.7670 | + |
| 15, 3 | -17141.80 | 0.9015D-02 | 5833.654 | 0.4541D 11 | 0.7784D 15 | 2.1765 | 4.7384 | - |
| 16, 3 | -16929.80 | 0.1607D-01 | 5906.745 | 0.7796D 11 | 0.1320D 16 | 2.1700 | 4.7101 | + |
| 17, 3 | -16720.80 | 0.2575D-01 | 5980.57[illegible] | 0.1204D 12 | 0.2013D 16 | 2.1636 | 4.6822 | - |
| 18, 3 | -16514.80 | 0.3651D-01 | 6055.174 | 0.1563D 12 | 0.2746D 16 | 2.1573 | 4.6546 | + |
| 19, 3 | -16311.80 | 0.4683D-01 | 6130.531 | 0.2032D 12 | 0.3315D 16 | 2.1511 | 4.6274 | - |
| 20, 3 | -16111.80 | 0.5171D-01 | 6206.671 | 0.2163D 12 | 0.3485D 16 | 2.1449 | 4.6009 | + |
| 21, 3 | -15914.80 | 0.4829D-01 | 6283.459 | 0.1946D 12 | 0.3098D 16 | 2.1390 | 4.5748 | - |
| 22, 3 | -15720.80 | 0.3608D-01 | 6360.999 | 0.1402D 12 | 0.2204D 16 | 2.1333 | 4.5501 | + |
| 23, 3 | -15529.80 | 0.1894D-01 | 6439.232 | 0.7094D 11 | 0.1102D 16 | 2.1284 | 4.5291 | - |
| 24, 3 | -15341.80 | 0.4348D-02 | 6518.139 | 0.1570D 11 | 0.2409D 15 | 2.1270 | 4.5183 | + |
| 25, 3 | -15156.80 | 0.3327D-03 | 6597.593 | 0.1159D 10 | 0.1756D 14 | 2.0797 | 4.3466 | + |
| 13, 4 | -18112.78 | 0.7188D-02 | 5520.964 | 0.4271D 11 | 0.7736D 15 | 2.2060 | 4.8678 | - |
| 14, 4 | -17894.78 | 0.1355D-01 | 5588.222 | 0.7765D 11 | 0.1389D 16 | 2.1996 | 4.8392 | + |
| 15, 4 | -17679.78 | 0.2274D-01 | 5656.180 | 0.1257D 12 | 0.2222D 16 | 2.1932 | 4.8110 | - |
| 16, 4 | -17467.78 | 0.3380D-01 | 5724.826 | 0.1801D 12 | 0.3147D 16 | 2.1869 | 4.7832 | + |
| 17, 4 | -17258.78 | 0.4402D-01 | 5794.153 | 0.2263D 12 | 0.3906D 16 | 2.1807 | 4.7559 | - |
| 18, 4 | -17052.78 | 0.4938D-01 | 5864.145 | 0.2449D 12 | 0.4176D 16 | 2.1746 | 4.7290 | + |
| 19, 4 | -16849.78 | 0.4624D-01 | 5934.795 | 0.2212D 12 | 0.3727D 16 | 2.1687 | 4.7028 | - |
| 20, 4 | -16649.78 | 0.3401D-01 | 6006.084 | 0.1570D 12 | 0.2613D 16 | 2.1630 | 4.6775 | + |
| 21, 4 | -16452.78 | 0.1699D-01 | 6077.999 | 0.7567D 11 | 0.1245D 16 | 2.1579 | 4.6543 | - |
| 22, 4 | -16258.78 | 0.3334D-02 | 6150.322 | 0.1433D 11 | 0.2330D 15 | 2.1556 | 4.6407 | + |
| 23, 4 | -16067.78 | 0.5613D-03 | 6223.634 | 0.2328D 10 | 0.3741D 14 | 2.1276 | 4.5417 | + |
| 24, 4 | -15879.78 | 0.1016D-01 | 6297.315 | 0.4068D 11 | 0.5460D 15 | 2.1339 | 4.5567 | - |
| 25, 4 | -15694.78 | 0.2507D-01 | 6371.544 | 0.9693D 11 | 0.1521D 16 | 2.1297 | 4.5367 | + |
| 13, 5 | -18645.23 | 0.1823D-01 | 5363.301 | 0.1182D 12 | 0.2203D 16 | 2.2219 | 4.9379 | - |
| 14, 5 | -18427.23 | 0.2898D-01 | 5420.751 | 0.1813D 12 | 0.3341D 16 | 2.2156 | 4.9[illegible] | + |
| 15, 5 | -18212.23 | 0.3306D-01 | 5490.815 | 0.2427D 12 | 0.4407D 16 | 2.2094 | 4.8817 | - |
| 16, 5 | -18000.23 | 0.4741D-01 | 5555.434 | 0.2765D 12 | 0.4977D 16 | 2.2032 | 4.8543 | + |
| 17, 5 | -17791.23 | 0.4607D-01 | 5620.740 | 0.2624D 12 | 0.4676D 16 | 2.1972 | 4.8274 | - |
| 18, 5 | -17585.24 | 0.3612D-01 | 5686.383 | 0.1954D 12 | 0.3454D 16 | 2.1914 | 4.8012 | + |
| 19, 5 | -17382.24 | 0.1929D-01 | 5752.999 | 0.1013D 12 | 0.1761D 16 | 2.1859 | 4.7764 | - |
| 20, 5 | -17182.24 | 0.4499D-02 | 5819.964 | 0.2282D 11 | 0.3921D 15 | 2.1820 | 4.7564 | + |
| 21, 5 | -16985.24 | 0.2216D-03 | 5887.460 | 0.1086D 10 | 0.1845D 14 | 2.1553 | 4.66[illegible]0 | + |
| 22, 5 | -16791.24 | 0.9489D-02 | 5955.487 | 0.4019D 11 | 0.6748D 15 | 2.1640 | 4.6862 | - |
| 23, 5 | -16600.24 | 0.2205D-01 | 6024.012 | 0.1[illegible]D 12 | 0.1675D 16 | 2.1596 | 4.5650 | + |
| 24, 5 | -16412.24 | 0.2837D-01 | 6093.015 | 0.1281D 12 | 0.2102D 16 | 2.1545 | 4.6422 | - |
| 25, 5 | -16227.24 | 0.2237D-01 | 6163.473 | 0.9432D 11 | 0.1531D 16 | 2.1498 | 4.6203 | + |

Appendix Vb. Molecular Chlorine and Molecular Chlorine Anion Franck-Condon Overlap Factors (con't)

| V*,V** | T(cm$^{-1}$) | Q | Lambda | QT**3 | QT**4 | RC | R**2C | Phase |
|---|---|---|---|---|---|---|---|---|
| 13, 6 | -19172.12 | 0.3429D-01 | 5215.908 | 0.2417D 12 | 0.4633D 16 | 2.2374 | 5.0068 | - |
| 14, 6 | -18954.12 | 0.4426D-01 | 5275.859 | 0.3014D 12 | 0.5713D 16 | 2.2312 | 4.9785 | + |
| 15, 6 | -18739.12 | 0.4757D-01 | 5336.431 | 0.3130D 12 | 0.5866D 16 | 2.2250 | 4.9508 | - |
| 16, 6 | -18527.12 | 0.4067D-01 | 5397.494 | 0.2586D 12 | 0.4792D 16 | 2.2190 | 4.9236 | + |
| 17, 6 | -18318.12 | 0.2499D-01 | 5459.075 | 0.1536D 12 | 0.2815D 16 | 2.2133 | 4.8973 | - |
| 18, 6 | -18112.12 | 0.8158D-02 | 5521.164 | 0.4847D 11 | 0.8779D 15 | 2.2082 | 4.8726 | + |
| 19, 6 | -17909.12 | 0.6300D-04 | 5583.747 | 0.3619D 09 | 0.6481D 13 | 2.2223 | 4.8967 | - |
| 20, 6 | -17709.12 | 0.5429D-02 | 5646.807 | 0.3015D 11 | 0.5339D 15 | 2.1923 | 4.8103 | - |
| 21, 6 | -17512.12 | 0.1866D-01 | 5710.330 | 0.1002D 12 | 0.1755D 16 | 2.1878 | 4.7880 | + |
| 22, 6 | -17318.12 | 0.2725D-01 | 5774.298 | 0.1416D 12 | 0.2451D 16 | 2.1827 | 4.7644 | - |
| 23, 6 | -17127.12 | 0.2266D-01 | 5838.693 | 0.1139D 12 | 0.1950D 16 | 2.1777 | 4.7414 | + |
| 24, 6 | -16939.12 | 0.8924D-02 | 5903.494 | 0.4337D 11 | 0.7347D 15 | 2.1737 | 4.7215 | - |
| 25, 6 | -16754.12 | 0.8260D-04 | 5968.680 | 0.3884D 09 | 0.6508D 13 | 2.2010 | 4.7995 | + |
| 13, 7 | -19693.39 | 0.4664D-01 | 5077.847 | 0.3562D 12 | 0.7015D 16 | 2.2526 | 5.0745 | - |
| 14, 7 | -19475.39 | 0.4551D-01 | 5134.686 | 0.3362D 12 | 0.6548D 16 | 2.2464 | 5.0462 | + |
| 15, 7 | -19260.39 | 0.3336D-01 | 5192.004 | 0.2384D 12 | 0.4591D 16 | 2.2404 | 5.0185 | - |
| 16, 7 | -19048.39 | 0.1530D-01 | 5249.788 | 0.1058D 12 | 0.2014D 16 | 2.2346 | 4.9915 | + |
| 17, 7 | -18839.39 | 0.1912D-02 | 5308.023 | 0.1279D 11 | 0.2409D 15 | 2.2303 | 4.9672 | - |
| 18, 7 | -18633.39 | 0.1824D-02 | 5366.710 | 0.1180D 11 | 0.2199D 15 | 2.2193 | 4.9324 | - |
| 19, 7 | -18430.39 | 0.1357D-01 | 5425.821 | 0.8493D 11 | 0.1565D 16 | 2.2152 | 4.9091 | + |
| 20, 7 | -18230.39 | 0.2522D-01 | 5485.346 | 0.1528D 12 | 0.2786D 16 | 2.2099 | 4.8842 | - |
| 21, 7 | -18033.39 | 0.2478D-01 | 5545.269 | 0.1453D 12 | 0.2621D 16 | 2.2046 | 4.8597 | + |
| 22, 7 | -17839.39 | 0.1241D-01 | 5605.572 | 0.7044D 11 | 0.1257D 16 | 2.1998 | 4.8368 | - |
| 23, 7 | -17648.39 | 0.1079D-02 | 5666.239 | 0.5934D 10 | 0.1047D 15 | 2.1992 | 4.8255 | + |
| 24, 7 | -17460.39 | 0.3095D-02 | 5727.249 | 0.1647D 11 | 0.2877D 15 | 2.1831 | 4.7723 | + |
| 25, 7 | -17275.39 | 0.1592D-01 | 5788.581 | 0.8206D 11 | 0.1418D 16 | 2.1801 | 4.7546 | - |
| 13, 8 | -20208.99 | 0.4233D-01 | 4948.293 | 0.3494D 12 | 0.7060D 16 | 2.2675 | 5.1410 | - |
| 14, 8 | -19990.99 | 0.2624D-01 | 5002.254 | 0.2096D 12 | 0.4191D 16 | 2.2613 | 5.1125 | + |
| 15, 8 | -19775.99 | 0.8130D-02 | 5056.637 | 0.6288D 11 | 0.1243D 16 | 2.2555 | 5.0843 | - |
| 16, 8 | -19563.99 | 0.4417D-05 | 5111.432 | 0.3308D 08 | 0.6471D 12 | 2.2791 | 5.0428 | + |
| 17, 8 | -19354.99 | 0.6917D-02 | 5166.627 | 0.5015D 11 | 0.9707D 15 | 2.2421 | 5.0305 | + |
| 18, 8 | -19148.99 | 0.2074D-01 | 5222.207 | 0.1457D 12 | 0.2789D 16 | 2.2367 | 5.0038 | - |
| 19, 8 | -18945.99 | 0.2657D-01 | 5278.161 | 0.1807D 12 | 0.3423D 16 | 2.2311 | 4.9776 | + |
| 20, 8 | -18745.99 | 0.1780D-01 | 5334.473 | 0.1173D 12 | 0.2198D 16 | 2.2255 | 4.9526 | - |
| 21, 8 | -18548.99 | 0.4012D-02 | 5391.123 | 0.2561D 11 | 0.4750D 15 | 2.2215 | 4.9299 | + |
| 22, 8 | -18354.99 | 0.6472D-03 | 5448.109 | 0.4002D 10 | 0.7346D 14 | 2.2079 | 4.8850 | + |
| 23, 8 | -18163.99 | 0.1076D-01 | 5505.397 | 0.6449D 11 | 0.1171D 16 | 2.2070 | 4.8733 | - |
| 24, 8 | -17975.99 | 0.2081D-01 | 5562.975 | 0.1209D 12 | 0.2173D 16 | 2.2023 | 4.8505 | + |
| 25, 8 | -17790.99 | 0.1635D-01 | 5620.922 | 0.9207D 11 | 0.1638D 16 | 2.1976 | 4.8279 | - |

Appendix Vb. Molecular Chlorine and Molecular Chlorine Anion Franck-Condon Overlap Factors (con't)

| V*,V** | T(cm$^{-1}$) | Q | Lambda | QT**3 | QT**4 | RC | R**2C | Phase |
|---|---|---|---|---|---|---|---|---|
| 13. 9 | -20718.88 | [illegible] | 4826.517 | 0.1795D 12 | 0.3719D 16 | 2.2821 | 5.2062 | - |
| 14. 9 | -20500.88 | [illegible] | 4877.841 | 0.3077D 11 | 0.6308D 15 | 2.2760 | 5.1783 | + |
| 15. 9 | -20285.88 | [illegible] | 4929.528 | 0.9146D 10 | 0.1855D 15 | 2.2689 | 5.1572 | + |
| 16. 9 | -20073.88 | 0.1289D-01 | 4981.599 | 0.1043D 12 | 0.2094D 16 | 2.2633 | 5.1246 | - |
| 17. 9 | -19864.88 | 0.2520D-01 | 5034.011 | 0.1976D 12 | 0.3925D 16 | 2.2575 | 5.0966 | + |
| 18. 9 | -19658.88 | 0.2379D-01 | 5086.760 | 0.1807D 12 | 0.3553D 16 | 2.2518 | 5.0692 | - |
| 19. 9 | -19455.88 | 0.1008D-01 | 5139.834 | 0.7423D 11 | 0.1444D 16 | 2.2464 | 5.0447 | + |
| 20. 9 | -19255.88 | 0.2114D-03 | 5193.219 | 0.1509D 10 | 0.2906D 14 | 2.2462 | 5.0212 | - |
| 21. 9 | -19058.88 | 0.5437D-02 | 5246.898 | 0.3764D 11 | 0.7174D 15 | 2.2332 | 4.9912 | - |
| 22. 9 | -18864.88 | 0.1758D-01 | 5300.855 | 0.1180D 12 | 0.2226D 16 | 2.2284 | 4.9667 | + |
| 23. 9 | -18673.88 | 0.1955D-01 | 5355.074 | 0.1273D 12 | 0.2377D 16 | 2.2234 | 4.9427 | - |
| 24. 9 | -18485.88 | 0.8364D-02 | 5409.534 | 0.5284D 11 | 0.9768D 15 | 2.2188 | 4.9200 | + |
| 25. 9 | -18300.88 | 0.1573D-04 | 5464.218 | 0.9639D 08 | 0.1764D 13 | 2.2547 | 4.9848 | - |
| 13.10 | -21222.99 | 0.1147D-02 | 4711.871 | 0.1096D 11 | 0.2327D 15 | 2.2959 | 5.2620 | - |
| 14.10 | -21004.99 | 0.3784D-02 | 4760.773 | 0.3507D 11 | 0.7366D 15 | 2.2903 | 5.2505 | - |
| 15.10 | -20789.99 | 0.1824D-01 | 4810.007 | 0.1639D 12 | 0.3408D 16 | 2.2841 | 5.2183 | + |
| 16.10 | -20577.99 | 0.2632D-01 | 4859.561 | 0.2337D 12 | 0.4809D 16 | 2.2780 | 5.1894 | - |
| 17.10 | -20368.99 | 0.1897D-01 | 4909.423 | 0.1595D 12 | 0.3248D 16 | 2.2721 | 5.1612 | + |
| 18.10 | -20163.00 | 0.4122D-02 | 4959.580 | 0.3379D 11 | 0.6813D 15 | 2.2666 | 5.1327 | - |
| 19.10 | -19960.00 | 0.8813D-03 | 5010.021 | 0.7008D 10 | 0.1399D 15 | 2.2588 | 5.1136 | - |
| 20.10 | -19760.00 | 0.1191D-01 | 5060.730 | 0.9186D 11 | 0.1815D 16 | 2.2542 | 5.0837 | + |
| 21.10 | -19563.00 | 0.2051D-01 | 5111.691 | 0.1535D 12 | 0.3003D 16 | 2.2489 | 5.0577 | - |
| 22.10 | -19369.00 | 0.1401D-01 | 5162.890 | 0.1018D 12 | 0.1972D 16 | 2.2437 | 5.0326 | + |
| 23.10 | -19178.00 | 0.1995D-02 | 5214.309 | 0.1407D 11 | 0.2698D 15 | 2.2399 | 5.0092 | - |
| 24.10 | -18990.00 | 0.2279D-02 | 5265.930 | 0.1554D 11 | 0.2952D 15 | 2.2300 | 4.9804 | - |
| 25.10 | -18805.00 | 0.1408D-01 | 5317.736 | 0.9363D 11 | 0.1761D 16 | 2.2262 | 4.9574 | + |
| 13.11 | -21721.28 | 0.5965D-02 | 4603.781 | 0.7139D 11 | 0.1551D 16 | 2.3111 | 5.3447 | + |
| 14.11 | -21503.28 | 0.2234D-01 | 4650.454 | 0.2222D 12 | 0.4777D 16 | 2.3046 | 5.3120 | - |
| 15.11 | -21288.28 | 0.2633D-01 | 4697.421 | 0.2540D 12 | 0.5407D 16 | 2.2983 | 5.2818 | + |
| 16.11 | -21076.28 | 0.1359D-01 | 4744.671 | 0.1272D 12 | 0.2681D 16 | 2.2922 | 5.2520 | - |
| 17.11 | -20867.28 | 0.8400D-03 | 4792.192 | 0.7633D 10 | 0.1593D 15 | 2.2862 | 5.2148 | + |
| 18.11 | -20661.28 | 0.4430D-02 | 4839.971 | 0.3907D 11 | 0.8072D 15 | 2.2803 | 5.2044 | + |
| 19.11 | -20458.28 | 0.1730D-01 | 4887.995 | 0.1431D 12 | 0.3030D 16 | 2.2745 | 5.1746 | - |
| 20.11 | -20253.28 | 0.1933D-01 | 4936.253 | 0.1607D 12 | 0.3256D 16 | 2.2689 | 5.1474 | + |
| 21.11 | -20061.28 | 0.7452D-02 | 4984.726 | 0.6017D 11 | 0.1207D 16 | 2.2636 | 5.1206 | - |
| 22.11 | -19867.28 | 0.8892D-05 | 5033.401 | 0.6973D 08 | 0.1385D 13 | 2.2394 | 5.1375 | - |
| 23.11 | -19676.28 | 0.7377D-02 | 5082.261 | 0.6000D 11 | 0.1181D 16 | 2.2516 | 5.0727 | + |
| 24.11 | -19488.28 | 0.1732D-01 | 5131.289 | 0.1252D 12 | 0.2498D 16 | 2.2466 | 5.0475 | - |
| 25.11 | -19303.28 | 0.1190D-01 | 5180.466 | 0.8563D 11 | 0.1653D 16 | 2.2415 | 5.0229 | + |
| 13.12 | -22213.67 | 0.2519D-01 | 4501.732 | 0.2751D 12 | 0.6132D 16 | 2.3250 | 5.4063 | + |
| 14.12 | -21995.67 | 0.2469D-01 | 4546.349 | 0.2627D 12 | 0.5779D 16 | 2.3185 | 5.3747 | - |
| 15.12 | -21780.67 | 0.9039D-02 | 4591.227 | 0.9340D 11 | 0.2034D 16 | 2.3120 | 5.3424 | + |
| 16.12 | -21568.67 | 0.7165D-05 | 4636.354 | 0.7189D 08 | 0.1551D 13 | 2.3207 | 5.5164 | + |
| 17.12 | -21359.67 | 0.3070D-02 | 4681.720 | 0.8839D 11 | 0.1888D 16 | 2.3005 | 5.2955 | - |
| 18.12 | -21153.67 | 0.2037D-01 | 4727.311 | 0.1928D 12 | 0.4078D 16 | 2.2945 | 5.2651 | + |

Appendix Vb. Molecular Chlorine and Molecular Chlorine Anion Franck-Condon Overlap Factors (con't)

| V*,V** | T(cm-1) | Q | Lambda | QT**3 | QT**4 | RC | R**2C | Phase |
|---|---|---|---|---|---|---|---|---|
| 19.12 | -20950.68 | 0.1549D-01 | 4773.115 | 0.1425D 12 | 0.2935D 16 | 2.2886 | 5.2364 | - |
| 20.12 | -20750.68 | 0.2472D-02 | 4819.120 | 0.2208D 11 | 0.4593D 15 | 2.2830 | 5.2093 | + |
| 21.12 | -20553.68 | 0.2100D-02 | 4865.310 | 0.1823D 11 | 0.3748D 15 | 2.2770 | 5.1923 | + |
| 22.12 | -20359.68 | 0.1353D-01 | 4911.669 | 0.1142D 12 | 0.2325D 16 | 2.2717 | 5.1619 | - |
| 23.12 | -20168.68 | 0.1635D-01 | 4958.184 | 0.1341D 12 | 0.2705D 16 | 2.2663 | 5.1356 | + |
| 24.12 | -19980.68 | 0.5520D-02 | 5004.836 | 0.4403D 11 | 0.8798D 15 | 2.2614 | 5.1095 | - |
| 25.12 | -19795.68 | 0.3697D-03 | 5051.608 | 0.2868D 10 | 0.5678D 14 | 2.2521 | 5.0917 | - |
| 13.13 | -22700.11 | 0.2277D-01 | 4405.265 | 0.2663D 12 | 0.6045D 16 | 2.3387 | 5.4684 | + |
| 14.13 | -22482.11 | 0.5668D-02 | 4447.981 | 0.6441D 11 | 0.1448D 16 | 2.3316 | 5.4324 | - |
| 15.13 | -22267.11 | 0.8662D-03 | 4490.929 | 0.9564D 10 | 0.2130D 15 | 2.3288 | 5.4353 | - |
| 16.13 | -22055.11 | 0.1351D-01 | 4534.097 | 0.1449D 12 | 0.3196D 16 | 2.3206 | 5.3873 | + |
| 17.13 | -21846.11 | 0.2111D-01 | 4577.474 | 0.2201D 12 | 0.4809D 16 | 2.3143 | 5.3558 | - |
| 18.13 | -21640.11 | 0.1078D-01 | 4621.048 | 0.1092D 12 | 0.2364D 16 | 2.3081 | 5.3249 | + |
| 19.13 | -21437.11 | 0.1745D-03 | 4664.807 | 0.1719D 10 | 0.3685D 14 | 2.3001 | 5.2625 | - |
| 20.13 | -21237.11 | 0.6497D-02 | 4708.738 | 0.6223D 11 | 0.1322D 16 | 2.2971 | 5.2802 | - |
| 21.13 | -21040.11 | 0.1693D-01 | 4752.826 | 0.1577D 12 | 0.3319D 16 | 2.2912 | 5.2503 | + |
| 22.13 | -20846.11 | 0.1227D-01 | 4797.057 | 0.1111D 12 | 0.2317D 16 | 2.2857 | 5.2224 | - |
| 23.13 | -20655.11 | 0.1121D-02 | 4841.416 | 0.9879D 10 | 0.2040D 15 | 2.2804 | 5.1895 | + |
| 24.13 | -20467.11 | 0.3703D-02 | 4885.887 | 0.3175D 11 | 0.6498D 15 | 2.2744 | 5.1785 | + |
| 25.13 | -20282.11 | 0.1459D-01 | 4930.453 | 0.1218D 12 | 0.2470D 16 | 2.2692 | 5.1500 | - |
| 13.14 | -23180.53 | 0.3467D-02 | 4313.966 | 0.4319D 11 | 0.1001D 16 | 2.3511 | 5.5217 | + |
| 14.14 | -22962.53 | 0.2581D-02 | 4354.921 | 0.3125D 11 | 0.7177D 15 | 2.3486 | 5.5223 | + |
| 15.14 | -22747.53 | 0.1709D-01 | 4396.082 | 0.2012D 12 | 0.4577D 16 | 2.3407 | 5.4800 | - |
| 16.14 | -22535.53 | 0.2020D-01 | 4437.438 | 0.2312D 12 | 0.5211D 16 | 2.3340 | 5.4470 | + |
| 17.14 | -22326.53 | 0.6518D-02 | 4478.977 | 0.7254D 11 | 0.1619D 16 | 2.3273 | 5.4125 | - |
| 18.14 | -22120.53 | 0.4030D-03 | 4520.687 | 0.4362D 10 | 0.9649D 14 | 2.3256 | 5.4266 | - |
| 19.14 | -21917.53 | 0.1129D-01 | 4562.558 | 0.1188D 12 | 0.2605D 16 | 2.3167 | 5.3692 | + |
| 20.14 | -21717.53 | 0.1742D-01 | 4604.575 | 0.1784D 12 | 0.3874D 16 | 2.3106 | 5.3384 | - |
| 21.14 | -21520.53 | 0.7184D-02 | 4646.725 | 0.7160D 11 | 0.1541D 16 | 2.3046 | 5.3079 | + |
| 22.14 | -21326.53 | 0.6035D-04 | 4688.995 | 0.5854D 09 | 0.1248D 14 | 2.3031 | 5.3524 | + |
| 23.14 | -21135.53 | 0.8720D-02 | 4731.369 | 0.8233D 11 | 0.1740D 16 | 2.2940 | 5.2653 | - |
| 24.14 | -20947.53 | 0.1530D-01 | 4773.832 | 0.1406D 12 | 0.2946D 16 | 2.2885 | 5.2368 | + |
| 25.14 | -20762.53 | 0.6280D-02 | 4816.363 | 0.5621D 11 | 0.1167D 16 | 2.2830 | 5.2083 | - |
| 13.15 | -23654.85 | 0.4466D-02 | 4227.463 | 0.5912D 11 | 0.1398D 16 | 2.3688 | 5.6160 | - |
| 14.15 | -23436.85 | 0.1970D-01 | 4266.785 | 0.2537D 12 | 0.5945D 16 | 2.3608 | 5.5742 | + |
| 15.15 | -23221.85 | 0.1848D-01 | 4306.290 | 0.2314D 12 | 0.5373D 16 | 2.3538 | 5.5392 | - |
| 16.15 | -23009.85 | 0.3368D-02 | 4345.965 | 0.4103D 11 | 0.9440D 15 | 2.3461 | 5.4983 | + |
| 17.15 | -22800.85 | 0.2349D-02 | 4385.802 | 0.2784D 11 | 0.6348D 15 | 2.3439 | 5.5010 | + |
| 18.15 | -22594.85 | 0.1519D-01 | 4425.787 | 0.1752D 12 | 0.3958D 16 | 2.3362 | 5.4591 | - |
| 19.15 | -22391.85 | 0.1557D-01 | 4465.910 | 0.1749D 12 | 0.3915D 16 | 2.3298 | 5.4267 | + |
| 20.15 | -22191.85 | 0.2953D-02 | 4506.158 | 0.3233D 11 | 0.7174D 15 | 2.3230 | 5.3899 | - |
| 21.15 | -21994.85 | 0.2033D-02 | 4546.518 | 0.2163D 11 | 0.4758D 15 | 2.3199 | 5.3898 | - |
| 22.15 | -21800.85 | 0.1313D-01 | 4586.977 | 0.1362D 12 | 0.2966D 16 | 2.3132 | 5.3521 | + |
| 23.15 | -21609.85 | 0.1291D-01 | 4627.519 | 0.1303D 12 | 0.2816D 16 | 2.3073 | 5.3225 | - |
| 24.15 | -21421.85 | 0.1362D-02 | 4668.130 | 0.1831D 11 | 0.3922D 15 | 2.3013 | 5.2875 | + |
| 25.15 | -21236.85 | 0.3021D-02 | 4708.795 | 0.2893D 11 | 0.5145D 15 | 2.2969 | 5.2821 | + |

Appendix Vb. Molecular Chlorine and Molecular Chlorine Anion Franck-Condon Overlap Factors (con't)

| V*,V** | T(cm$^{-1}$) | Q | Lambda | QT**3 | QT**4 | RC | R**2C | Phase |
|---|---|---|---|---|---|---|---|---|
| 13,16 | -24123.01 | 0.2152D-01 | 4145.420 | 0.3020D 12 | 0.7286D 16 | 2.3811 | 5.6701 | - |
| 14,16 | -23905.01 | 0.1664D-01 | 4183.224 | 0.2274D 12 | 0.5435D 16 | 2.3736 | 5.6327 | + |
| 15,16 | -23690.01 | 0.1423D-02 | 4221.189 | 0.1892D 11 | 0.4482D 15 | 2.3640 | 5.5788 | - |
| 16,16 | -23478.01 | 0.5097D-02 | 4259.305 | 0.6596D 11 | 0.1549D 16 | 2.3633 | 5.5899 | - |
| 17,16 | -23269.01 | 0.1770D-01- | 4297.562 | 0.2230D 12 | 0.5190D 16 | 2.3557 | 5.5501 | + |
| 18,16 | -23063.01 | 0.1251D-01- | 4335.947 | 0.1535D 12 | 0.3539D 16 | 2.3489 | 5.5154 | - |
| 19,16 | -22860.01 | 0.5483D-03 | 4374.451 | 0.6550D 10 | 0.1497D 15 | 2.3389 | 5.4543 | + |
| 20,16 | -22660.01 | 0.5755D-02 | 4413.060 | 0.6696D 11 | 0.1517D 16 | 2.3388 | 5.4742 | + |
| 21,16 | -22463.01 | 0.1547D-01- | 4451.763 | 0.1753D 12 | 0.3938D 16 | 2.3321 | 5.4392 | - |
| 22,16 | -22269.01 | 0.8744D-02 | 4490.545 | 0.9656D 11 | 0.2150D 16 | 2.3259 | 5.4071 | + |
| 23,16 | -22078.01 | 0.2000D-04 | 4529.393 | 0.2152D 09 | 0.4752D 13 | 2.3052 | 5.2272 | - |
| 24,16 | -21890.01 | 0.7375D-02 | 4568.293 | 0.7735D 11 | 0.1693D 16 | 2.3159 | 5.3666 | - |
| 25,16 | -21705.01 | 0.1403D-01- | 4607.231 | 0.1434D 12 | 0.3113D 16 | 2.3099 | 5.3353 | + |
| 13,17 | -24584.92 | 0.1521D-01 | 4067.534 | 0.2260D 12 | 0.5556D 16 | 2.3937 | 5.7280 | - |
| 14,17 | -24366.92 | 0.4479D-03 | 4103.924 | 0.6480D 10 | 0.1579D 15 | 2.3793 | 5.6424 | + |
| 15,17 | -24151.92 | 0.7927D-02 | 4140.457 | 0.1117D 12 | 0.2697D 16 | 2.3832 | 5.6828 | + |
| 16,17 | -23939.92 | 0.1894D-01 | 4177.123 | 0.2599D 12 | 0.6221D 16 | 2.3754 | 5.6425 | - |
| 17,17 | -23730.92 | 0.9234D-02 | 4213.911 | 0.1234D 12 | 0.2928D 16 | 2.3680 | 5.6043 | + |
| 18,17 | -23524.93 | 0.2989D-04 | 4250.810 | 0.3892D 09 | 0.9155D 13 | 2.3897 | 5.7817 | + |
| 19,17 | -23321.93 | 0.9835D-02 | 4287.810 | 0.1248D 12 | 0.2909D 16 | 2.3579 | 5.5623 | - |
| 20,17 | -23121.93 | 0.1547D-01 | 4324.899 | 0.1912D 12 | 0.4421D 16 | 2.3511 | 5.5269 | + |
| 21,17 | -22924.93 | 0.4497D-02 | 4362.064 | 0.5418D 11 | 0.1242D 16 | 2.3440 | 5.4894 | - |
| 22,17 | -22730.93 | 0.1050D-02 | 4399.293 | 0.1233D 11 | 0.2804D 15 | 2.3430 | 5.5010 | - |
| 23,17 | -22539.93 | 0.1151D-01 | 4436.572 | 0.1318D 12 | 0.2971D 16 | 2.3346 | 5.4521 | + |
| 24,17 | -22351.93 | 0.1165D-01 | 4473.887 | 0.1301D 12 | 0.2907D 16 | 2.3284 | 5.4200 | - |
| 25,17 | -22166.93 | 0.1047D-02 | 4511.225 | 0.1141D 11 | 0.2529D 15 | 2.3209 | 5.3747 | + |
| 13,18 | -25040.52 | 0.8608D-04 | 3993.528 | 0.1352D 10 | 0.3384D 14 | 2.3837 | 5.6376 | - |
| 14,18 | -24822.52 | 0.1040D-01 | 4028.601 | 0.1591D 12 | 0.3949D 16 | 2.4033 | 5.7788 | - |
| 15,18 | -24607.52 | 0.1931D-01 | 4063.799 | 0.2878D 12 | 0.7082D 16 | 2.3952 | 5.7366 | + |
| 16,18 | -24395.52 | 0.6407D-02 | 4099.114 | 0.9302D 11 | 0.2269D 16 | 2.3869 | 5.6934 | - |
| 17,18 | -24186.52 | 0.9390D-03 | 4134.535 | 0.1329D 11 | 0.3213D 15 | 2.3884 | 5.7173 | - |
| 18,18 | -23980.52 | 0.1331D-01 | 4170.051 | 0.1835D 12 | 0.4401D 16 | 2.3772 | 5.6525 | + |
| 19,18 | -23777.52 | 0.1372D-01 | 4205.653 | 0.1844D 12 | 0.4384D 16 | 2.3700 | 5.6153 | - |
| 20,18 | -23577.52 | 0.1447D-02 | 4241.329 | 0.1896D 11 | 0.4470D 15 | 2.3608 | 5.5634 | + |
| 21,18 | -23380.52 | 0.4122D-02 | 4277.065 | 0.5269D 11 | 0.1232D 16 | 2.3606 | 5.5778 | + |
| 22,18 | -23186.52 | 0.1395D-01 | 4312.851 | 0.1739D 12 | 0.4032D 16 | 2.3533 | 5.5382 | - |
| 23,18 | -22995.52 | 0.7697D-02 | 4348.673 | 0.9360D 11 | 0.2152D 16 | 2.3466 | 5.5034 | + |
| 24,18 | -22807.52 | 0.2041D-04 | 4384.519 | 0.2422D 09 | 0.5523D 13 | 2.3655 | 5.6880 | + |

Appendix Vb. Molecular Chlorine and Molecular Chlorine Anion Franck-Condon Overlap Factors (con't)

| V*,V** | T(cm$^{-1}$) | Q | Lambda | QT**3 | QT**4 | RC | R**2C | Phase |
|---|---|---|---|---|---|---|---|---|
| 25.18 | -22622.52 | 0.8687D-02 | 4420.374 | 0.1006D 12 | 0.2275D 16 | 2.3370 | 5.4642 | - |
| 13.19 | -25489.70 | 0.1231D-01 | 3923.153 | 0.2033D 12 | 0.5196D 16 | 2.4240 | 5.8792 | + |
| 14.19 | -25271.70 | 0.1933D-01 | 3956.995 | 0.3121D 12 | 0.7886D 16 | 2.4153 | 5.8331 | - |
| 15.19 | -25056.70 | 0.4317D-02 | 3990.949 | 0.6791D 11 | 0.1702D 16 | 2.4058 | 5.7821 | + |
| 16.19 | -24844.70 | 0.2639D-02 | 4025.003 | 0.4047D 11 | 0.1005D 16 | 2.4066 | 5.7990 | + |
| 17.19 | -24635.70 | 0.1578D-01 | 4059.150 | 0.2360D 12 | 0.5814D 16 | 2.3966 | 5.7447 | - |
| 18.19 | -24429.70 | 0.1110D-01 | 4093.377 | 0.1619D 12 | 0.3954D 16 | 2.3888 | 5.7043 | + |
| 19.19 | -24226.70 | 0.8989D-04 | 4127.677 | 0.1278D 10 | 0.3096D 14 | 2.3642 | 5.5457 | - |
| 20.19 | -24026.70 | 0.7960D-02 | 4162.036 | 0.1104D 12 | 0.2653D 16 | 2.3792 | 5.6636 | - |
| 21.19 | -23829.70 | 0.1417D-01 | 4196.443 | 0.1917D 12 | 0.4568D 16 | 2.3718 | 5.6250 | + |
| 22.19 | -23635.70 | 0.3721D-02 | 4230.887 | 0.4913D 11 | 0.1161D 16 | 2.3641 | 5.5834 | - |
| 23.19 | -23444.70 | 0.1590D-02 | 4265.356 | 0.2049D 11 | 0.4803D 15 | 2.3640 | 5.5978 | - |
| 24.19 | -23256.70 | 0.1188D-01 | 4299.835 | 0.1494D 12 | 0.3475D 16 | 2.3554 | 5.5491 | + |
| 25.19 | -23071.70 | 0.8799D-02 | 4334.314 | 0.1081D 12 | 0.2493D 16 | 2.3487 | 5.5138 | - |
| 13.20 | -25932.39 | 0.1950D-01 | 3855.182 | 0.3400D 12 | 0.8817D 16 | 2.4359 | 5.9330 | + |
| 14.20 | -25714.39 | 0.3001D-02 | 3888.874 | 0.5102D 11 | 0.1312D 16 | 2.4246 | 5.8712 | - |
| 15.20 | -25499.39 | 0.4549D-02 | 3921.663 | 0.7542D 11 | 0.1923D 16 | 2.4264 | 5.8929 | - |
| 16.20 | -25287.39 | 0.1733D-01 | 3954.541 | 0.2803D 12 | 0.7088D 16 | 2.4164 | 5.8394 | + |
| 17.20 | -25078.39 | 0.8430D-02 | 3987.497 | 0.1330D 12 | 0.3334D 16 | 2.4077 | 5.7938 | - |
| 18.20 | -24872.39 | 0.2706D-03 | 4020.522 | 0.4164D 10 | 0.1036D 15 | 2.4176 | 5.8702 | - |
| 19.20 | -24669.39 | 0.1150D-01 | 4053.606 | 0.1726D 12 | 0.4258D 16 | 2.3982 | 5.7532 | + |
| 20.20 | -24469.39 | 0.1258D-01 | 4086.738 | 0.1843D 12 | 0.4509D 16 | 2.3904 | 5.7124 | - |
| 21.20 | -24272.39 | 0.9823D-03 | 4119.907 | 0.1405D 11 | 0.3410D 15 | 2.3792 | 5.6477 | + |
| 22.20 | -24078.39 | 0.4935D-02 | 4153.101 | 0.6889D 11 | 0.1659D 16 | 2.3814 | 5.6756 | + |
| 23.20 | -23887.39 | 0.1316D-01 | 4186.309 | 0.1794D 12 | 0.4286D 16 | 2.3737 | 5.6342 | - |
| 24.20 | -23699.39 | 0.4777D-02 | 4219.519 | 0.6359D 11 | 0.1507D 16 | 2.3662 | 5.5942 | + |
| 25.20 | -23514.39 | 0.1012D-02 | 4252.715 | 0.1316D 11 | 0.3094D 15 | 2.3663 | 5.6139 | + |

# REFERENCES

1. R. Wildt, Astrophys. J. 89, 295 (1939).

2. W. Gerlach and F. Gromann, Z. Phys. 18, 239 (1923).

3. L. M. Branscomb and B.E.F. Pagel, Roy. Astronomical Soc. (London) Monthly Notices, 118, 258 (1959).

4. Ya. L. Al'pert, Radio Wave Propagation and the Ionosphere (Consultants' Bureau, New York, 1963), p. 91.

5. E. E. Ferguson, Kinetics of Ion-Molecule Reactions, edited by P. Ausloos, NATO Adv. Study Inst. Series B (Plenum, New York, 1979).

6. E. E. Ferguson, F. C. Fehsenfeld and D. L. Albritton, Gas Phase Ion Chemistry, edited by M. T. Bowers (Academic, New York, 1979), p. 45.

7. a. A. N. Hayhurst and N. R. Telford, Combustion and Flame 28, 67 (1977).
   b. A. N. Hayhurst, D. B. Kittleson, and N. R. Telford, Combustion and Flame 28, 123 (1977).
   c. A. N Hayhurst and D. B. Kittleson, Combustion and Flame 31, 37 (1978).

8. G. Moreau, Compt. Rend. 148, 342 (1909).

9. D. K. Bohme, Kinetics of Ion-Molecule Reactions, edited by P. Ausloos, NATO Adv. Study Inst. Series B (Plenum, New York, 1979), p. 323.

10. G. S. Aravin and E. S. Semenov, Combustion, Explosions and Shock Waves 15, 589 (1979).

11. Ch. K. Rhodes, Excimer Lasers, Topics in Applied Physics, (Springer-Verlag, Berlin, 1979) Vol. 30.

12. a. S. K. Searles and C. A. Hart, Appl. Phys. Lett. 27, 243 (1975).
    b. R. Burnham, D. Harris, and N. Djeu, Appl. Phys. Lett. 28, 86 (1976).

13. P. J. Jay, W. R. Wadt, and T. H. Dunning, Jr., Ann. Rev. Phys. Chem. 30, 311 (1979).

14. D. W. Trainer and J. H. Jacob, Appl. Phys. Lett. 35, 920 (1979).

15. a. M. G. Thackston, F. L. Eisele, W. M. Pope, H. W. Ellis, E. W. McDaniel, and I. R. Gatland, J. Chem. Phys. 73, 3183 (1980).
    b. R. C. Sze, A. E. Greene, and C. A. Brau, J. Appl. Phys. 53, 1312 (1982).

16. D. J. Ehrlich and R. M. Osgood, Jr., J. Chem. Phys. 73, 3038 (1980).

17. L. G. Christophorou, Adv. in Electron. and Electron Phys., edited by L. Marton (Academic, New York, 1978), Vol. 46, p. 55.

18. G. E. Streit and T. W. Newton, J. Chem. Phys. 73, 3178 (1980).

19. J. N. Bardsley and F. Mandl, Rep. Prog. Phys. 31, 471 (1968).

20. B. K. Janousek and J. I. Brauman, Gas Phase Ion Chemistry, edited by M. T. Bowers (Academic, New York, 1979), p. 53.

21. C. A. Dowell, Physical Chemistry: An Advanced Treatise, edited by D. Henderson (Academic, New York, 1969), Vol. 3, p. 495.

22. L. N. Branscomb, Adv. in Electron. and Electron Phys., edited by L. Marton (Academic, New York, 1957), Vol. 9, p. 43.

23. H.S.W. Massey, Negative Ions (Cambridge Univ. Press, Cambridge 1950).

24. D. B. Dunkin, F. C. Fehsenfeld, and E. E. Ferguson, Chem. Phys. Lett. 15, 257 (1972).

25. C. Lifshitz, B. M. Hughes, and T. O. Tiernan, Chem. Phys. Lett. 7, 469 (1970).

26. A. P. Hickman and K. T. Gillen, J. Chem. Phys. 73, 3672 (1980).

27. M. W. Siegel, R. J. Celotta, J. L. Hall, J. Levine, and R. A. Bennett, Phys. Rev. 6, 631 (1972).

28. F. Breyer, P. Frey, and H. Hotop, Z. Phys. A 286, 133 (1978).

29. J. M. Slater, F. H. Reed, S. E. Novick, and W. C. Lineberger, Phys. Rev. A 17, 201 (1978).

30. P. C. Cosby, R. A. Bennett, J. R. Peterson, and J. T. Moseley, J. Chem. Phys. 63, 1612 (1975).

31. T. A. Lehman and M. M. Bursey, Ion Cyclotron Resonance Spectrometry (Wiley-Interscience, New York, 1976).

32. J. D. Baldeschwieler and S. S. Woodgate, Acc. Chem. Res. 4, 114 (1971).

33. L. N. Morgenthaler, Ph. D. dissertation, Univ. of Florida, Gainesville, FL 32611 (1979).

34. H. O. Pritchard, Chem. Rev. 52, 529 (1953).

35. W. B. Person, J. Chem. Phys. 38, 109 (1963).

36. R. S. Mulliken and W. B. Person, Physical Chemistry: An Advanced Treatise, edited by D. Henderson (Academic, New York, 1969), Vol. 3, p. 537.

37. a. W. F. Scheehan, J. Am. Chem. Soc. 100, 1348 (1978).
    b. G. V. Karachevtsev, Zh. Fiz. Khim. 52, 2740 (1978).

38. H. A. Kurtz, Ph. D. dissertation, Univ. of Florida, Gainesville, FL 32611 (1978).

39. J. Simons and W. D. Smith, J. Chem. Phys. 58, 4899 (1973).

40. E. Steiner, The Determination and Interpretations of Molecular Wave Functions (Cambridge Univ. Press, Cambridge, 1976).

41. a. E. P. Wigner, Phys. Rev. 73, 1002 (1948).
    b. E. P. Wigner and L. Eisenbud, Phys. Rev. 72, 29 (1947).

42. A. M. Lane and R. G. Thomas, Rev. Mod. Phys. 30, 257 (1958).

43. S. Geltman, Phys. Rev. 112, 176 (1958).

44. S. Seely and A. D. Poularikas, Electromagnetics: Classical and Modern Theory and Applications (Marcel Dekker, New York, 1979).

45. T. G. Northrop, The Adiabatic Motion of Charged Particles, Interscience Tracts on Physics and Astronomy (Interscience, New York, 1963) No. 21.

46. R. T. McIver, Jr., Rev. Sci. Instrum. 41, 555 (1970).

47. T. E. Sharp, J. R. Eyler, and E. Li, Int. J. Mass Spectrom. and Ion Phys. 9, 421 (1972).

48. C. E. Berry, J. Appl. Phys. 25, 28 (1954).

49. J. D. Jackson, Classical Electrodynamics (J. Wiley and Sons, New York, 1975).

50. A. Warnick, L. R. Anders, and T. E. Sharp, Rev. Sci. Instrum. 45, 929 (1974).

51. a. R. A. Brooks, Rev. Sci. Instrum. 43, 807 (1972).
    b. Y. T. Yang and T. C. Chen, Rev. Sci. Instrum. 36, 706 (1965).
    c. J. R. Singer and S. D. Johnson, Rev. Sci. Instrum. 30, 92 (1959).

52. R. T. McIver, Jr., Rev. Sci. Instrum. 44, 1071 (1973).

53. R. J. Dugan, L. N. Morgenthaler, R. O. Daubach, and J. R. Eyler Rev. Sci. Instrum. 50, 691 (1979).

54. Kepco, Inc. 131-38 Sanford Ave., Flushing, NY 11352.

55. CVC Products, Inc., P. O. Box 1886, Rochester, NY 14603.

56. Varian Associates, Palo Alto Vacuum Div., 611 Hansen Way, Palo Alto, CA 94303.

57. Varian V-5900 Ion Cyclotron Resonance Spectrometer Component, Varian Associates, 611 Hansen Way, Palo Alto, CA 94303.

58. Candela Corporation, 96 South Ave., Natick, MA 01760.

59. Candela Corporation, 96 South Ave., Natick, MA 01760. Manual on the operation of an ED-100U Head Assembly.

60. Micropump Corp., 1935 Shary Ct., Concord, CA 94518.

61. F. P. Schafer, Dye Lasers (Springer-Verlag, Berlin, 1977), p. 61.

62. Pall Corp./Mectron Industries, Inc., 330 Turnbull Canyon Rd., City of Industry, CA 91744.

63. Exciton Chemical Co., Inc., P. O. Box 3204, Overlook Station, Dayton, OH 45431.

64. PTR Optics Corp., 145 Newton St., Waltham, MA 02154.

65. Bausch and Lomb, Inc., Instrum. and Systems Div., 42 East Ave., Rochester, NY 14603.

66. Edmund Scientific, Inc., 101 E. Gloucester Pike, Barrington, NJ 08007.

67. Burleigh Instruments, Inc., Burleigh Park, Fishers, NY 14453.

68. American Instrument Co. (S-L-M Instrument Co.), 810 W. Anthony Drive, Urbana, IL 61801.

69. Instruments SA, Inc., J-Y Optical Systems Div., 173 Essex Ave., Metuchen, NJ 08840.

70. Gen Tec Inc., 2625 Dalton, Ste-foy, Quebec, Canada G1P 359.

71. Spectra-Physics, Inc., 1250 W. Middlefield Road, Mountain View, CA 94042.

72. L. Anders, J. Beauchamp, R. Dunbar, and J. Baldeschwieler, J. Chem. Phys. 45, 1062 (1966).

73. MOS Technology, Inc., 950 Rittenhouse Road, Norristown, PA 19401.

74. S.J. Smith, Methods Exptl. Phys. 7a, 179 (1968).

75. O.I. Asubiojo, H. L. McPeters, W. N. Olmstead, and J. I. Brauman, Chem. Phys. Lett. 48, 127 (1977).

76. J.J. DeCorpo and J. L. Franklin, J. Chem. Phys. 54, 1885 (1971).

77. D. E. Milligan, M.E. Jacox, and W. A. Guillory, J. Chem. Phys. 52, 3864 (1970).

78. D. B. Dunkin, F. C. Fehsenfield, and E. E. Ferguson, Chem. Phys. Lett. 15, 257 (1972).

79. B. M. Hughes, C. Lifschitz, and T. O. Tiernan, J. Chem. Phys. 59, 3162 (1973).

80. C. Lifshitz, B. M. Hughes, and T. O. Tiernan, Chem. Phys. Lett. 7, 469 (1970).

81. J. Berkowitz, W. A. Chupka, and D. Gutman, J. Chem. Phys. 55, 2733 (1971).

82. K. Lacmann and D. R. Herschbach, Bull. Am. Phy. Soc. 16, 213 (1971).

83. P. Warneck, Chem. Phys. Lett. 3, 532 (1969).

84. K. Smyth, Ph. D. dissertation, Stanford Univ., Palo Alto, CA 94303 (1972).

85. E. Herbst, T. A. Patterson, and W. C. Lineberger, J. Chem. Phys. 61, 1300 (1974).

86. J.H. Richardson, L. M. Stephenson, and J. I. Brauman, Chem. Phys. Lett. 25, 318 (1974).

87. R. M. Hochstrasser and A. P. Marchetti, J. Chem. Phys. 50, 1727 (1969).

88. G. Herzberg, Spectra of Diatomic Molecules (Van Nostrand, Princeton, 1950):
    a. 195
    b. 519
    c. 215
    d. 512

89. B. A. Huber, P. C. Cosby, J. R. Peterson, and J. T. Moseley, J. Chem. Phys. 66, 4520 (1977).

90. J. A. Stockdale, F. J. Davis, R. N. Compton, and C. E. Klots, J. Chem. Phys. 60, 4279 (1974).

91. I. D. Roberts, R. Stewart, and M. C. McGovern, Organic Chemistry (Benjamin, Menlo Park, 1971), p. 25.

92. S. A. Sullivan, B. S. Freiser, and J. L. Beauchamp, Chem. Phys. Lett. 48,294 (1977).

93. W. C. Tam and S. F. Wong, J. Chem. Phys. 68, 5625 (1978).

94. R. E. Fox, Phys. Rev. 109, 2008 (1958).

95. T. L. Gilbert and A. C. Wahl, J. Chem. Phys. 55, 5247 (1971).

96. P. W. Tasker, G. G. Balint-Kurti, and R. N. Dixon, Molec. Phys. 32, 1651 (1976).

97. L. Andrews, J. Am. Chem. Soc. 98, 2147 (1976).

98. C. J. Delbecq, B. Smaller, and P. H. Yuster, Phys. Rev. 111, 1235 (1958); C. J. Delbecq, W. Haynes, and P. H. Yuster, Phys. Rev. 121,1043 (1958).

99. D. L. Griscom, J. Chem. Phys. 51, 5186 (1969).

100. J. H. D. Eland, Photoelectron Spectroscopy (J. Wiley and Sons, NY, 1974).

101. P. M. Morse, Phys. Rev. 34, 57 (1929).

102. H. M. Hulburt and J. O. Hirschfelder, J. Chem. Phys. 9, 61 (1941).

103. A. L. G. Rees, Proc. Phys. Soc. 59, 998 (1947).

104. J. L. Dunham, Phys. Rev. 41, 721 (1932).

105. A. C. Hurley, Introduction to the Electron Theory of Small Molecules (Academic, New York, 1976), p. 1.

106. O. Klein, Z. Physik. 76, 226 (1932).

107. R. N. Zare and J. K. Cashion, UCRL-10881 (1963).

108. J. W. Cooley, Math. of Computation 15, 363 (1961).

109. A. E. Douglas and A. R. Hoy, Canadian J. Phys. 53, 1965 (1975).

110. B. Rosen, Spectroscopic Data Relative to Diatomic Molecules (Pergamon, New York, 1970), p. 121.

111. J. A. Coxon, Mol. Spectros. 1, 177 (1973).

112. M. V. Kurepa, D. S. Babic, and D. S. Belic, Chem. Phys. 59, 125 (1981).

113. J. A. Ayala, W. E. Wentworth, and E. C. M. Chen, J. Phys. Chem. 85, 768 (1981).

114. M. Allan and S. F. Wong, J. Chem. Phys. 74, 1687 (1981).

115. K. Lacmann and D. D. Herschbach, Chem. Phys. Lett. 6, 106 (1970).

116. W. A. Chupka, J. Berkowitz, and D. Gutman, J. Chem. Phys. 55, 2724 (1971).

117. H. C. Mattraw, C. F. Pachucki, and N. J. Hawkins, J. Chem. Phys. 22, 1117 (1954).

118. H. G. Vesper and G. K. Rollesfson, J. Am. Chem. Soc. 56, 620 (1934).

119. R. N. Compton and L. G. Christophorou, Phys. Rev. 154, 110 (1967).

120. J. A. Stockdale, R. N. Compton, and P. W. Reinhardt, Phys. Rev. 184, 81 (1969).

121. A. H. Zimmermann, K. J. Reed, and J. I. Brauman, J. Am. Chem. Soc. 99, 7203 (1977).

122. R. L. Jackson, A. H. Zimmermann, and J. I. Brauman, J. Chem. Phys. 71, 2088 (1979).

# BIOGRAPHICAL SKETCH

Ronald O. Daubach was born in Belleville. Illinois, on August 12, 1952. He graduated from Althoff Catholic High School in 1970 and Knox College in 1974. He attended the University of Florida from 1974 to 1983. During the final three years of this period, he worked as a research associate with the Magnetohydronamic Energy Center, Mississippi State University, Starkville, Mississippi. On August 22, 1981, he married Joni Meno. He is currently employed with the Magnetohydronamic Energy Center.

I certify that I have read this study and that in my opinion it conforms to acceptable standards of scholarly presentation and is full adequate, in scope and quality, as a dissertation for the degree of Doctor of Philosophy.

John R. Eyler

John R. Eyler, Chairman
Associate Professor of Chemistry

I certify that I have read this study and that in my opinion it conforms to acceptable standards of scholarly presentation and is full adequate, in scope and quality, as a dissertation for the degree of Doctor of Philosophy.

Wallace S. Brey

Wallace S. Brey
Professor of Chemistry

I certify that I have read this study and that in my opinion it conforms to acceptable standards of scholarly presentation and is full adequate, in scope and quality, as a dissertation for the degree of Doctor of Philosophy.

Martin Vala

Martin T. Vala
Professor of Chemistry

I certify that I have read this study and that in my opinion it conforms to acceptable standards of scholarly presentation and is full adequate, in scope and quality, as a dissertation for the degree of Doctor of Philosophy.

Richard T. Schneider

Richard T. Schneider
Professor of Nuclear Engineering

I certify that I have read this study and that in my opinion it conforms to acceptable standards of scholarly presentation and is full adequate, in scope and quality, as a dissertation for the degree of Doctor of Philosophy.

Thomas L. Bailey

Thomas L. Bailey
Professor of Physics

This dissertation was submitted to the Graduate Faculty of the Department of Chemistry in the College of Liberal Arts and Sciences and to the Graduate Council, and was accepted as partial fulfillment of the requirements for the degree of Doctor of Philosophy.

December 1983

Dean for Graduate Studies and Research